Modelling the grass cover erosion in the wave run-up zone of sea dikes

APPLYING AN OPENFOAM MODEL TO DELTA FLUME EXPERIMENTS

N. G. Bijen

UNIVERSITY OF TWENTE.

Photo cover image: Deltares delta flume (Deltares.nl).

Modelling the grass cover erosion in the wave run-up zone of sea dikes

By

N. G. Bijen

To obtain a Master of Science in Civil Engineering and Management

at the University of Twente.

Student number:	2213915	
Project duration:	September 23, 2020 – April 15, 2021	
Thesis committee:	Prof. dr. S. J. M. H. Hulscher,	University of Twente, chair supervisor
	Dr. J. J. Warmink,	University of Twente, committee member
	Dr. J. P. Aguilar-López,	TU Delft, external committee member
	V. M. van Bergeijk, (MSc.),	University of Twente, daily supervisor
	W. Chen, (MSc.),	University of Twente, daily supervisor

UNIVERSITY OF TWENTE.

Preface

This report is my thesis for the Master of Science in Civil Engineering and Management at the Water Engineering and Management department at the University of Twente. The project was interesting to work on due to the diversity of the subject and broad applicability of numerical modelling and data analysis. I worked on the thesis between September 2020 and April 2021 under supervision of Vera van Bergeijk, Weiqiu Chen, Jord Warmink, Juan Pablo Aguilar-López and Suzanne Hulscher.

My special thanks go to Vera van Bergeijk and Weiqiu Chen for their valuable feedback and guidance during the project. Their input and knowledge have significantly increased the quality of this thesis and were of great importance. I would like to thank Jord Warmink, Juan Pablo Aguilar-López and Suzanne Hulscher for their supervision and valuable input, helping me to narrow down the research.

I would also like to express my gratitude towards Mark Klein Breteler from Deltares, for supplying me with all the necessary data from the delta flume experiments, for analysis and creation of the OpenFOAM model.

N. G. Bijen
April 2021

Summary

New flood standards came into effect recently whereby the design water level reached above the hard revetment of outer slopes of many sea dikes. Consequently, the grass revetment on the dike slope is subject to wave impact and wave run-up erosion whereby it is not known which erosion process is dominant. Scale tests are performed in the delta flume at Deltares in order to test the erosion resistance of the sea dikes along the Wadden Sea coast with the new flood standards. The erosion resistance of different grass and clay qualities are tested to provide insights into the effect of the cover layer quality on erosion rate. The objective of this study is to determine how grass covers on the outer dike slope erode and which hydraulic variables can be used to predict the erosion. This study is divided into three parts: (1) analysis of erosion data from the delta flume experiment, (2) creating a hydrodynamic model in OpenFOAM to simulate a dike from the delta flume experiments with and without grass cover erosion, and (3) computing the erosion using the OpenFOAM model results.

In the first part of this study, elevation data of a laser scanner measuring grass revetment profile changes after each delta flume test were analysed and the maximum erosion depth and erosion volume was determined. The results showed that the grass cover eroded three times faster when the grass is dried out compared to normal grass. Therefore, it is suggested that the effect of dry summers, especially in the wake of expected climate change, are considered in the design of dikes with grass covers. The analysis on clay erosion showed that the higher quality clay contributed to a roughly 35% increase in erosion resistance compared to low quality clay. However, the clay quality did not seem to have a significant effect on the erosion of the grass cover.

In the second part of the study, an OpenFOAM model was created and validated to describe the effect of an erosion profile on simulated hydraulic load. The model results showed that the hydraulic load on the eroded grass revetment profile is generally lower than on the initial profile. The lower half of the eroded grass revetment profile is mostly sheltered by the, not erodible, hard revetment slope, experiencing little hydraulic loading. However, a cliff is present towards the end of the grass revetment surface, which endures high dynamic pressures, flow velocities and shear stresses. Although the dynamic pressures at the cliff in the eroded profile are not higher than on the dike without erosion, the velocities and shear stresses are significantly larger.

For the third part, results of the OpenFOAM model were used to compute the erosion that occurred in the experiment. Several empirical relations describing wave impact and wave run-up erosion were used and calibrated. The results show that wave impact relations using dynamic pressures and wave run-up relations using flow velocities are both capable of describing the erosion depth of the grass revetment, which is mostly situated above the wave impact zone. However, dynamic pressures show to be the most accurate when replicating the erosion profile measured in the delta flume experiments. Additionally, a head cut erosion model was used to compute the cliff erosion using the flow velocities and the water layer thickness on the grass revetment.

To conclude; grass and clay quality have a major influence on the erosion rate of a grass revetment cover layer on the outer dike slope. The distribution of hydraulic variables on the grass revetment slope changes significantly when the grass revetment cover layer has eroded. Dynamic pressures can best be used for determining the erosion volume and the erosion depth, combined with a head cut erosion model to compute the erosion of significantly eroded cover layers.

List of figures

List of tables

List of symbols

The symbols used in this report as summarized below:

- A = Head cut advance rate load parameter [m/s$^{1/3}$]
- A = Empirical coefficient depending on grass quality [-]
- A_0 = Head cut advance rate threshold parameter [m/s$^{1/3}$]
- B = width of dike berm [m]
- C = Head cut advance rate coefficient [s$^{-2/3}$]
- C_E = Strength parameter [m^{-1}/s^{-1}]
- c_s = Clay cohesion [kN/m^2]
- $c_{v2\%}$ = Coefficient depending on dike slope [-]
- $c_{\%}$ = Weight percentage of clay in the soil [%]
- D = Empirical coefficient depending on grass quality [-]
- d = Depth under surface [cm]
- d = Grain size [mm]
- d_{cor} = Empirical coefficient depending on grass quality [-]
- d_i = Erosion depth resulting from a single wave breaker impact [m]
- dX/dt = Head cut advance [m/h]
- E = Erosion mass per unit area of the bed [kg]
- E_{soil} = Soil parameter [m/s]
- g = Acceleration due to gravity [m/s^2]
- H = Cliff height [m]
- H_s = Significant wave height [m]
- h = Water layer thickness [m]
- h_i = Water layer thickness at the ith node [m]
- J_s = Head cut soil material parameter [-]
- K_b = Particle size number [-]
- K_d = Interparticle bond strength [-]
- K_h = Head cut sediment parameter [-]
- k_{dp} = Detachability coefficient clay erosion amount [m^3/Pa]
- k_{dpi} = Erodibility coefficient clay erosion depth [m^3/Pa]
- k_{dgp} = Detachability coefficient grass cover erosion amount [m^3/Pa]
- k_{dgpi} = Erodibility coefficient grass cover erosion depth [m^3/Pa]
- L_{Berm} = total effective length of the berm [m]
- M = Sediment parameter erosion depth [kg/(m^{2}s)]
- M_s = Material strength number [-]
- $M2$ = Sediment parameter erosion volume [kg/(m^{2}s)]
- m = Mass of the sediment on the bed [kg/m^2]
- n = Amount of data points [-]
- p_i = Impact pressure at ith node [N/m^2]
- P_{max} = Maximum impact pressure [kPa]
- $p_{max,2\%}$ = 2% boundary impact pressures [Pa]
- $R_{d,p}$ = Volume of soil eroded after a single impact event [cm^3]
- $R_{\text{u2\%}}$ = Run-up height exceeded by 2% of the incomming waves [m]
- R^2 = Coefficient of determination [-]
- $RMSE$ = Root Mean Square Error [-]
- RVR = Root Volume Ratio [%]

- r_B = influence of the berm width [-]
- r_{db} = vertical difference between the SWL and middle of the berm [-]
- r_0 = Turbulence intensity [m/s]
- t = Time [s]
- T = Wave period [s]
- U_c = Critical flow velocity [m/s]
- U_0 = Depth averaged flow velocity [m/s]
- $v_{\mathrm{A},2\%}$ = Run-up flow velocity exceeded by 2% of the incomming waves [m/s]
- w = Damping coefficient [-]
- wc = Clay water content [-]
- $\bar{y}$ = Mean of the measured data [-]
- γ_b = influence factor for berm [-]
- γ_f = Influence factor for roughness elements on a slope [-]
- y_i = Measured data [-]
- $\hat{y}_i$ = Computed value [-]
- y_m = Erosion depth [m]
- γ_β = Influence factor for oblique wave attack [-]
- z_A = Difference between SWL and height measuring point [m]
- α = Angle of the dike [deg]
- Δd = Difference in erosion depth [m]
- Δt = Difference in time [s]
- ξ_d = Iribarren number [-]
- ρ_{cw} = Density of the clay-water mixtures [kg/m^3]
- ρ_s = Density of soil [kg/m^3]
- ρ_w = Water density [kg/m^3]
- σ_g = Grass cohesion [kN/m^2]
- τ_c = Critical bed shear stress [m^2/s^2]
- τ_0 = Bed shear stress [m^2/s^2]
- ϕ'_{r} = Friction angle [-]

Table of Contents

1 Introduction

1.1 Relevance of research

This document describes the analysis of grass cover erosion in the run-up zone of sea dikes using data from delta flume experiments and an OpenFOAM model. Coastal defences such as sea dikes need to be improved to account for the effect of climate change such as sea level rise and drought (Neumann et al., 2015).

Countries will need to adapt to the changing climate, requiring large investments to retain a sufficiently protected coastline. The Netherlands recently adopted a new flood safety standard for the Dutch primary flood defences. Consequently, over 1.000 km of dikes along the Dutch coastline have been rejected due to the new standards. Necessary dike reinforcements will cost approximately 7.3 billion euros (HWBP, 2020). The Dutch Flood Protection Program (Hoog Water Beschermings Programma, HWBP) which is an alliance consisting of Dutch water authorities and Rijkswaterstaat, is tasked with the reinforcement of the Dutch water defences. The water boards have already decided on several dike reinforcements projects which require the asphalt revetment to be extended to the crest of dikes at the Wadden Sea (Klein Breteler, 2020). These conventional hard structures are expensive and do not contribute to nature or a diverse landscape.

Figure 1-1 shows the different layers of a sea dike with the grass revetment which is a dike cover consisting of a grass cover layer and a clay layer. The grass cover in Figure 1-1 is classified as the first 20 cm from the surface which consists of a mixture between clay and grass roots. The clay layer below the grass cover contains few roots and has a thickness of approximately 130 cm. Dutch dikes generally consist of a sand core, which is referred to as the core material in Figure 1-1. The sand core will erode quickly when the cover layer has been eroded. Furthermore, current regulations in the Statutory Assessment Instruments (Wettelijk Beoordelingsinstrumentarium, WBI) prescribe that a dike with a grass revetment fails when an erosion depth of 20 cm has been reached (erosion of the grass cover layer in Figure 1-1).

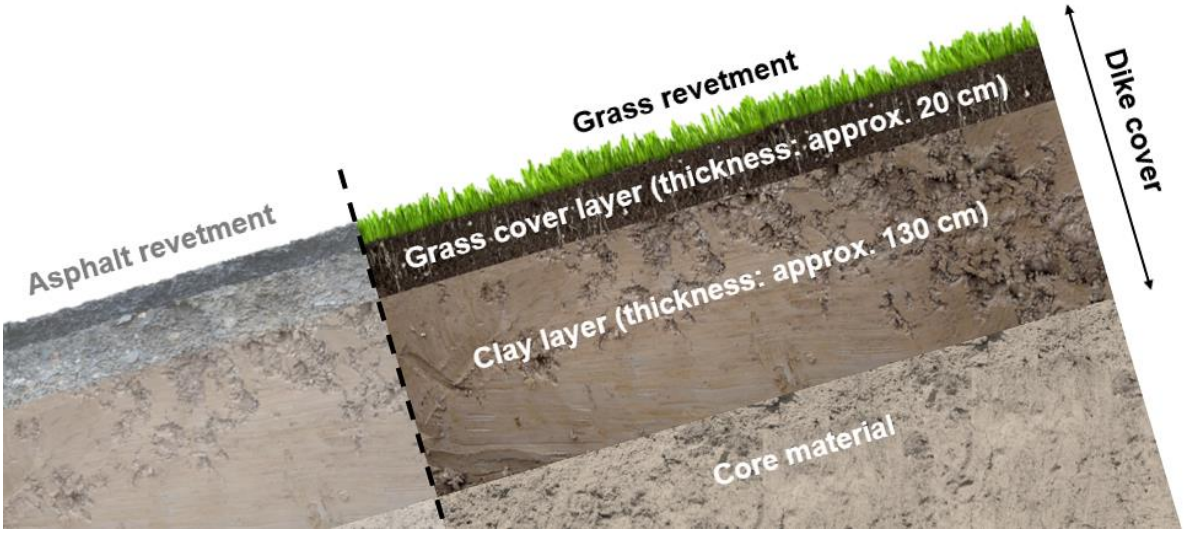

Figure 1-1 Dike slope with asphalt and grass revetment, a clay layer and a sand core (core material), different layers of the dike and the grass cover thickness are highlighted.

However, the dike can likely sustain significantly more damage until the dike has fully eroded (Klein Breteler, 2020; Van Bergeijk et al., 2021). It is yet unknown how much more erosion the dike can sustain before absolute failure of the dike occurs, as well as the rate of erosion of the grass revetment on the seaward outer slope of the dike. In addition, the storm surge water level for several dikes at the Wadden Sea is around the transition from the hard revetment to grass cover, possibly subjected to wave impact and wave run-up flow. However, it is unclear how much influence wave impact has on erosion in combination with wave run-up.

1.2 Problem definition

Grass revetment on the seaside slope of dikes at the Wadden Sea provides insufficient flood protection according to new safety standards from the WBI-2017 assessment. Erosion of the grass revetment under design storm conditions becomes larger than the allowed erosion given by the new, stricter regulations, resulting in failure of the dike. The projected increase in sea water level causes the Still Water Level (SWL) to be above the transition from hard to grass revetment on the outer dike slope. Therefore, the grass revetment may be eroded by wave impact load and wave run-up which was previously not the case. Consequently, the increase in SWL makes it unclear whether erosion of the grass revetment is caused by wave run-up, wave impact or both.

Several dikes located at the Wadden Sea have been reproduced in the delta flume at Deltares in order to test the erosion resistance of the grass revetment on the outer slope of sea dikes. The reconstructed dikes have been subjected to design storm conditions for many hours to determine the erosion resistance of grass revetment and clay layers. Although the experiments give insights into the total amount of erosion for every test (dependent on the duration of each experiment), these experiments do not supply information about what the erosion is caused by. Further investigation is required because the grass revetment in the delta flume experiments start below the SWL and therefore it is suspected that erosion is caused by wave run-up and wave impact. Because dikes are deemed to be failing after 20 cm of grass and clay revetment has been eroded, it is unclear what the effect is of a largely eroded dike profile on impact pressures and wave run-up and subsequently erosion. Lastly, it is not defined what hydraulic variables and processes are dominant in determining erosion for grass revetment dike covers and what the effect of an eroded grass revetment slope is on determining erosion.

1.3 Research objective

The objective of this study is to determine how outer dike slope grass covers erode and what hydraulic variables can be used to predict the erosion of the grass revetment on the seaside slope of the dike. Firstly, the amount of erosion is determined by analysing the FARO3D laser scanner data of the eroded dike profiles after every test, which is scaled for the duration of the tests. Secondly, two tests of the first experiment from the delta flume experiments at Deltares will be simulated in a 2DV numerical model using OpenFOAM. The results will be used to calculate the amount of erosion during the first 600 s of the test. The measured erosion volume and erosion depth for the first 600 s of each test is compared to simulated data from the OpenFOAM model of Lauwersmeerdijk-Vierhuizengat. Consequently, the computed erosion volumes from the numerical model were used to obtain a relation between the erosion rate and hydraulic load. The main research question is:

"How does the grass revetment on the seaside slope of a dike erode and what influences the erosion process and the erosion rate?"

The following sub-questions give direction to the answer to the main research question.

1. *How is the dynamics of the grass cover and clay layer erosion in the delta flume experiments affected by the clay and grass quality?*
2. *How does an eroded dike profile affect the simulated dynamic pressures and run-up velocities in the OpenFOAM model?*
3. *How accurately can the erosion as a result of wave run-up, wave impact and head cut be predicted using the existing empirical equations and OpenFOAM model results?*
4. *For which part of the dike slope can wave impact be used to predict erosion and for what part of the dike slope are wave run-up or head cut erosion models applicable?*

The research activities are summarized in the flowchart in Figure 1-2 summarizing the steps taken to answer the main and sub research questions. The document can be classified in 4 objectives (P1 – P4 in Figure 1-2) where:

- The first objective (P1) is to obtain the erosion volume and erosion depth from the delta flume experiments and to determine the effect of clay and grass quality on erosion rate. The erosion data were obtained from interpolated elevation profiles which were measured with a FARO3D laser scanner after each delta flume test.
- The second objective (P2) is to adapt an OpenFOAM model to simulate a part of the experiments analysed in part 1. The OpenFOAM model consists of geometry that is implemented as a mesh with boundary conditions and wave generation to create the same waves as in the experiments. The main objective is to investigate the effect of erosion on wave loads by constructing two models of a dike, with and without erosion.
- The third objective (P3) is to determine what hydraulic variables obtained from the OpenFOAM simulation can, in combination with empirical erosion relations, be used to compute the erosion that occurred during the delta flume experiments. Several erosion relations will be calibrated to obtain the best fit between the data from the experiment and the erosion using simulated hydraulic variables.
- The fourth objective (P4) is to determine what erosion relations can best be used to compute the erosion depth and volume, and to quantify what part of the dike slope experiences wave impact, wave run-up and/or head cut erosion. The accuracy of the calibrated relations will be determined using coefficient of determination (R^2) and Root Mean Square Error (RMSE) to determine which hydraulic variables can best be used to predict erosion.

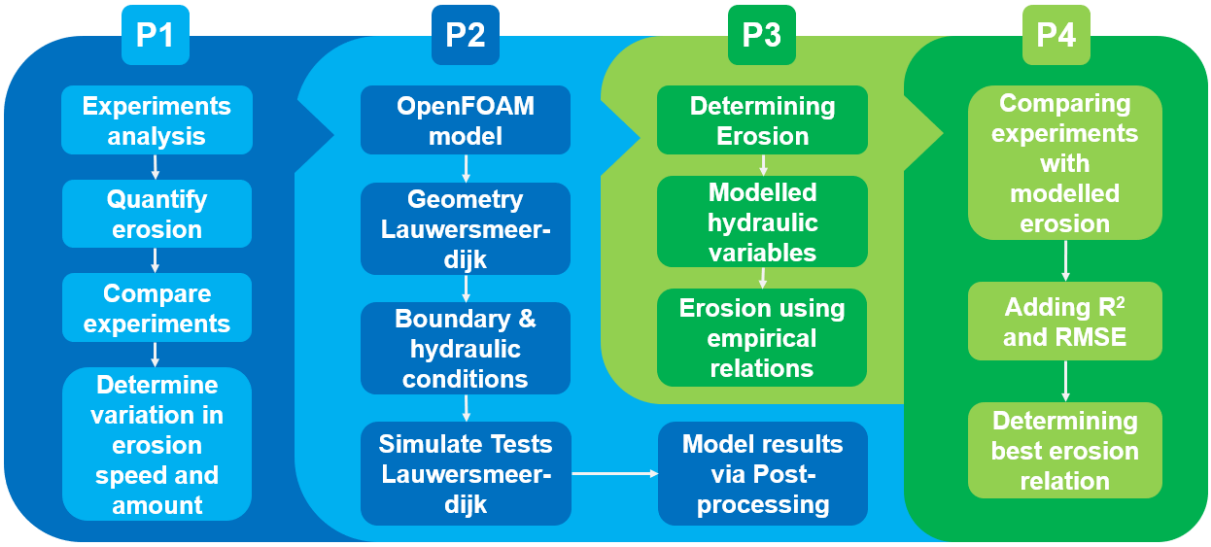

Figure 1-2 Flowchart of research steps taken to answer the main research question, referred to as P1 – P4.

1.4 Report outline

The report is structured as follows:

Chapter 2	**Background**	The following subjects will be introduced in this chapter, outlining the subjects in this research: experiment set-up, clay (block) properties, grass cover erosion and the numerical model.
Chapter 3	**Methodology**	The data analysis on the 3D laser of the delta flume experiments, OpenFOAM model set-up, validation and the model results will be described in this chapter. Lastly, the method for calibrating erosion relations used for computing erosion with the OpenFOAM simulation data will be described.
Chapter 4	**Results**	This chapter provides the results used for answering the research questions. The research steps and activities as described in the methodology were used to derive the results.
Chapter 5	**Discussion**	In this chapter the meaning and significance of the results will be discussed as well as the applicability and limitations of the research findings.
Chapter 6	**Conclusion**	In this final chapter each sub-research question is answered followed by the conclusion of the main research question. The conclusion also provides recommendations for further research.

2 Background

In The Netherlands most dikes have hard revetment on the seaside slope of sea dikes with grass revetment on the upper part and crest of the dike. With the new regulations following the WBI-2017, most of the sea dikes do not comply. This means that the risk of failure is too high based on the predicted grass cover erosion during extreme storm events.

There are two types of failure mechanisms for describing the erosion of the outer slope of a dike described by Van Hoven (2015). The first failure mechanism is the 'grass revetment sliding off outside cover' (GABU). This occurs when the internal water pressure in the dike is higher than the outside pressure on the dike plus the weight and cohesive forces of the outer clay layer itself, as illustrated in the right picture of Figure 2-1. Part of the clay layer can then 'press up' and break loose from the top layer which can occur in combination with shearing of the clay layer shown in the left picture of Figure 2-1. Shearing of the clay layer can occur with a steep seaside slope of the dike or with low quality of clay in the top layer leading to erosion more quickly. The clay gets mobilized and slides downward where the clay slab likely breaks out at the lowest point of the wave (Van Hoven, 2015). This exposes the sand core from the point of the tear to the top of the clay slab with erosion as a consequence which leads to failure of the dike over time. The clay slab break out is illustrated by the tear in the clay layer and press up at the wave trough in the left picture of Figure 2-1.

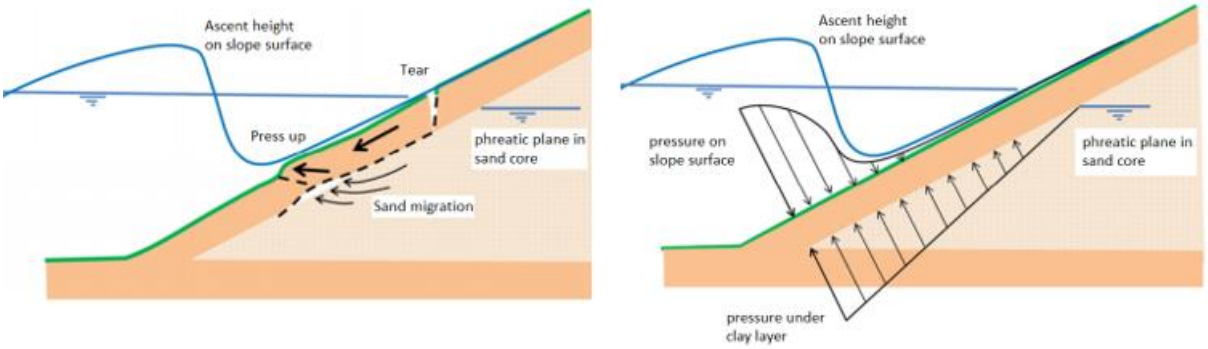

Figure 2-1 Pressing up and shearing of clay layer due to wave attack and forces on dike when wave impacts dike outer slope (after: Hoven, 2015).

The second failure mechanism is outer dike slope failure method, also described by Van Hoven (2015), which is the erosion of the top layer and grass revetment of the dike, 'Gras Erosie BUitentalud' (GEBU). The GEBU failure mechanism occurs in two ways: (1) by wave impact load and (2) by wave run-up. The wave impact on the dike results in a short period of high water pressures on the slope which can damage the grass sods with pressure gradients pushing the grass sods in inward and sideward directions. The wave run-up on the dike causes friction between the water layer and grass revetment, causing erosion.

As mentioned, failure of the dike occurs when 20 cm of the cover layer is eroded (Van Hoven, 2015). However, the actual failure probability is likely much lower because the underlying clay layer can aid significantly in erosion resistance of the dike. The hydraulic load during design storm events can result in significant damage of grass cover. However, it is not defined when the erosion of the grass cover results into failure. Before the dike fails, the clay layer has to be eroded as well as a part of the sand core, after which the crest of the dike gets eroded, lowers, and finally results into collapse of the dike (Van Hoven, 2015). Because erosion due to wave impact only occurs between the water level and half the significant wave

height below the water level, it is unlikely that complete failure occurs during heavy storm events due to wave attack only. Therefore, experiments were conducted in the Delta flume at Deltares to gain knowledge about dike erosion during extreme storm events to determine new design methodology for sea dikes.

2.1 Dike locations

For the delta flume experiments, two dikes in northern Friesland were chosen. These locations are shown in Figure 2-2 as the Koehool-Lauwersmeerdijk (blue) and the Lauwersmeerdijk-Vierhuizengat (green). Further specifications of the experiments are found in the methodology (Chapter 3).

Figure 2-2 Locations Lauwersmeerdijk-Vierhuizengat (green) and Koehool-Lauwersmeerdijk (blue) in Friesland (The Netherlands) (after: Klein Breteler, 2020).

These two dike locations have been chosen because they are up for renovation and following WBI-2017, the hard revetment needs to be extended to the crest which will cost millions of euros (Klein Breteler, 2020). The experiments were conducted to determine the waterside slope erosion of the grass revetment. Erosion on the crest and erosion at the landward slope due to overtopping, will not be measured.

2.2 Outline delta flume experiments by Deltares

A total of 6 experiments were conducted by Deltares and tested dikes were recreated in the delta flume at Deltares on a 1:1 scale. The delta flume at Deltares is 300 m long, 9.5 m deep and 5 m wide (Deltares, 2020). The wave paddle in the flume can generate waves with a maximum height of 4.5 m and a maximum significant wave height of 2 m (Deltares, 2020).

The results from the experiments can be used to create new design standards for Dutch sea dikes including the Koehool-Lauwersmeerdijk and Lauwersmeerdijk-Vierhuizengat as tested in the delta flume. New design standards are required because the current standards possibly lead to conservative estimates and therefore lead to unnecessary investments.

The waves created in the flume have a significant wave height of $H_s = 2$ m and a wave period of $T = 5.5$ s. Consequently, the wave length can be computed as follows: $\lambda = \frac{gT^2}{2\pi} = \frac{9.81 \times 5.5^2}{2\pi} = 47.23\ m$. However, the exact conditions vary slightly from test to test. Wave impact erosion occurs when plunging breakers are present, which is proved as follows: the outer dike has a slope of 1:4, the Iribarren number can then be calculated as $\xi_d = \frac{\tan(\alpha)}{\sqrt{H_s/\lambda}} = \frac{\tan(14.04)}{\sqrt{2/47.23}} \approx 1.22\ [-]$. The waves in the Wadden Sea during storm conditions with an Iribarren number of 1.22 can then be classified as having plunging breakers (Table 2-1).

Dike slope 1:n	Plunging breaker	Collapsing breaker	Surging breaker
1:6	$\xi_d < 2.1$	$2.1 < \xi_d < 2.8$	$\xi_d > 2.8$
1:4	$\xi_d < 2.4$	$2.4 < \xi_d < 3.1$	$\xi_d > 3.1$
1:3	$\xi_d < 2.6$	$2.6 < \xi_d < 3.3$	$\xi_d > 3.3$
mean	$\xi_d < 2.3$	$2.3 < \xi_d < 3.0$	$\xi_d > 3.0$

Table 2-1 Classification of breaking types on sea dikes (after: Stanczak et al., 2008).

The erosion during the storm mainly occurs at the maximum water level of approximately 6.5 m above the bottom of the flume, because the grass revetment starts at a height of around 6.4 m above the bottom of the flume for the Lauwersmeerdijk-Vierhuizengat and 6.5 m above the bottom of the flume for the Koehool-Lauwersmeerdijk. The maximum duration of wave load when two extremely high water levels occur is 8 h (Klein Breteler, 2021).

2.2.1 In-situ clay blocks

To recreate the dikes, grass blocks from in-situ locations were used containing clay with poor quality from the Lauwersmeerdijk-Vierhuizengat, clay with good quality from the Koehool-Lauwersmeerdijk at Holwerd and clay with good quality from the Koehool-Lauwersmeerdijk from Blija (Friesland). The grass blocks were extracted using steel moulds with a size of 2x2 m^2 and a thickness of around 0.8 m as shown in Figure 2-3. Using clay from in-situ location guarantees accurate test results. In the experiments two clay layers were used to create sufficient thickness where 15 -20 cm of the grass cover were removed from the bottom clay block.

Figure 2-3 Clay blocks with grass and steel moulds as used in the Deltares delta flume experiments.

The clay is taken from the in-situ locations to represent a clay layer that is restructured in the years after construction of the dike. This means that shrink-cracks in the clay layer have formed because of weather influences and the change in the seasons. The tears cause weak spots in the clay layer influencing the erosion speed and were accurately represented when using in-situ clay blocks (Klein-Breteler, 2020). The clay blocks were watered for half an hour each day at Deltares, with exceptions for rainy days and in the weekend, slightly increasing the water content. The grass is mowed to a height of 4 – 6 cm before the experiment. The clay layer rests on 15 cm of sand cement and is held in place by wooden planks. Empty spaces were filled in with sand to allow for quick rebuilding of the different dike set-ups. The total width of the flume is 5 m.

The experiments take climate change with increasing summer drought into account by placing blocks with dry grass in the model set-up for experiment 5. The grass blocks were deprived of water until the blocks were dried out, after which the blocks will be watered for a month. The drying of the grass blocks is also visible in the blocks in the white tent in Figure 2-3.

2.2.2 Delta flume experiments set-up

The 6 experiments conducted in the delta flume at Deltares are classified as experiments K1 – K6. Experiment K2 had an extremely low erosion rate. Therefore, it was split into experiments K2 and K3 where the set-up of K3 was the same as that of K2, except that the berm in K3 was lowered. Experiment K5 was also split into experiment K5 and K6. The berm in experiment K6 was removed after an erosion depth of 0.5 m was measured (Klein Breteler, 2021). Summary of the experiments conducted in the Deltares delta flume including the number of tests and clay are found in Table 2-2.

Experiment	Tests	Profile	slope	Clay origin
K1	K101 – K114	Lauwersmeerdijk-Vierhuizengat	1:4	Lauwersmeerdijk
K2	K201 – K208	Koehool-Lauwersmeerdijk	1:5	Holwerd
K3	K301 – K3_10	Koehool-Lauwersmeerdijk (lowered berm)	1:5	Holwerd
K4	K4_01 – K4_17	Lauwersmeerdijk-Vierhuizengat	1:4	Blija
K5	K5_01 – K5_06	2 blocks with dry grass	1:5	Holwerd
K6	K6_01 – K6_10	No berm, 2 blocks with dry grass	1:5	Holwerd

Table 2-2 The different experiments conducted in the Deltares delta flume.

Three types of clay were used in the 6 delta flume experiments, the characteristics of the clays is given in Table 2-3:

Clay origin	Lutum	Sand
Lauwersmeerdijk	24%	40%
Holwerd	25%	31%
Blija	44%	14%

Table 2-3 Characteristics of the different clay types from the delta flume experiments (Klein Breteler, 2020).

2.2.3 Lauwersmeerdijk-Vierhuizengat test set-up

The profile experiment K1 and experiment K4, which used the Lauwersmeerdijk-Vierhuizengat profile is schematized in Figure 2-4. Figure 2-4 shows the water depth of 6.5 m in the flume, height of the transition between hard and grass revetment at 6.4 m, as well as different slopes of the waterside slope. In this report the bottom of the flume is used as the reference height of the dikes, not NAP, since the bottom of the delta flume is also the bottom

of the dike set-up. Therefore, the most important parameters are the height of transition from the bottom of the flume (6.4 m), the water depth (6.5 m), the slope used for the hard revetment and the slope of the grass revetment (1:4).

The profile used in the experiments is slightly altered from the real dike to facilitate rapid rebuilding for multiple experiment set-ups. The bottom slope has been altered from 1:4.4 to 1:4 and the berm at the bottom of the dike has been removed because the berm does not alter the water movement near the experiment set up (Klein Breteler, 2020). The slope at the toe of the dike has also been increased to reduce the size of the dike since it does not influence the water movement near the dike.

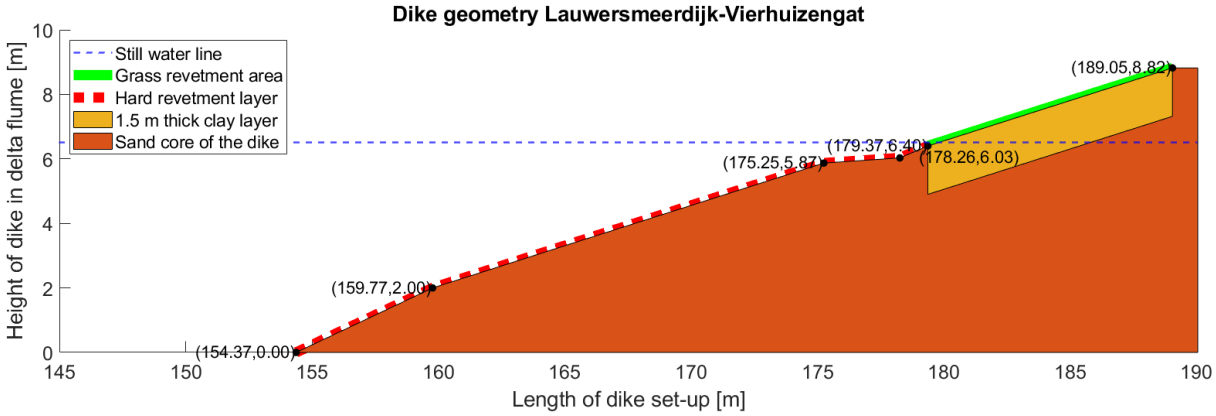

Figure 2-4 Cross-section of Lauwersmeerdijk-Vierhuizengat set up for experiments K1 & K4 at Deltares (adapted from Klein Breteler, 2020).

2.2.4 Koehool-Lauwersmeerdijk test set-up

The dike profile of the Koehool-Lauwersmeerdijk is used for experiments K2 - K3 and experiments K5 – K6. A different dike set-up is used with a dike slope of 1/5 and the height of the transition is at 7.15 m from the bottom of the flume, as shown in Figure 2-5.

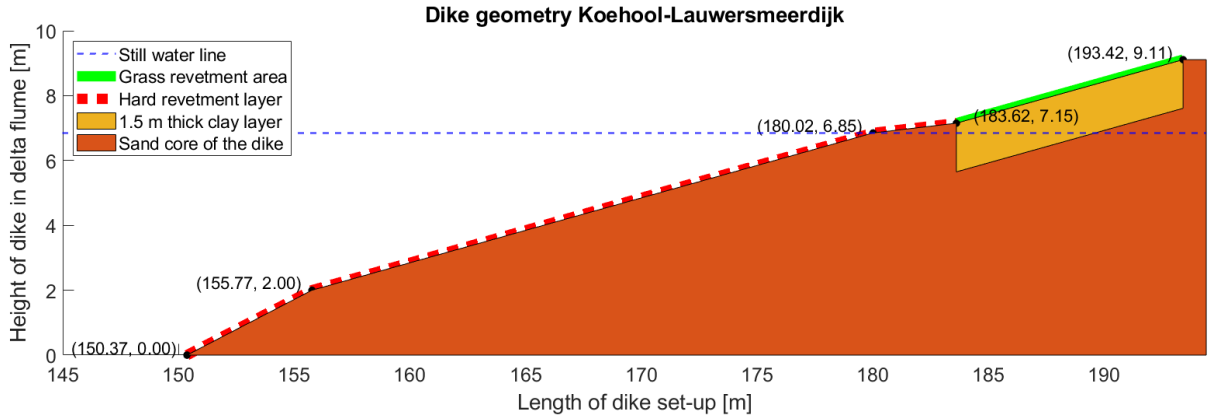

Figure 2-5 Cross-section of Koehool-Lauwersmeerdijk set-up for experiments K2 and K3, variation of this set-up is used for experiments K5 and K6 at Deltares (adapted from Klein Breteler, 2020).

2.3 Impact pressure

The impact pressures can be used for determining wave impact erosion and modelled impact pressures can be validated against exceedance values. The empirical 2%, 5% and 10% exceedance values of the maximum pressure can be determined using the relation found in Peters (2017) and Horstman (2020). Peters (2017) described the dimensionless impact

pressure value ($\frac{p_{max,2\%}}{\rho_w g H_s}$) for the lower boundary of the top 2% impact pressure values and is given below:

$$\frac{p_{max,2\%}}{\rho_w g H_s} = 8 - 1.6\xi_d - \frac{2}{(\xi_d - 0.2)^2} \tag{2.1}$$

In which:

- $p_{max,2\%}$ = 2% boundary impact pressures [Pa];
- ρ_w = Water density [kg/m^3];
- ξ_d = Iribarren number [-];
- H_s = Significant wave height [m];
- g = Acceleration due to gravity [m/s^2].

Secondly, the relations found in Horstman (2020) will also be used to validate the pressures and can be used on the 2%, 5% and 10% of the exceedance values.

$$\frac{P_{2\%,max}}{\rho_w g H_s} = 14.28 \tan(\alpha) - 0.36 \tag{2.2}$$

$$\frac{P_{10\%,max}}{\rho_w g H_s} = 5.18 \tan(\alpha) + 0.33 \tag{2.3}$$

$$\frac{P_{5\%,max}}{\rho_w g H_s} = 2.24 \tan(\alpha) + 0.44 \tag{2.4}$$

In which α is the angle of the dike slope and $P_{n\%,max}$ is the maximum impact pressure, referred to percentage of waves that exceed this value. The n% highest pressures can be used for validation of the dynamic pressures using the highest pressure of each wave measured at the dike surface.

2.4 Wave run-up

The 2% exceedance flow velocity of wave run-up can be computed as described in the EurOtop overtopping manual (2018):

$$v_{\mathrm{A},2\%} = c_{v2\%}\left(g(R_{\mathrm{u}2\%} - z_A)\right)^{0.5} \tag{2.5}$$

Where:

- $v_{\mathrm{A},2\%}$ = Run-up flow velocity exceeded by 2% of the incomming waves [m/s];
- z_A = Difference between SWL and height measuring point [m];
- $c_{v2\%}$ = Coefficient which is 1.4 for dikes with a slope of 1:4 (EurOtop overtopping manual, 2018) [-];
- $R_{\mathrm{u}2\%}$ = Run-up height exceeded by 2% of the incomming waves [m].

The run-up height is calculated using the following expression for the relatively gentle dike slope as obtained from the EurOtop overtopping manual (2018):

$$R_{u2\%} = 1.65 \times \gamma_b \times \gamma_f \times \gamma_\beta \times \xi_d \times H_s \tag{2.6}$$

With a maximum of:

$$R_{u2\%} = 1.0 \cdot \gamma_f \cdot \gamma_\beta \left(4 - \frac{1.5}{\sqrt{\gamma_b \cdot \xi_d}}\right) \times H_s \quad (2.7)$$

Where:

- γ_f = Influence factor for roughness elements on a slope [-];
- γ_β = Influence factor for oblique wave attack [-];
- γ_b = influence factor for berm [-].

The berm influence factor is determined as follows (EurOtop, 2018):

$$\gamma_b = 1 - r_B(1 - r_{db}) \quad 0.6 \leq \gamma_b \leq 1.0 \quad (2.8)$$

With:

$$r_{db} = 0.5 - 0.5 \times \cos\left(\pi \frac{d_b}{2 \times H_s}\right) \text{ for a berm below still water line} \quad (2.9)$$

And:

$$r_B = \frac{B}{L_{Berm}} \quad (2.10)$$

Where L_{Berm} is the total effective length of the berm, B the width of the berm, r_{db} stands for the vertical difference d_b between the SWL and middle of the berm and r_B stands for the influence of the berm width.

2.5 Erosion calculation models

2.5.1 Grass cover thickness

The erosion of the grass cover layer (Figure 1-1) is strongly related to the physical properties of the grass (Stanczak et al., 2008). For the typical structure of the grass cover layer that is used in sea-dikes, the following properties relating to the vertical succession of the root system and consequently the erosion resistance can be classified as follows (TAW, 1999):

- The upper layer, which is called stubble, has a thickness of up to 3.5 cm and consists of loose soil and plant remains. This layer is washed away within short time by waves;
- Below the upper layer is the soil closely rooted, this layer erodes slowly and has a thickness of 0.5 - 5 cm;
- The lower part of the grass cover layer where the number of roots is considerably smaller, has a thickness of 5 -10 cm. In the clay layer below the grass cover layer (Figure 1-1) the number of roots decreases significantly, which results in the reinforcement properties of the soil becoming almost negligible.

The total thickness of the grass cover layer is between 9 and 18.5 cm and is eroded by impact pressures from plunging breakers hitting the dike slope and run-up and run-down of waves. In this report, the thickness of the grass cover layer is assumed to be 20 cm, the erosion depth required for failure following WBI (2017) and Klein Breteler (2020).

2.5.2 Erosion depth caused by wave impact pressures

The wave impact erosion depth is obtained via the impact pressure and water depth at the probing locations on the outer dike slope. First, the erosion depth due to wave impact is described for the grass revetment and subsequently the clay layer below.

Erosion depth as a function of impact pressure and the detachability coefficient can be determined using the following expression which can be used for the grass cover and the clay layer using different detachability coefficients (Stanczak et al., 2007).

$$d_i = k_{dpi} \times p_i \times e^{-wh_i} \tag{2.11}$$

In which:

- d_i = Depth of erosion at i[th] node resulting from a single wave breaker impact [m];
- k_{dpi} = Soil detachability coefficient for a unit area calculated at the i[th] node [m^3/N];
- p_i = Impact pressure at i[th] node [N/m^2];
- w = Coefficient representing the damping effectiveness of a water layer [-];
- h_i = Water layer thickness at the i[th] node [m].

The clay empirical detachability coefficient depends on the type of clay and on the water content. For clay of the erosion resistance Category 1 according to Dutch requirements (TAW, 1996), the erodibility coefficient $k_{d,i}$ in [m^3/Pa] can be calculated using the following function of the water content wc that was derived by Husrin (2007):

$$k_{di} = 0.35 \times \arctan\left[110 - (wc - 0.434)\right] \times 10^{-12} \tag{2.12}$$

In the top layer of the clay cover, the soil is reinforced with grass roots. The modified erodibility coefficient $k_{d,g,p,i}$ for the grass revetment in [cm^3] is a function of the dimensionless parameter b that describes the influence of the roots on the erodibility and the Root Volume Ratio (RVR) which can be determined using the following expression:

$$k_{dgpi} = \frac{k_{dpi}}{b \times RVR_i^2} \tag{2.13}$$

The RVR [%] can be calculated as function of the depth under the grass surface. Two models that describe the distribution of the RVR underneath the soil surface are available (Sprangers, 1999 and Stanczak et al., 2007).

$$RVR = A \times D^{(d - d_{cor})} \tag{2.14}$$

Where A, D, and d_{cor} are empirical coefficients that depend on the quality of the grass cover and d is the depth under the surface in centimeters. The coefficients A and D should have a negative correlation with clay quality since stronger clay prevents the grow of a dense root network (Stanczak et al., 2008). Coefficients suggested by Sprangers (1999) and Stanczak et al. (2007) are shown in Table 2-4.

A	D	d_{cor}	b	Reference
2.67	0.8	1.5	-	Sprangers (1999)
1.58	0.75	2.0	5	Stanczak et al. (2007)

Table 2-4 Coefficients describing the grass roots distribution and their effects on soil erodibility (Stanczak et al., 2008).

The erodibility parameter for the whole revetment $k_{d,t,p,i}$ can then be calculated using the following expression:

$$k_{d,t,p,i} = \frac{k_{d,p,i}}{b \times RVR^2} \quad for \quad d < d_{crit}$$

$$k_{d,t,p,i} = k_{d,p,i} \quad for \quad d > d_{crit} \tag{2.15}$$

Where d_{crit} is the thickness of the grass revetment layer which is likely between 90 and 185 mm thick.

2.5.3 Erosion volume caused by wave impact pressures

The amount of erosion that occurs due to the impact of a single wave can be derived from an empirical relation from Woolhiser et al. (1990) which is similar to 'splash erosion' and specified for clay with no significant pull-cracks. Pull-cracks usually occur when the soil contracts or shrinks and are differently orientated depending on the size of the crack. Larger pull-cracks (up to 1 m) are almost always vertical and begin directly at the dike surface, while smaller cracks (up to 20 cm) can occur anywhere in the clay layer in all directions (Stanczak et al., 2008). Shear cracks occur in all directions and are usually formed in shear areas and are smaller (up to 20 cm) and are caused by swelling of the clay layer. For clay layers without significant cracks the empirical formula (Stanczak et al., 2007) for determining erosion reads:

$$R_{d,p} = k_{d,p} \times p_{max} \times e^{-wh} \tag{2.16}$$

In which:

- $R_{d,p}$ = The volume of soil eroded after a single impact event [cm^3];
- $k_{d,p}$ = The empirical detachability coefficient [cm^3/kPa];
- P_{max} = Maximum impact pressure [kPa];
- w = The empirical coefficient describing the effectiveness of a water layer [-];
- h = The water layer thickness [m].

The values of the empirical detachability parameter and the empirical coefficient describing the effectiveness of a water layer were calibrated and given in Table 2-5.

Type of soil	$k_{d,p}$ [cm^3/kPa]	w [-]
Weak clay	1.09	0.25
Moderate clay	0.99	1.0
Strong clay	0.85	0.1

Table 2-5 The values of $k_{d,p}$ and w calibrated for types of clay soil (Stanczak et al., 2007).

2.5.4 Wave run-up erosion using the Turf Element Model

The strength of the dike vegetation and soil can be approximated with the turf element model which describes the forces acting on a turf cube with a 10 cm length (Hoffmans et al., 2018). Turf is specified as the 2 lower cm of grass vegetation plus 8 cm of clay including that part of the root system, as shown in Figure 2-6. Turf is porous, has a high root density and is elastic in moist conditions (Hoffmans et al., 2008).

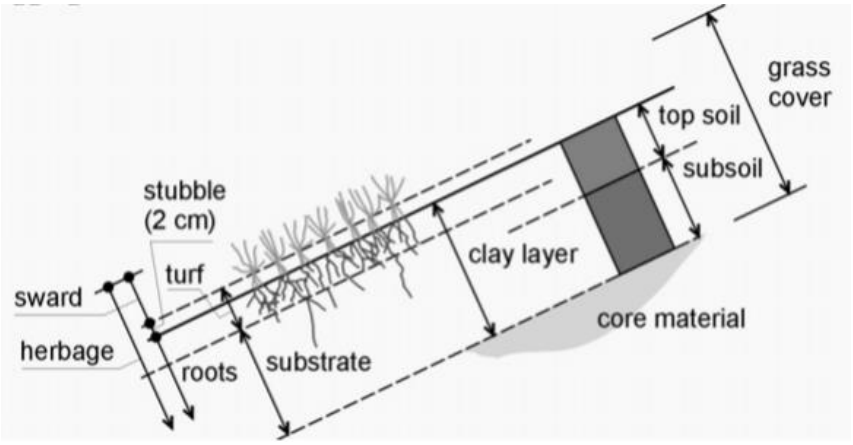

Figure 2-7 top layer of grass covered dike and forces on grass root (Hoffmans et al., 2008).

2.5.5 Turf Element Model erosion volume

The erosion volume can be calculated following the relation found in Hoffmans et al., (2008) which reads:

$$E = \frac{\mathrm{d}m}{\mathrm{d}t} = \frac{M}{\tau_c}(\tau_0 - \tau_c) \tag{2.17}$$

Where E is the erosion mass per unit area of the bed, m the mass of the sediment on the bed [kg/m^2], M a coefficient depending on the sediment characteristics (0.00001 to 0.0005 kg/(m^{2}s)), t the time [s], τ_0 the bed shear stress [m^2/s^2] and τ_c the critical bed shear stress [m^2/s^2]. The relation adapted to compute the erosion depth reads:

$$\Delta d = \frac{M \times \Delta t}{\tau_c \times \rho_s}(\tau_0 - \tau_c) \tag{2.18}$$

In which ρ_s is the soil density [kg/m^3], Δt is the difference in time [s] and Δd the difference in erosion depth [m]. The critical bed shear stress including clay cohesion and grass can be estimated using the relation found in Hoffmans et al., (2008) as follows:

$$\tau_c = \alpha_r \left((\rho_s - \rho_w) g d + c_s + \sigma_g\right) \text{ with } \alpha_\tau = 1/18 = 0.056 \tag{2.19}$$

In which d is the grain size [mm], c_s is the clay cohesion [kN/m^2] and σ_g is the grass cohesion [kN/m^2]. The bed shear stress can be obtained via Hoffmans et al., (2008) and reads:

$$\tau_0 = \frac{1}{c_0^2}\rho_w (r_0 U_0)^2 = 0.7 \rho_w (r_0 U_0)^2 \tag{2.20}$$

In which c_0 is a constant [-] equal to 1.21, U_0 is the depth averaged flow velocity [m/s] and r_0 is the turbulence intensity.

2.5.6 Turf Element Model erosion depth

The erosion depth due to wave run-up can be calculated using the scouring model for determining erosion on inner dike slopes covered with grass found by Van den Bos (2006):

$$y_m = (E_{\text{soil}})^{-1}(\alpha U_0 - U_c)^2 t \tag{2.21}$$

In which y_m is the erosion depth [m], U_c is the critical flow velocity [m/s], t is the time [s], $\alpha (= 1.5 + 0.5 r_0)$ the turbulence coefficient using the turbulence intensity (r_0) and E_{soil} is a soil parameter [m/s] described by:

$$E_{\text{soil}} \equiv \rho_s U_c^2 (M)^{-1} \equiv (C_E)^{-1} \tag{2.22}$$

Where C_E is the strength parameter [m^{-1}/s^{-1}] and the critical flow velocity can be calculated using the following relation found in Hoffmans et al., (2008):

$$U_c = \frac{\alpha_0}{r_0}\sqrt{\Delta g d + \frac{c_s}{\rho} + \frac{\sigma_g}{\rho}} \text{ with } \alpha_0 = \sqrt{\alpha_\tau c_0^2} = 0.29 \tag{2.23}$$

2.5.7 Run-up and run-down erosion due to shear stress

Erosion of the soil occurs due to run-up and run-down flow occurs when the effective shear stress is greater than the critical shear stress of the soil. The erosion is then calculated according to the excess effective stress approach following Meyer (1964):

$$\frac{dz}{dt} = k_d(\tau_0 - \tau_c)dt \tag{2.24}$$

In which:

- τ_c = Critical shear stress for the soil type [N/m^2];
- τ_0 = Shear stress for the soil type [N/m^2];
- k_d = Detachability coefficients that depends on the soil properties [m*N^{-1}s^{-1}];
- dz = Incremental erosion depth [m];
- dt = Time step [s].

Equation (2.24) describes the erosion depth due to wave run-up on clay soil and is therefore not applicable for calculating erosion on the dike slope when grass revetment is present. The detachability coefficient k_d is then calculated as follows (Temple and Hanson, 1994):

$$k_d = 10^{-6}\frac{10\rho_w}{\rho_s} exp\left[-0.121 c_{\%}^{0.406}\left(\frac{\rho_s}{\rho_w}\right)^{3.1}\right] \tag{2.25}$$

In which $c_{\%}$ is the weight percentage of clay in the soil [%]. The critical shear stress τ_c is calculated as (D'Eliso, 2007):

$$\tau_c = 5.43 \times 10^{-6}\left(\rho_s \times \frac{\rho_{cw}-\rho_w}{\rho_s - \rho_w}\right)^{2.28} \tag{2.26}$$

Where ρ_{cw} denotes the density of the clay-water mixtures, which is usually equal to around 1100 kg/m^3. The critical shear stress for the grass cover is in the range of $\tau_c = 34.8 - 184.2\ N/m^2$ depending on grass quality (Fischerich, 2001).

2.5.8 Calculating head cut advance

The head cut advance model as described in The US model SSEA, Sites Spillway Erosion Analysis (NRCS, 1997), describes the cliff erosion due to wave overtopping on dikes. The description found by SSEA and Van Hoven (2014) described the erosion progress in three phases where:

- Phase 1 is the erosion of the grass cover;
- Phase 2 is the mostly vertical erosion of the clay layer below the grass cover creating cliffs in the dike profile (head cuts);
- Phase 3 horizontal advance and deepening of head cut resulted from flow over the (near) vertical cliff.

The erosion due to phase 1 and 2 can be computed using equations (2.11)-(2.23) and the rate of advance of a head cut (phase 3) can be described using the following relation (NRCS, 1997):

$$dX/dt = C(A - A_0) \tag{2.27}$$

In which dX/dt is the head cut advance [m/h], C is the head cut advance rate coefficient [s$^{-2/3}$], A is the head cut advance rate load parameter [m/s$^{1/3}$] and A_0 is the head cut advance rate threshold parameter [m/s$^{1/3}$]. The parameters C, A and A_0 are computed as follows:

$$A = (qH)^{1/3} \tag{2.28}$$

$$A_0 = \left[189 \cdot K_h^{1/2} \cdot \exp\left(\frac{-3{,}23}{\ln(101 \cdot K_h)}\right)\right]^{1/3} \tag{2.29}$$

$$C = 3.04 - 0.79 \cdot \ln(K_h) \tag{2.30}$$

In which K_h is the sediment parameter [-], q $(= uh)$ the average overtopping discharge [m^3/s/m] and H is the cliff height [m]. Where:

$$K_h = M_s \cdot K_b \cdot K_d \cdot J_s \tag{2.31}$$

Where M_s is the material strength number [-], J_s is the soil material parameter [-], $\mathrm{K_d} \cong \tan \phi'_\mathrm{r}$ is the interparticle bond strength [-], with ϕ'_r the friction angle [-] and K_b is the particle size number [-].

2.6 Model accuracy

In this section two models that can be used to determine the quality of a model compared to data are discussed.

2.6.1 Coefficient of determination

The coefficient of determination can be used to quantify how well a model can predict the data. The coefficient of determination (R^2) can be computed following Draper and Smith (1966) as follows:

$$R^2 = 1 - \frac{\sum_{i=1}^{n} (y_i - \hat{y}_i)^2}{\sum_{i=1}^{n} (y_i - \bar{y})^2} \tag{2.32}$$

Where y_i is the measured data, $\hat{y}_i$ is the computed value, $\bar{y}$ is the mean of the measured data and n is the amount of data points. The coefficient of determination has a value between 0 and 1 where a value of 1 represents a perfect fit and a value of 0 a horizontal line. The model prediction compared to the data is worse than a horizontal line if the coefficient of determination is negative. The coefficient of determination is generally used for linear models.

2.6.2 Root Mean Square Error (RMSE)

The Root Mean Square Error (RMSE) is the standard deviation of the predication errors (residuals).The RMSE is a measure of how concentrated the data is around the model. The RMSE can be computed following Barnston (1992):

$$\mathrm{RMSE} = \sqrt{\frac{\sum_{i=1}^{n} (\hat{y}_i - y_i)^2}{n}} \tag{2.33}$$

For computation of the RMSE the same parameters are used as for computation of the coefficient of determination. A RMSE of close to 0 indicates that the model can predict the data well. Therefore, the model with the lowest RMSE is the most accurate model.

2.7 OpenFOAM model

OpenFOAM is an acronym for Open source Field Operation And Manipulation, which is an open-source Computational Fluid Dynamics (CFD) toolbox. OpenFOAM is operated via text files that are coded with C++ and is operated with commands, not via a user friendly Graphical User Interface (GUI). OpenFOAM allows for an unlimited amount of calculations for free and is constantly updated because of its open source code. OpenFOAM models have been used in simulating the effect of convex and concave structures on wave run-up.

OpenFOAM can be used to model wave breaking, wave run-up and the effects of bottom friction (Higuera et al., 2013).

2.7.1 OpenFOAM governing equations

OpenFOAM is based on the Reynolds Averaged Navier-Stokes equations (RANS) for two incompressible phases using a finite volume discretization and the Volume Of Fluid (VOF) method (Higuera et al., 2013). This makes the model able to perform complex computations with higher efficiency than other CFD models such as DualSPHysics model. Moreover, the OpenFOAM models are implemented using Eularian method making it more efficient than the DualSPHysics model which is implemented by the Lagrangian method. The Lagrangian method deals with individual particles and their separate trajectory whereas the Eularian method deals with clusters of particles and computes the overall diffusion and convection of a number of particles (Saidi et al., 2014). The governing equations are as follows (Higuera et al., 2013):

$$\nabla \cdot \mathbf{U} = 0 \tag{2.34}$$

$$\frac{\partial \rho \mathbf{U}}{\partial t} + \nabla \cdot (\rho \mathbf{U}\mathbf{U}) - \nabla \cdot (\mu_{\text{eff}} \nabla \mathbf{U}) = -\nabla p^* - \mathbf{g} \cdot X \nabla \rho + \nabla \mathbf{U} \cdot \nabla \mu_{eff} + \sigma \kappa \nabla \alpha \tag{2.35}$$

$$\frac{\partial \alpha}{\partial t} + \nabla \cdot \mathbf{U}\alpha + \nabla \cdot \mathbf{U}_c \alpha (1 - \alpha) = 0 \tag{2.36}$$

In which all the bold letters indicate a vector field, $\mathbf{U}$ is the velocity vector, $\mathbf{U}_c$ is the compression velocity vector, $\mathbf{g}$ the graviational acceleration, σ is the surface tension coefficient, X is the position vector, μ is the dynamic molecular viscosity, p^* is the pseudodynamic pressure, α is the VOF indicater, ρ is the density which is calculated as $\rho = \alpha \rho_{\text{water}} + (1 - \alpha)\rho_{\text{air}}$, μ_{eff} is the efficient dynamic viscosity, $\mathbf{U}_c$ is the compression velocity and $\kappa = \nabla \times \frac{\nabla \alpha}{|\nabla \alpha|}$ is the curvature of the interface.

2.7.2 OpenFOAM waves2Foam solver

Waves2Foam is a toolbox applied as a plug-in to OpenFOAM used for generation an absorption of free surface waves (Jacobsen et al., 2012). The waves2Foam toolbox was later expended with the possibility of modelling the interaction between free surface waves and a permeable medium (Jensen et al., 2014). The OpenFOAM momentun equations are used for waves2Foam with the advection of the VOF field, F is computed as:

$$\frac{\partial F}{\partial t} + \nabla \cdot \mathbf{u}F + \nabla \cdot \mathbf{u}_r (1 - F)F = 0 \tag{2.37}$$

Where, $\mathbf{u}_r$ is a relative velocity as further explained by Berberović et al., (2009) and F is used to evaluate the spatial variation in density and dynamic viscosity as below:

$$\rho = F\rho_1 + (1 - F)\rho_0 \text{ and } \mu = F\mu_1 + (1 - F)\mu_0 \tag{2.38}$$

Where subscript 1 refers to material properties corresponding to F = 1 and subscript 0 refers to material properties corresponding to F = 0 where F = 1 indicates water and F = 0 indicates air in waves2Foam.

3 Methodology

The methodology describes the research activities conducted to obtain the results required for answering the research questions described in section 1.3. The methodology is divided in four main parts:

- Calculating erosion depth and volume using FARO3D laser scanner data of delta flume experiments at Deltares, determining the variation in erosion rate per experiment and quantify the effect of grass and clay quality on erosion rate to subsequently answer the first research question;
- OpenFOAM model description for models of test K101 without erosion and test K114, with significantly eroded grass revetment. The simulated hydraulic variables from the two OpenFOAM models were compared to determine the effect of an eroded dike slope profile on wave impact and run-up velocities in order to answer the second research question;
- The OpenFOAM models were validated by determining the accuracy of the simulated dynamic pressures and flow velocities by comparing the model results to empirical relations. The hydraulic variables of the validated OpenFOAM models were used to compute the erosion using empirical relations required for answering research question 3 and 4;
- Computation and calibration process of applying empirical erosion relations to determine wave run-up, wave impact and head cut erosion using OpenFOAM model results. The erosion computed by using the simulated hydraulic variables in combination with the calibrated erosion relations were compared to the erosion from the experiment in order to answer research questions 3 and 4.

3.1 Erosion delta flume experiments

The set-up of the delta flume experiments is described in section 2.2. The elevation of the grass revetment slope has been measured after each test. This was used to compute the erosion depth and volume for each experiment to quantify the effect of clay and grass quality on erosion rate and subsequently answer the first research question. The data of the delta flume experiments is also used to answer research question 3 and 4.

3.1.1 FARO3D laser scanner data

The grass revetment profiles were measured using a FARO3D laser scanner. Data of this scanner consists of XYZ points where:

- The X points represent the length of the dike, which is 10 m, from toe of the dike to the crest;
- The Y points represent the width of the dike set up, which stretches for 1.93 m;
- The Z points represent the height of the profile.

All measurement data is given in meters and the dike slope is not measured; the dike slope is added in MATLAB to improve the visualization. The sloped profile was created using the height at the transition, which is 6.5 m above the bottom of the delta flume and the 1/4 dike slope. After every test, summarized in appendix A, the dike surface is scanned which contains information about the height of the dike profile. The profile after the first wave impact test, during which no erosion occurred, is compared to all other profiles for each experiment to calculate the amount of erosion and erosion depth. The FARO3D scanner measured almost the whole width of the dike, the measured width is 1.93 m as mentioned

before. The experiments that were conducted in the Delta flume at Deltares are summarized in Table 2-2.

3.1.2 Erosion depth and volume using FARO3D data

The maximum erosion depth and change after each test has been derived from processing the FARO3D data in order to determine the erosion rate. The FARO 3D laser scanner data contained a large number of data points which were linearly interpolated with a resolution of 1x1 cm significantly reducing the amount of data. A part of the hard revetment was also measured with the FARO3D scanner of which 50 cm was included in creating the surface profiles, resulting in a grid size of 200 by 1050 data points displaying the height relative to a flat plane shown in Figure 3-1. After each test, the profile was compared to the result of the first test of the experiment. The profiles were subtracted from the profile of the first tests, after which the maximum erosion depth was found, which is located at a different location along the dike slope for each test. Figure 3-1 shows the erosion surface with a colorbar identifying the erosion depth and the point of maximum erosion depth marked by a red dot.

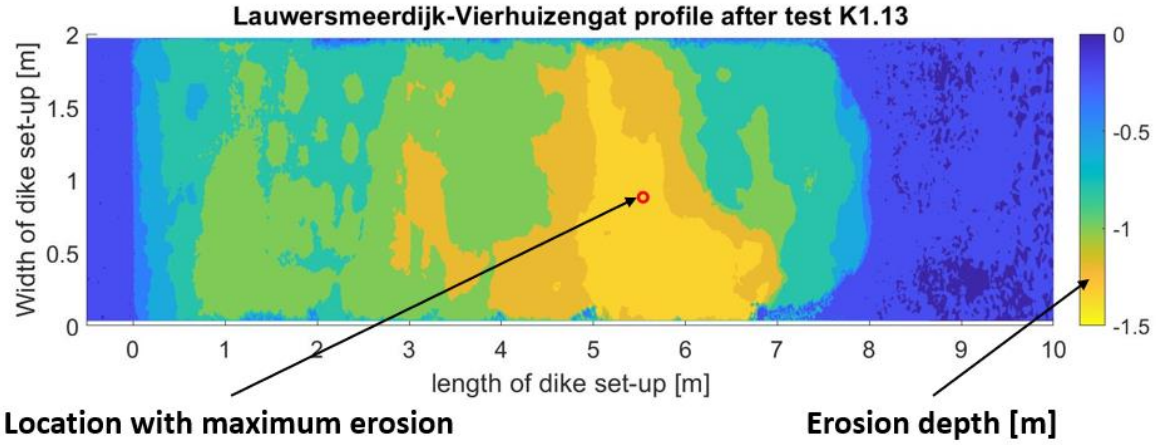

Figure 3-1 A colour map showing the erosion after experiment K1 test K113 with a red dot indicating the location of maximum erosion.

The maximum erosion depth is calculated by finding the profile with the highest surface height difference between erosion profile of first test and every other test in direction of the length of the dike set-up in the delta flume. The profile in length direction is then plotted, which includes the point that is marked by the red dot in Figure 3-1. The colour map in Figure 3-1 consists of 200 erosion profiles in length direction (x-axis in Figure 3-1). The profile along the dike with the averaged erosion depth, shown in Figure 3-2, has been determined by computing the average erosion depth of the 200 interpolated points in the width direction for all 1050 points in length direction of the grass revetment. Consequently, the total erosion volume has been computed by integrating the difference between two erosion profiles and multiplying the integrated erosion area by the total width of the test set up.

Two types of cross-sections from every test were produced: the maximum erosion profile and the average erosion profile. The maximum erosion profile is the profile that includes the point in the surface with maximum erosion depth. The average erosion profile is averaged along the dike and used to calculate the total erosion volume. In Figure 3-2 the erosion figures are explained, where the top plot shows the 2D profile with the highest erosion depth based on the erosion surface from Figure 3-1 and the bottom plot shows the average erosion profile, used to calculate the total amount of erosion after each experiment, shown by the red shaded area in Figure 3-2. The blue line is the average dike profile after test K101 and the red line the erosion profile after test K113. The erosion surface is marked in red in Figure

3-2, including the location of the transition (shown in Figure 3-2) from hard to grass revetment and initial profile before erosion after test K101. Because experiment K3 and K6 are continuations of experiment K2 and K5, the maximum erosion depth has been measured compared to test K201 and K301 for experiment K3 and to K501 and K601 for experiment K6.

The erosion data obtained from the FARO3D laser scanner for each test in experiments K1 – K6 is summarized in appendix A. The erosion profiles and surfaces of experiments K1-K6 are found in appendix C.

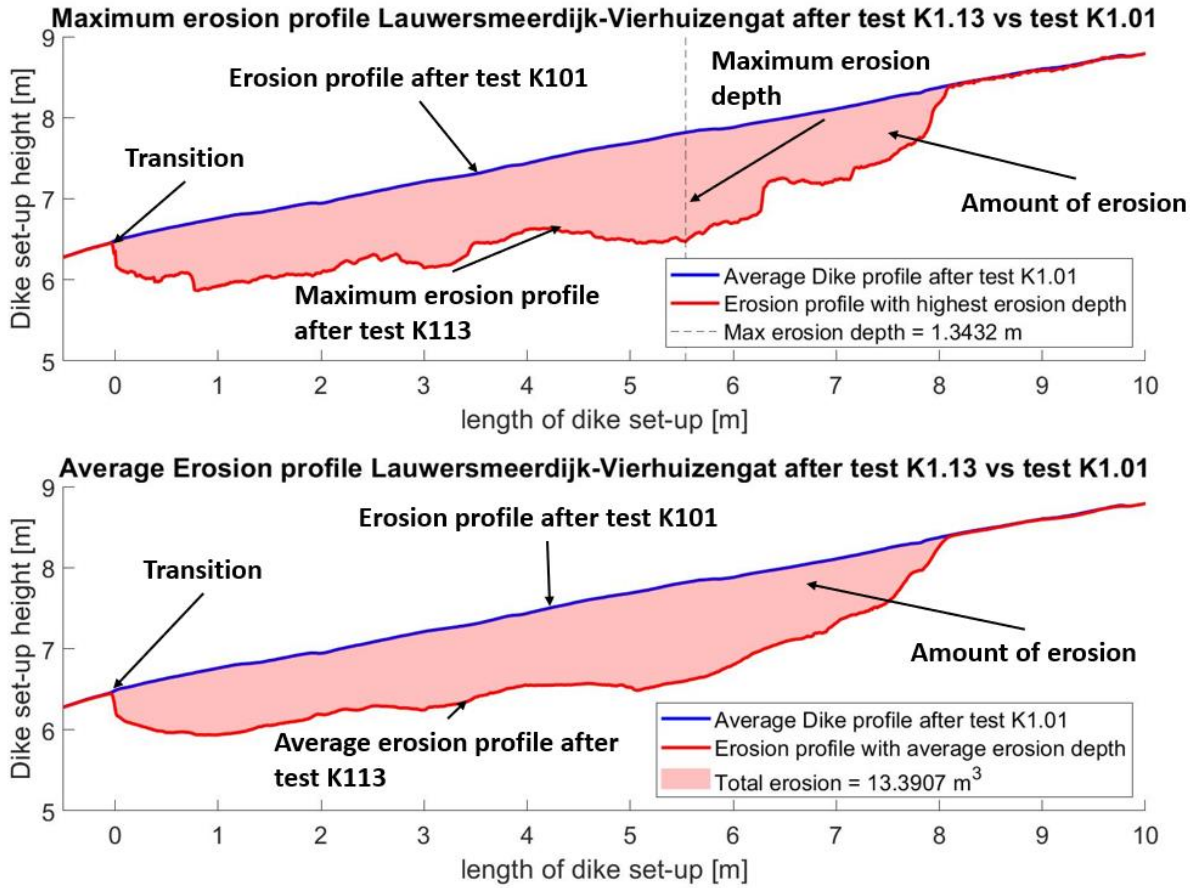

Figure 3-2 Cross sections of erosion profile along the dike that includes the maximum erosion depth and averaged erosion profile along the dike after test K113 of experiment K1.

3.1.3 Effect clay and grass quality on erosion rate

Experiment K1 is compared to experiment K4 to investigate the effect of clay quality on erosion rate and experiments K2 - K3 is compared to experiments K5 - K6 to determine the effect of grass quality on erosion rate. The experiments were compared using a percentage of the maximum for each value of erosion depth and volume. Consequently, the absolute difference between each experiment is neglected and the erosion development can be directly compared. Additionally, the erosion after each experiment is known as well as the duration of each experiment which is used to derive the erosion per minute, assuming linear erosion rate during the experiment. It is unlikely that the erosion occurs exactly linear during each experiment, but no data is available to determine erosion during the experiment.

3.2 OpenFOAM Model description

A 2DV OpenFOAM model is created to simulate the wave impact pressures and velocities on the dike. The erosion models use the simulated hydraulic variables as input. The computed erosion depth and volume is then compared to the delta flume experiments to determine the relation between hydraulic load and erosion.

The implementation of the OpenFOAM model is schematized in Figure 3-3 first, 2DV meshes of the delta flume were created including the dike profiles of the Lauwersmeerdijk-Vierhuizengat after test K101 and test K114. Thereafter, boundary conditions were added as well as friction and probes for measuring flow velocity, pressures and shear stresses, followed by validation of the models. After the models were created, the experiments were simulated for a duration of 600 s and the modelled data were processed. The post-processed model data were later used to compute the erosion due to wave impact, run-up and head cut erosion. The simulations were ran using the waveIsoFoam solver, which simulates wave propagation with a higher accuracy than the waveFoam solver, as tested by Chen et al. (2021).

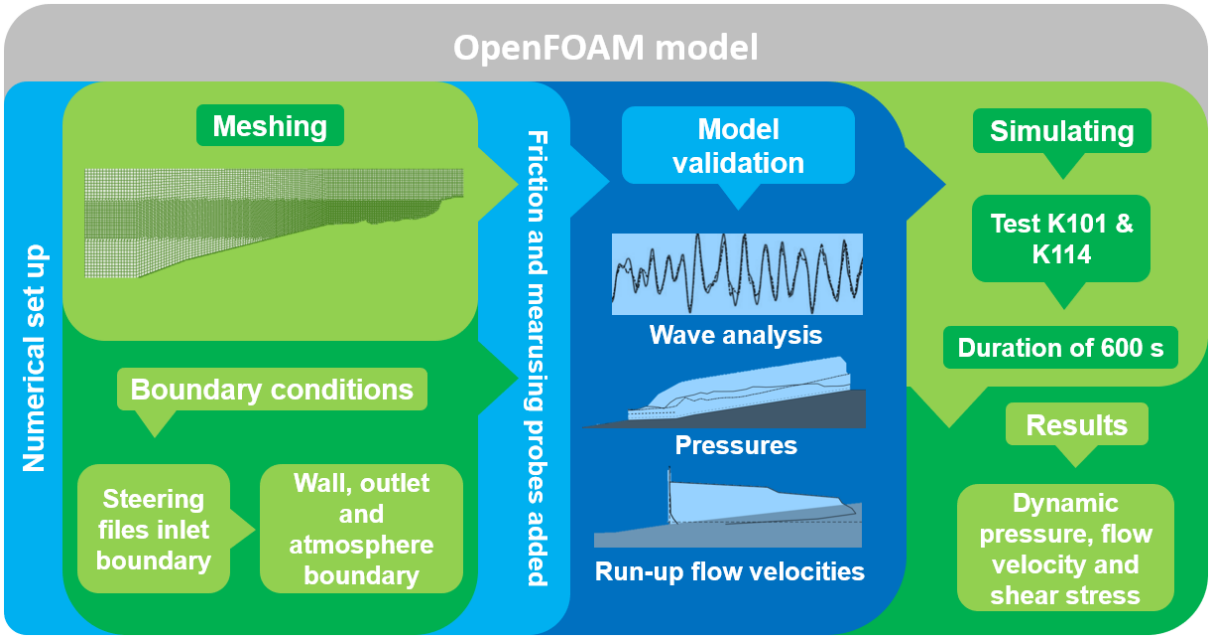

Figure 3-3 Flowchart of the OpenFOAM model set-up showing a schematization of simulation steps and numerical set-up.

3.2.1 Waves2Foam

Waves2foam has been used extensively for a large number of papers and reports ranging from validation to application of the toolbox and the free surface capabilities of OpenFOAM (e.g., Paulsen et al., 2014 and Jacobsen et al., 2014). Therefore, waves2Foam is used to simulate the propagating waves for the OpenFOAM models in this report. Relaxation zones were utilized in the OpenFOAM models, which is a technique meant to remove the spurious reflections from the numerical simulations included in the waves2Foam toolbox (Jacobsen, 2017). The relaxation zone technique is based on a weighing between the computed flow velocity field and the indicator field with a target solution. The specification of the location of the relaxation zones in the computational domain is described in section 3.2.4.

3.2.2 Turbulence model

The Reynolds shear stresses require additional modelling to close the RANS equation for solving which leads to turbulence models. There are three turbulence models available, the

$\kappa - \epsilon$ model which is the kinetic energy (κ) and dissipation (ϵ), $\kappa - \omega$ model that predicts turbulence by kinetic energy and specific rate of dissipation and the $\kappa - \omega$ Shear Stress Transport (SST) turbulence model. A stabilized $\kappa - \omega$ model was used by Chen et al. (2021). They showed that the aforementioned turbulence model can be used to simulate wave run-up and overtopping at dikes with higher accuracy than the $\kappa - \omega$SST and laminar model. Therefore, the stabilized $\kappa - \omega$ model was used for the OpenFOAM model of the Lauwersmeerdijk-Vierhuizengat.

3.2.3 Geometry Lauwersmeerdijk-Vierhuizengat

In this study, simulations were performed for two dike profiles: the regular dike profile measured at the end of test K101 and the profile after experiment K114 with significant erosion to the grass revetment. The first simulation consists of the outer dike slope and a part of the dike crest using a non-eroded surface (test K101). The second simulation uses the dike geometry after experiment K114 with significant erosion to the grass revetment. The waterside slope dike profiles from Lauwersmeerdijk-Vierhuizengat are shown in Figure 3-4 with the coloured surface representing the dike profile after experiment K114 and the orange surface plus the area up to the dashed line representing the dike before erosion.

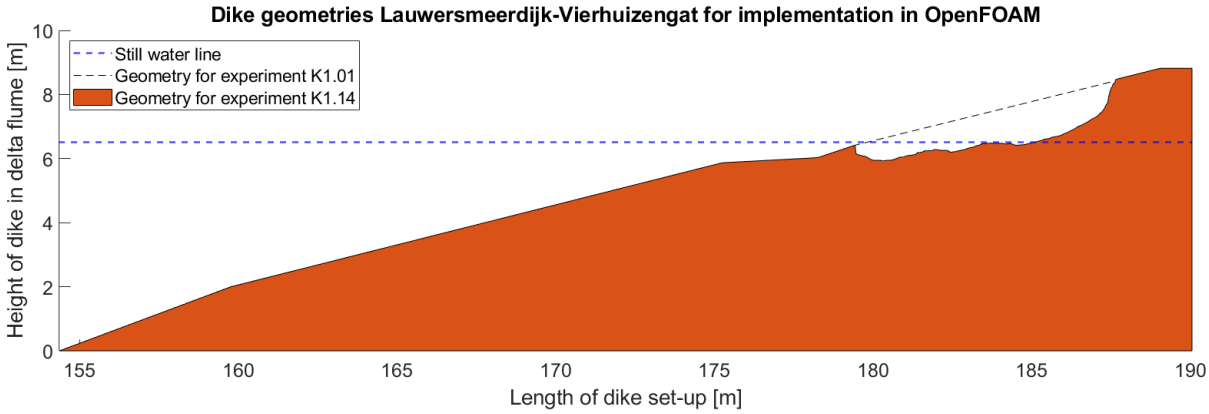

Figure 3-4 Dike geometry as implemented in OpenFOAM showing the initial and eroded grass cover, with a berm between x = 175 – 178 m.

The model representation of the Lauwersmeerdijk-Vierhuizengat has a total height (from the bottom of the flume) of 8.87 m and a waterside slope length (from bottom to crest) of 34.68 m. The blue dashed line in Figure 3-4 shows the water level, which is 6.5 m in the first simulation and 6.65 m in the second simulation. The grass revetment spans from a height (from the bottom of the flume) of 6.4 m to the crest of the dike.

3.2.4 Wave generation, model domain and boundary conditions

The waves for the OpenFOAM simulation will be generated using OceanWave3D (OCW3D) and the steering files from experiments K101 and K114. The wave conditions applied in the experiments were reproduced in the OpenFOAM model. The wave conditions with the significant wave height $H_s = 2$ m and period $T = 5.5$ s were used to replicate the Lauwersmeerdijk-Vierhuizengat in experiment K1 to simulate storm conditions in the Wadden Sea (Klein Breteler, 2020). Waves were generated by inputting the wave board signal files that were used in the experiments. The generated nonlinear irregular waves in OCW3D provide input for waves2Foam (Chen et al., 2020).

The waves were implemented in OpenFOAM from the inlet boundary. The OpenFOAM model domain could be shortened by using OCW3D which reduces computation time. Therefore, the flume is simulated in OpenFOAM from 50 m followed by an inlet relaxation zone between 50 and 100 m as shown in Figure 3-5. OCW3D simulates waves for a length

of 100 m, which is roughly two wavelengths with one wavelength overlap in the OpenFOAM model at the location of the inlet relaxation zone (between 50 and 100 m). The free zone, between the inlet relaxation zone and the toe of the dike contains three wave gauges that measure the simulated incoming and reflected wave heights and were used to validate the modelled waves. The wave-structure interaction zone as highlighted in Figure 3-5 is the area where the waves break and impact pressures were measured.

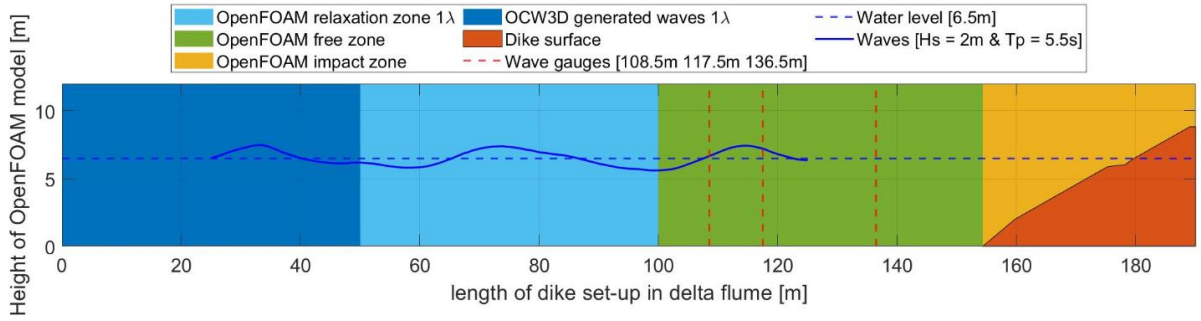

Figure 3-5 OpenFOAM model sections showing wave generation using OceanWave3D into the relaxation zone where wave propagation is calculated with waves2foam solver.

Boundary conditions

The model uses non-slip wall boundary conditions for the flume bottom and dike profile. An atmosphere boundary condition is present in the top of the model which allows water and air to flow out and air to flow in. A zeroGradient boundary condition is present in the outlet, allowing water and air to flow out of the model domain. No relaxation zone is present at the outlet. The boundary conditions of the patches for the model parameters are summarized in the table below:

Parameter	Inlet	Outlet	Atmosphere	Bottom/slope
U (m/s)	zeroGradient	zeroGradient	pressureInlet-OutletVelocity	fixedValue (no-slip)
p (Pa)	zeroGradient	fixedValue	totalPressure	zeroGradient
alpha.water	zeroGradient	zeroGradient	inletOutlet	zeroGradient

Table 3-1 Boundary conditions for extracted parameters of patches in the OpenFOAM model.

3.2.5 Mesh properties

The dike set up of the Lauwersmeerdijk-Vierhuizengat starts at 154.37 m from the start of the flume. The domain that is simulated in OpenFOAM begins 50 m from the start of the flume and ends at the crest of the experimental dike set-up. The length of the entire modelling domain is 150 m and is shown in Figure 3-6. The figure also shows the refinement surface in dark blue until the dike slope to accurately simulate wave breaking required for obtaining the dynamic pressures at the grass revetment.

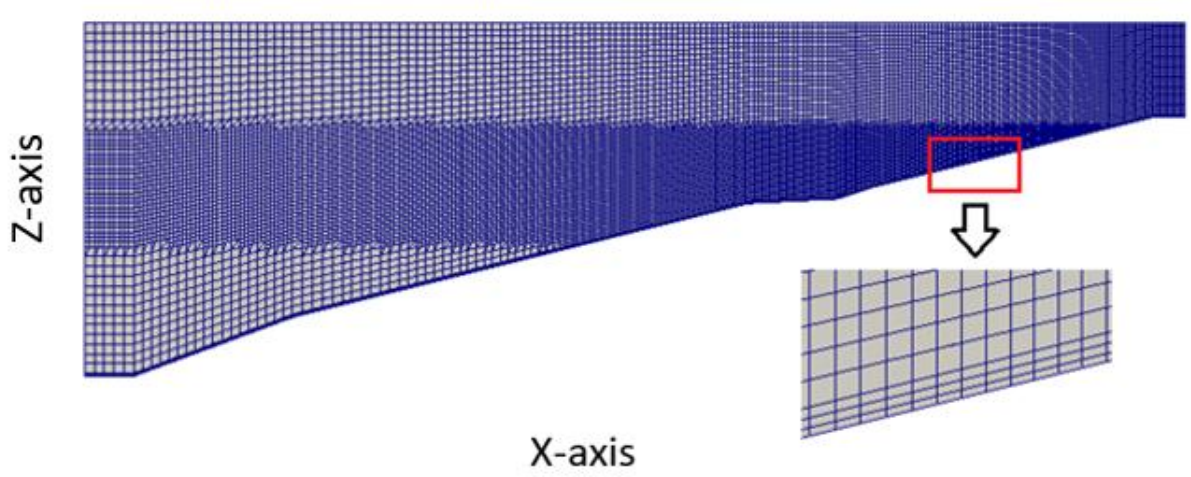

Figure 3-6 OpenFOAM model mesh near dike surface with refinement surface of experiment K101.

The mesh for both was created using blockMesh and snappyHexMesh which are utilities in OpenFOAM. A background mesh for the dike in experiment K101 was created which includes the dike profile as shown in Figure 3-6. The number of cells in the vertical y-direction is constant in the mesh. The vertical height of the mesh decreases with the inclusion of the dike profile as visible in Figure 3-6. Consequently, the size of the cells decreases and the cell density increases on the slope of the dike. Therefore, more cells were added in the horizontal x-direction to maintain an aspect ratio close to 1. 12 cells in z-direction are required to accurately resolve the wave height (Larsen et al., 2019). The cell size between the inlet and the toe of the dike is 33x33 cm (between 50 and 154.37 m in Figure 3-5) which is not sufficient to simulate the propagating waves with a significant wave height of 2 m with 12 cells in the z-direction. Therefore, a refinement surface has been added between 4.5 and 8.5 m in z-direction, in which the cell density is twice as high as in the surrounding mesh, resulting in a sufficient amount of cells to simulate wave propagation. In order to increase the computational speed, simulations were ran with a shortened refinement surface. However, this had a significant effect on the model results and therefore the refinement surface is applied over the entire length of the model as further elaborated in Appendix E.1.

The second OpenFOAM simulation was conducted on the final erosion profile of the Lauwersmeerdijk-Vierhuizengat after experiment K114. The mesh for experiment K114 is similar to the mesh used for experiment K101 but with an extension at the grass revetment location to accommodate the erosion profile. The dike profile of experiment K114 was then created by fitting the dike surface with the grass revetment erosion profile, obtained from the FARO3D laser scanner, to the blockMesh using snappyHexMesh. Several average cell sizes from different locations in the model are summarized in Table 3-2. Note that the cells in the refinement surface are not per definition twice as small since the cell size also increases higher up the outer dike slope.

	Not in refinement surface [x*z]	In refinement surface [x*z]
Wave propagation zone cell size [cm]	33 x 33	17.5 x 17.5
Lower dike slope [cm]	25 x 25	11 x 11
Grass revetment slope [cm]	15 x 15	10 x 10

Table 3-2 Cell sizes at different location in the OpenFOAM model mesh, which are very similar for test K101 and test K114.

The OpenFOAM meshes for simulation of test K101 and K114 can be found in Appendix D.

Wall function

Wall functions were applied in the bottom and dike boundary layers instead of resolving the boundary, which saves computational time. The wall function was applied by placing the first grid-cell layer in the log layer. Therefore, the mesh near dike surface was refined, resulting in the grid size near the wall of $\Delta y \approx 0.0033$ m for the first three layers which is constant throughout the simulation.

Courant number

The model stability is indicated by the courant number which has to be lower than a pre-defined value. The maximum Courant number for the simulations is 0.3 [-] with a variable time step of Δt of around 1 ms. Since the wave celerity and mesh resolution cannot be altered during the simulation, only the time step can be changed to ensure a sufficiently low Courant number (Larsen et al., 2018).

3.2.6 Friction of grass revetment and clay layer

Friction has been added in the OpenFOAM models by adding a patch on the location of the grass revetment and applying the roughness height to 8 mm as found by a recent study (Van Bergeijk et al., 2020).

The roughness height of clay has been determined using the Manning coefficient where the roughness can be described following Marriott & Jayaratne (2010) in the relation below:

$$k_s = \left(\frac{n}{0.012}\right)^6 \tag{3.1}$$

Where k_s is the roughness height in mm and n is the Manning roughness. The Manning roughness is 0.016 for the clay in the eroded dike profile following from Chow (1959), resulting in a roughness height of 6 mm for the eroded area in the model of experiment K114. The roughness is constant throughout the OpenFOAM simulation.

3.2.7 Probe locations

Probes have been placed at a height of 20 cm above the dike surface from the start of the berm (x = 175 m) until the crest of the dike in the numerical model of experiment K101 (Figure 3-7). The distance between each probe is approximately 40 cm in x-direction in order to reduce the amount of data points and to increase computational and processing speed. Elaboration on the height of the measuring probes is found in Appendix E.2.

The probes for the model of experiment K114 have been placed at the same x-locations but with varying z-locations because of the eroded grass revetment profile. The y-locations have been determined by linearly interpolating the erosion profile obtained from the FARO3D laser scanner data over 20 points, ensuring accurate measuring points 20 cm above the profile at the same locations as the probes from experiment K101 (Figure 3-8).

A vertical probe measuring the water flow velocity and pressure over depth is placed at the transition between hard and grass revetment from the dike surface (x = 179.6 m) to a height of 10 m in both profiles. The vertical probe contains 15 measuring points for every cell in the vertical direction.

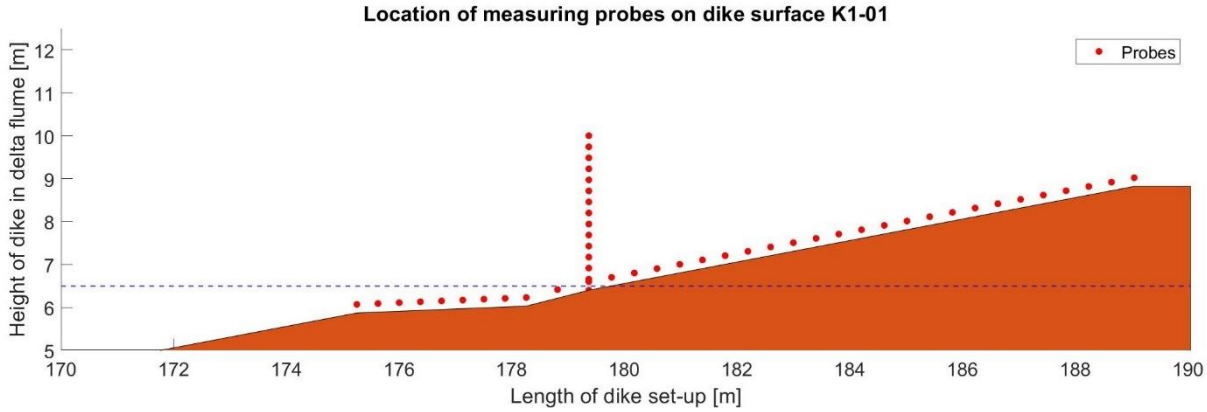

Figure 3-7 Probe locations of final OpenFOAM model of Lauwersmeerdijk-Vierhuizengat of experiment K101.

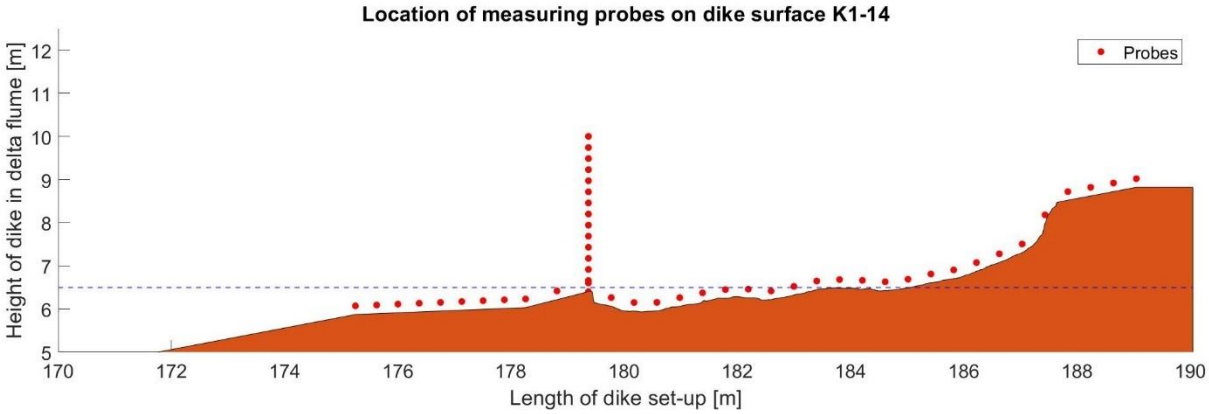

Figure 3-8 Probe locations of final OpenFOAM model of Lauwersmeerdijk-Vierhuizengat of experiment K114.

Measured parameters

The simulated pressures at the probe locations were saved every time step in the OpenFOAM model. There are three different pressures that were measured with the probes in the model. All of the measured parameters including the three different pressures are:

- P_rgh [-] which is the total pressure minus rho*g*h but OpenFOAM has difficulty determining the water depth making the value of p_rgh somewhat unreliable;
- P [Pa] which is the hydrostatic pressure;
- Total-P [Pa] which is the total modelled pressure, which is the sum of the hydrostatic and hydrodynamic pressure ;
- U [m/s] which is the flow velocity measured in x, y and z direction;
- Alpha.water [-] contains the water content of each cell that includes a probe. If alpha.water is close to 1 it is almost filled with water and the cell is empty when alpha is 0. Since only the velocities of water are of interest, the decision has been made to use the velocities of the cells that have an alpha.water larger than 0.6. The flow velocity is not used if the cell water content is below 0.6.

Additionally, the wall shear stress [m^2/s^2] is measured to determine the stress on the dike profile due to wave run-up that is used to calculate the wave run-up erosion. However, the wall shear stresses can only be measured at the cell closest to the boundary. Therefore, a layer of extra probing points has been placed at the grass revetment 1 cm above the dike surface at the same x-location as the probes shown in Figure 3-7 and Figure 3-8.

3.3 OpenFOAM model validation

The simulated incoming waves from OpenFOAM were validated against the incoming waves from the delta flume experiment. The energy density spectrum of the wave heights were validated to show that OpenFOAM is able to accurately model the wave height and wave period using a steering file from OceanWave3D (OCW3D). No measurements were available for validating the modelled pressure and flow velocity. Therefore, the pressure and flow velocity of the model were compared to empirical formulas discussed in the background.

3.3.1 OpenFOAM model wave height validation

The OpenFOAM model of both experiments has been validated using measured time series of water surface elevation from the delta flume experiments that were compared to those at the same locations in the OpenFOAM model. The locations of the wave gauges in the OpenFOAM model as shown in Figure 3-5 are the same as those in the delta flume experiment. The measured simulated waves and measured waves data contain the wave height of the incoming and reflected waves which were separated for analysis to remove randomness in the wave signal. The wave separation is conducted based on the Mansard-Funke procedure (Mansard et al., 1980) using uniform water depth and waves propagating in only the x-direction. The sampling frequency of the wave gauges in OpenFOAM was 1000 Hz while the sampling frequency for the wave height of the experiment was 20 Hz. Therefore, the sampling frequency of the OpenFOAM data for the wave separation has been reduced to 20 Hz to match the data from the experiment.

The input wave height is the only parameter from the steering files that can be altered in OCW3D. The steering files contained an initial significant wave height of 2.3 m which has been lowered to a significant wave height of 1.8 m to match the experimental wave height.

Comparing the modelled incoming and reflected waves directly to the incoming and reflected waves of the delta flume experiments did not yield accurate results. There is a lag between the model and the experiment, the duration of which has been determined using cross-correlation analysis.

3.3.2 Dynamic pressure validation

The data from the model has been validated against empirical relations that give an indication of the maximum impact pressures. The impact pressure is equal to the dynamic pressure output of OpenFOAM that has been obtained by extracting p_rgh, which is the pressure without hydrostatic pressure or pressure minus rho*g*h. However, the value of p_rgh is not reliable because OpenFOAM cannot accurately determine the water depth causing uncertainty in the results. Therefore, the dynamic pressure is also obtained via determining the total pressure and subtracting the hydrostatic pressure. Calculating the dynamic pressure using the total pressure should give accurate results since it is calculated independent of the water depth.

The dynamic pressure is calculated for every calculation step in OpenFOAM. The maximum dynamic pressures of the model were compared to empirical relations to roughly validate the simulated data. Therefore, the 2%, 5% and 10% exceedance values of the maximum pressure were determined over the total simulation duration for every probe location and compared to the empirical determined value. The relations found in Peters (2017) and Horstman (2020) as described in the background were used to determine the 2%, 5% and 10% exceedance pressures. The n% highest pressures have been used for validation of the dynamic pressures using the highest pressure of each wave measured at the dike surface.

The exceedance dynamic pressures are based on the maximum impact pressure per wave, which was determined by finding the peak pressure for every spike in the OpenFOAM

pressure data. After defining the maximum dynamic pressure for each wave at each location, the pressures were sorted and the waves exceeding the top 10%, 5% and 2% of dynamic pressures were determined. The noisy data in between the peaks has not been used in determining the peak pressures and the number of impact pressure events depends on the location of the probe, since probes located higher on the seaside slope experience fewer impact events.

3.3.3 Flow velocity validation

OpenFOAM obtains the flow velocity in cartesian coordinates separately per probe. This means that, aside from temporal interpolation to create equal time steps over the data, the velocities have to be separated for defining the flow velocity magnitude parallel to the dike slope. The velocity parallel to the slope is determined using a rotation matrix, where the x-coordinate parallel to the dike slope can be obtained using the following equation:

$$x' = x\cos + y\sin\theta \tag{3.2}$$

In which θ is the slope angle. The slope angle θ = 14 degrees with a slope of 1/4 at the grass revetment of test K101. The slope angle in experiment K114 changes due to the geometry of the eroded grass revetment profile. In order to determine the slope angle for each of the 25 probing locations on the grass revetment of test K114, the surface vector (Sf) for every cell in the grass revetment has been determined in OpenFOAM. The surface vector has been transformed to the slope angle and interpolated over 25 locations to obtain the slope angle for every probe on the grass revetment of test K114.

However, the flow velocity includes the velocity of air which is not of interest for validation and calculation of the wave run-up. Therefore, the water velocities were obtained by multiplying with the water fraction alpha.water. After interpolating the data, obtaining the normal flow velocity magnitude, and adjusting for water content, the flow velocity data could be used for analysis and validation.

The flow velocities have been validated using equations (2.5)-(2.10), where the 2% exceedance value of the wave run-up has been calculated with the run-up height using influence factors for oblique waves. The roughness elements have been set to 1 and the influence factor for the berm has been set to 0.6 based on equations (2.8)-(2.10). The 2% exceedance run-up flow velocity has been compared to the velocities measured by the probes on the grass revetment dike slope. The peak run-up velocities have been determined for every wave run-up event occurring after each wave impact where the number of peaks depend on the location of the probe. The 2% exceedance run-up flow velocity has then been determined by finding the 2% highest peak velocities for each location of the grass revetment area above the SWL.

3.3.4 Effect of eroded profile on model results

The 2%, 5% and 10% exceedance values of the dynamic pressure, flow velocity and shear stress from the model of test K101 and K114 were compared against each other to determine the effect of a grass revetment erosion profile on model results. Additionally, the mean and maximum water depth were compared to identify the difference in water depth which might influence the pressures, velocities and stresses of the model. The data were compared by plotting the results of the probes on the grass revetment and berm between x = 175 m and x = 189 m on the dike slope.

3.4 Estimation of erosion using the OpenFOAM output

The erosion depth and volume measured during experiment K101 and K114 can be computed using the erosion relations in Chapter 2 (equations (2.11)-(2.26)) and the model output of the OpenFOAM model. Erosion is computed either by wave impact or wave run-up. No relations considering both impact and run-up erosion are found in literature. There are 25 probes 0.2 m above the surface of the erodible grass revetment area used to compute the erosion following the relations found in equations (2.11)-(2.26). These erosion relations describe the amount of erosion depth or erosion volume that has occurred due to a single wave impact event (e.g., Stanczak et al., 2007 and Stanczak et al., 2008) using wave impact pressures or shear stress or flow velocity induced by wave run-up (Hoffmans et al., 2008). The wave impact and wave run-up erosion will be calculated simultaneously using equations (2.11)-(2.26) in order to determine the effect of predicting erosion using currently existing relations. Because relations describing the erosion volume are available, both the erosion depth and volume have been computed using the OpenFOAM model data. These relations require information on the cover strength and hydraulic load.

The erosion volume and erosion depth for each test in experiment K1 is known from the analysis of the FARO3D scanner. Equations (2.11)-(2.26) will be used to compute the erosion volume and erosion depth as close to the test results as possible using the validated OpenFOAM data from experiment K101 and K114. The grass revetment after experiment K101 is almost undamaged allowing for greater erosion resistance which is accounted for by the different detachability coefficients and artificial grass cohesion.

3.4.1 Cover strength

Little information was available about the properties of the grass of the Lauwersmeerdijk-Vierhuizengat. The erosion resistance of the grass cover, including the clay layer of the Lauwersmeerdijk-Vierhuizengat is poor, with an average water content of 30% (Klein Breteler, 2020). Therefore, the assumption has been made that the grass is of poor quality and the following empirical coefficients have been chosen for computing the erosion (following Hoffmans et al., 2008, Stanczak et al., 2007 and Stanczak et al., 2008). The coefficients have been chosen based on suggested ranges by the abovementioned authors and are given in Table 3-3. Head cut erosion parameters are excluded from the table and calibrated separately described in section 3.4.5.

Coefficient	Coefficient symbol	Source	Value grass	Value clay
Damping coefficient erosion depth	w [-]	Stanczak et al. (2007) & Stanczak et al. (2008)	-	2
Damping coefficient erosion volume	w [-]	Stanczak et al. (2007) & Stanczak et al. (2008)	-	0.25
Detachability coefficient erosion depth	$k_{d,p,i}/k_{d,g,p,i}$ [m^3/N]	Stanczak et al. (2007) & Stanczak et al. (2008)	-	1.09
Detachability coefficient erosion depth	$k_{d,p}/k_{d,g,p}$ [cm^3/kPa]	Stanczak et al. (2007) & Stanczak et al. (2008)	-	$0.55*10^{-12}$
Empirical coefficient	A [-]	Stanczak et al. (2007)	1.58	-
Empirical coefficient	D [-]	Stanczak et al. (2007)	0.75	-
Empirical coefficient	d_{cor} [-]	Stanczak et al. (2007)	2	-
Depth under surface	d [cm]	Stanczak et al. (2007)	Increases during test	-
Empirical coefficient	b [-]	Stanczak et al. (2007)	5	-
Water content	wc [-]	Husrin (2007)	-	0.3

Weight percentage soil	$c_{\%}$ [%]	Temple and Hanson, (1994)	-	82.4
Grain size	d [mm]	Hoffmans et al. (2008)	-	10^{-3}
Sediment coefficient	M [kg/(m^{2}s]	Hoffmans et al. (2008)	-	$2*10^{-4}$
Soil density	ρ_s [kg/m^3]	Hoffmans et al. (2008)	-	1700
Water density	ρ_w [kg/m^3]	Hoffmans et al. (2008)	1000	1000
Turbulence intensity	r_0 [-]	Hoffmans et al. (2008)	0.2	0.2
Timestep	t [s]	Hoffmans et al. (2008)	0.1	0.1
Strength parameter	C_E [m^{-1}/s^{-1}]	Hoffmans et al. (2008)	$0.033*10^{-4}$	$4.3*10^{-4}$
Clay cohesion	c_s [kN/m^2]	Hoffmans et al. (2008)	-	0
Grass cohesion	σ_g [kN/m^2]	Hoffmans et al. (2008)	5.6	-

Table 3-3 Coefficients used in equations (2.11)-(2.26) for computing erosion volume and erosion depth.

3.4.2 Calibration of erosion coefficients representing cover strength

Some of the erosion coefficients given in Table 3-3 have to be calibrated because of the large uncertainty regarding clay and grass cover strength. The empirical values of the detachability coefficient, damping coefficient, sediment coefficient and grass cohesion have been chosen for calibration because the soil and grass properties are unknown and the aforementioned parameters are the most uncertain. Single and multivariate analysis have been performed to determine the optimal value of multiple constants over possible ranges found in (Stanczak et al., 2007, Stanczak et al., 2008 and Hoffmans et al., 2008) summarized in Table 3-4.

Optimized coefficient	Symbol	Suggested range	Source	Tested ranges K101	Tested ranges K114
Damping Coefficient erosion depth	w [-]	0.1 - 4	Stanczak et al. (2007) & Stanczak (2008)	0.1 - 4	0.1 - 4
Damping Coefficient erosion volume	w [-]	0.1 - 4	Stanczak et al. (2007) & Stanczak et al. (2008)	0.1 - 4	0.1 - 4
Detachability coefficient erosion depth clay	$k_{d,p,i}$ [m^3/N]	$0.1*10^{12}$ – $0.7*10^{12}$	Stanczak et al. (2008)	-	0 – $0.5*10^{-6}$
Detachability coefficient erosion depth grass	$k_{d,g,p}$ [m^3/N]	$\frac{k_{d,p,i}}{b \times RVR^2}$	Stanczak et al. (2007)	0 – 10^{-8}	-
Detachability coefficient erosion volume clay	$k_{d,p}$ [cm^3/kPa]	0.85 – 1.09	Stanczak et al. (2007) & Stanczak et al. (2008)	-	10^{-4}-0.01
Detachability coefficient erosion volume grass	$k_{d,g,p}$ [cm^3/kPa]	$\frac{k_{d,p}}{b \times RVR^2}$	Stanczak et al. (2008)	10^{-6}– 10^{-3}	-
Sediment coefficient erosion depth	M [kg/(m^{2}s]	10^{-5}– $5*10^{-4}$	Hoffmans et al. (2008)	10^{-4}– 0.1	10^{-5}– 10^{-3}
Sediment coefficient erosion volume	M [kg/(m^{2}s]	10^{-5}– $5*10^{-4}$	Hoffmans et al. (2008)	10^{-6}– 10^{-4}	10^{-4}– $5*10^{-3}$
Grass cohesion	σ_g [kN/m^2]	2.8 – 11.2	Hoffmans et al. (2008)	2.8 – 8.4	-

Table 3-4 Possible ranges for different coefficients when calculating the erosion volume and depth (after: Stanczak et al., 2007, Stanczak et al., 2008 and Hoffmans et al., 2008).

The parameters in Table 3-4 have been chosen because they affect the clay and grass strength, the RVR of the grass cover layer is omitted by changing the grass detachability coefficient directly, because no knowledge about the grass strength is available. Initially, a global search was conducted to determine the general range the parameters as shown in Table 3-4 had to be calibrated. The ranges given in Table 3-4 were then used to determine the best fit for erosion volume and erosion depth of the 2D grass revetment profile between the experiment and OpenFOAM model results. The clay cohesion coefficient c_s [kN/m^2] has not been calibrated in the single and multivariate analysis since the cohesion of poor quality clay is 0 kN/m^2 and calibrated coefficients are greater than values in suggested ranges. Increasing clay cohesion will only further increase values of other calibrated coefficients. Varying the grass cohesion also varies the critical shear stress and critical flow velocity calculated using equations (2.20) and (2.23) because the critical flow velocity and shear stress are influenced by grass and clay cohesion.

Multivariate sensitivity analysis was conducted separately on erosion relations in equations (2.11) and (2.16) varying the detachability and damping coefficient and in equations (2.19) and (2.21) varying the sediment parameter and grass cohesion used to compute the critical shear stress and critical flow velocity. The erosion volume and depth were then computed using 50 different values equally spread in the ranges given in Table 3-4 resulting in a 50 x 50 grid with erosion profiles calculated using varying empirical parameters. The computed erosion profile with the maximum erosion depth and volume closest to the delta flume experiments as shown in Table 3-5 were chosen as most accurate. The accuracy of the computed erosion profile is determined using the coefficient of determination and RMSE as further discussed in section 3.4.6.

While conducting the calibration of the parameters given in Table 3-4, several ranges were tested before accurate results could be found. The ranges given in Table 3-4 show values that are above and below the optimum value. In the multivariate sensitivity analysis, multiple combinations of parameters could be chosen to compute the erosion. However, the chosen combination of parameters for each calibrated erosion relation shows the highest similarity to the measured erosion depth and volume as occurred during the delta flume experiments.

3.4.3 Hydraulic load

Wave impact erosion occurs when a wave impacts the slope of the dike and exerts high dynamic pressures for a short duration causing movement of the soil in the dike (Van Hoven, 2015). Wave run-up erosion occurs when a critical shear stress or flow velocity has been exceeded. Peak values for flow velocity, shear stress and dynamic pressure have been determined as well as the half width of each peak to quantify the effect of wave impacting the dike slope. The width of the peak shows the duration of the impact in seconds and multiplying the width at half the peak prominence with the peak value resulted in the approximated surface area of the peak which has been used to compute the total impact pressures and shear stresses for each wave impact.

Peak values of the flow velocity, shear stress and dynamic pressure have been obtained for all 25 probes evenly spread above the grass revetment surface. The number of peaks at the probing location on the transition (X = 179.6 m) are roughly equal to the number of waves that impact the dike while the amount of peaks reduces higher up the grass revetment slope. The calibration was performed by changing the minimal duration between two peaks and a minimum peak prominence. Where a minimum duration between peaks of 2 s and a minimum peak prominence of the maximum value divided by 15 have been chosen to determine the peak values. The probe at the transition has been chosen for peak calibration because it is the lowest (Y = 6.4 m) and almost all waves impact this location. The amount of

peaks per probe location depends on the location of the probing location on the grass revetment slope, with less peaks higher up the slope.

The width of each flow velocity peak at half prominence has been used as the duration of the time step for equation (2.21). The noisy data from the small peaks that occur in between of each wave impact, have not been measured. The positive and negative peak velocities and shear stresses have been separated, in order to distinguish wave run-up and run-down erosion.

3.4.4 Erosion calculations

The erosion computed using equations (2.11)-(2.26) is compared to the erosion depth and volume measured using the FARO3D laser scanner data from experiment K1. The first 30 s of the 600 s simulation were ignored because waves had not reached the dike during that time. Scaling for the simulated duration of 570 s, the computed erosion using the OpenFOAM data of the model of Lauwersmeerdijk-Vierhuizengat test K101 and K114 should be close to the values shown in Table 3-5.

	K101	K114
Duration experiment [h]	1.96	1.17
Maximum erosion depth increase during test [m]	0.0735	0.206
Erosion volume increase during test [m^3/m]	0.0893	0.969
Depth increase scaled to duration simulation [m]	*0.00239*	*0.0670*
Volume increase scaled to duration of simulation [m^3/m]	*0.00717*	*0.0778*

Table 3-5 Increase in erosion volume and depth during OpenFOAM simulation for test K101 and K114 (after: Deltares, 2020).

The erosion volume computed with equations (2.4) and (2.17) gives the erosion per meter and since the probes have a spacing of approximately 40 cm is the erosion volume multiplied by 0.4. The maximum erosion depth and erosion volume give a sense of scaling for the calibration process, while the calibrated results will be compared against the difference in erosion profiles between K101 – K103 and K113 – K114 from the delta flume experiment.

3.4.5 Head cut advance eroded grass revetment profile

Computing the erosion depth and volume can describe the change in erosion profile of experiment K101. However, a cliff is present between 185 m and 188 m in the dike profile of experiment K114 with eroded grass cover and clay layer. The total height difference is approximately 1.75 m and erosion rate in this area is significantly higher than predicted using the empirical relations for erosion depth and volume. Therefore, the empirical relations from equations (2.23)-(2.31) were used to compute the cliff erosion for profile K114 between 185 m and 188 m, since that is the only location where a significant cliff is present.

Cliff erosion is computed using peak flow velocity run-up and water depth data from the OpenFOAM models. Cliff erosion is computed in m/h which has been scaled to m/s and multiplied with the half width of each flow velocity peak to obtain the erosion per wave impact. Only wave run-up data used since the relations from equations (2.23)-(2.31) were used for computing cliff erosion for overtopping waves, where wave run-down is not present. Therefore, cliff erosion due to wave run-down is not described in Van Hoven (2014) and neglected because the effect of cliff erosion due to wave run-down is unknown.

The soil parameter $\mathrm{K_h}$ found in equations (2.23)-(2.31) has been calibrated as a whole since the exact properties of the clay in the dike cover layer are unknown. Initial values of M_s = 0.1, K_b = 1, J_s = 1 and $\mathrm{K_d}$ = 0.47 have been assumed but gave no favourable results. During calibration it was noticed that the soil parameter is sensitive. Therefore, the soil parameter has been calibrated using 100 values in the narrow range between 0.01 and 0.02 [-] which

falls in low end the range of the suggested value for the soil parameter (NRCS, 1997). The effect of head cut erosion has been added to the wave erosion depth due to wave impact and run-up computed with equations (2.11)-(2.23). The head cut erosion has been calibrated separately to fit the computed wave impact and run-up erosion profile more accurately. To fit the experiment erosion profile, a head cut erosion model was used 2 m in seaward direction and 1 m in landward direction to the location of the cliff.

3.4.6 Model accuracy

The coefficient of determination and RMSE were used to determine how well the calibrated relations described in equations (2.11)-(2.26) for computing wave impact and run-up erosion can predict the erosion from the delta flume experiments. The coefficient of determination is computed using equation (2.32) and the RMSE is computed using equation (2.33). The model with the lowest RMSE is the most accurate compared to the data. However, this does not directly mean that the model with the lowest RMSE is accurate. Therefore, the coefficient of determination is defined, which is a value between 0 and 1 indicating how well the model predicts the data. Although mostly used for linear models, the coefficient of determination can still provide information about the model quality.

The erosion from the delta flume experiment determined as the difference between the erosion profiles of two tests is compared against 2 erosion models predicting wave impact erosion, and 2 models predicting wave run-up erosion, for the erosion of test K101 and K114. For the erosion of test K114 the coefficient of determination and RMSE were also determined for the models, including head cut erosion.

4 Results

4.1 Measured erosion depth and volume during the delta flume experiments

The maximum erosion depth and total erosion volume were obtained from the delta flume experiments and summarized in Table 4-1. The profile, erosion volume, maximum erosion depth and surface figures of the dikes after each test in all the experiments are shown in Appendix A.

Exper-iment	Profile	Clay origin	Clay quality	Maximum erosion depth [m]	Total erosion amount [m^3]
K1	Lauwersmeerdijk-Vierhuizengat	Lauwersmeer-dijk	poor	1.552	15.261
K2	Koehool-Lauwersmeerdijk	Holwerd	high	0.280	0.723
K3	Koehool-Lauwersmeerdijk (lowered berm)	Holwerd	high	0.924	5.865
K4	Lauwersmeerdijk-Vierhuizengat	Blija	high	1.465	13.162
K5	Koehool-Lauwersmeerdijk with 2 blocks with dry grass	Holwerd	high	0.579	1.280
K6	Koehool-Lauwersmeerdijk with berm, 2 blocks with dry grass	Holwerd	high	1.101	8.100

Table 4-1 Maximum erosion depth and volume for each experiment.

In the following sections, the erosion during each experiment is analysed as a percentage of maximum per test and scaled to the duration of each test. Artificial damage was created after some of the tests in the beginning of most experiments in order to accelerate the erosion process during the delta flume experiments. The effect of added artificial damage on the results are discussed in appendix B and also mentioned in the discussion.

4.1.1 Percentual change erosion depth and volume

Figure 4-1 shows the development of erosion over the tests in each experiment where the maximum erosion depth and total erosion volume is compared to the maximum of each test.

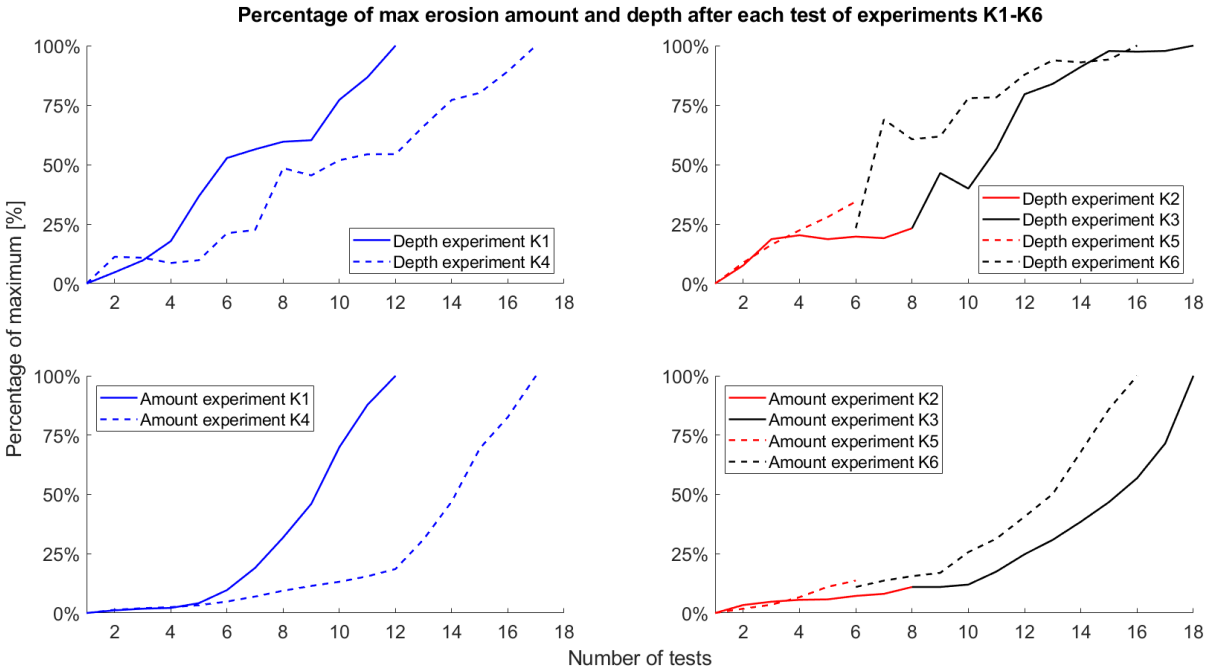

Figure 4-1 Percentage of erosion depth and volume of each test to the maximum of the experiment for Lauwersmeerdijk-Vierhuizengat (K1 and K4) differencing in clay quality and Koehool-Lauwersmeerdijk (K2-K3 and K5-K6) differencing in grass quality.

The difference in the total erosion depth and total volume between experiments is accounted for by relating the erosion to the maximum percentage. Experiment K1 and K4 of the Lauwersmeerdijk-Vierhuizengat profile (Figure 4-1) show the effect of clay quality on development of erosion. The erosion depth development is similar, but the stronger quality of clay results in strong erosion of the clay after test 7 (for experiment K4) instead of after test 4 (for experiment K1). The main effect of clay quality on the development of erosion depth seems to be increased resistance during the first 6 h of wave attack, which are the first 7 tests of experiment K4. The effect of the stronger clay quality on erosion volume is mainly visible between test 5 and 12 where the erosion rate of experiment K4 is significantly lower than that of experiment K1. The relative erosion volume of the first 5 tests of experiments K1 and K4 is very similar, likely due to the strength of the grass cover, which is the same for experiment K1 and K4.

The effects of the dried out grass blocks (grass blocks after a dry summer) is visible in the erosion rate difference between experiment K2 and K5 of the Koehool-Lauwersmeerdijk. Experiments K3 and K6 are a continuation of these experiments but the grass cover has then mostly eroded. The initial difference in the grass erosion depth and volume is minimal while after the third test the erosion rate of experiment K5 becomes much higher than that of experiment K2. Therefore, the effect of the dried grass is mostly visible during the time it takes to erode the grass cover while the erosion rate until grass cover failure is identical. The erosion depth and volume development between experiment K3 and K6 are similar. The difference in the grass cover quality does not seem to have a significant effect on the erosion of the underlying clay layer, which is shown using the black lines in Figure 4-1 for experiment K3 and K6.

In general, there is a clear difference visible between the development of erosion depth and erosion volume, where the erosion depth increases linearly and the erosion volume increases exponentially during the experiment. Therefore, an increase in erosion volume does not directly indicate a significant increase in erosion depth. Erosion depth increases

faster than the erosion volume in the first half of each experiment, while erosion volume increases faster than the erosion depth in the second half of each experiment.

4.1.2 Erosion experiments scaled to duration of tests

The duration of each experiment varies significantly due the the erosion rate, amount of tests and duration of these tests. Using the duration of the experiments, the erosion results have been adjusted for the duration of each test by deriving the maximum erosion depth and erosion volumes per minute. The amount of erosion changes during the test, which was not measured with the FARO3D laser scanner.

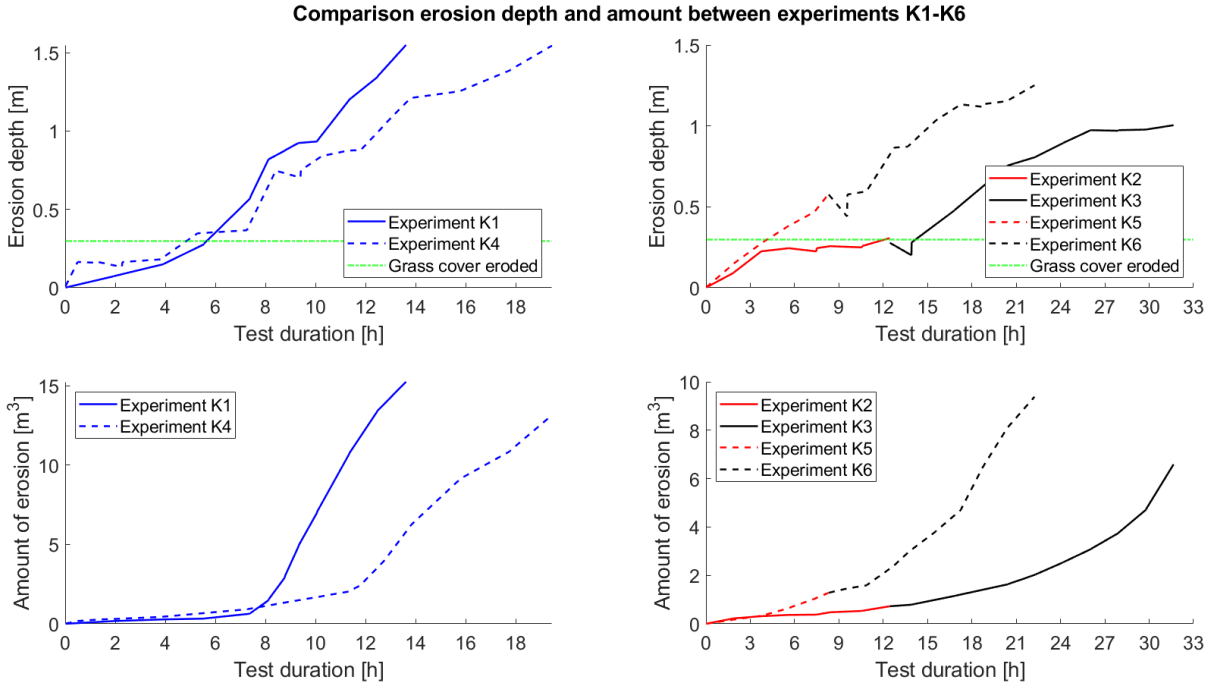

Figure 4-2 Erosion depth and volume scaled to the duration of wave impact for Lauwersmeerdijk-Vierhuizengat (K1 and K4) and Koehool-Lauwersmeerdijk (K2-K3 and K5-K6). The plots show the effect of the different clay qualities used in experiment K1 and K4 as well as the effect of dried out grass used in experiment K2 - K3 and K5 – K6.

The maximum erosion depth occurs at a different location in the dike profile for every test. Therefore, the figure shows the increase in maximum erosion depth over the whole profile, rather than the increase at one location. In addition, two clay blocks were stacked on top of each other for creation of the clay layer, where the grass cover has been removed for the bottom blocks (Klein Breteler, 2020). However, not all roots were removed, causing significant stagnation in the increase in erosion depth between 0.75 and 0.9 m, mainly visible in experiment K1 and K4.

Comparing experiment K1 with K4 in the left plots of Figure 4-2, no significant difference in erosion volume or depth is observed until the grass cover has eroded. The grass cover has eroded when an erosion depth of approximately 0.2 - 0.3 m has been reached, indicated by the green lines and also characterized by the sharp increase in erosion volume in Figure 4-2. The large increase in erosion volume during experiment K1 occurs after 8 h of impact, while a similarly large increase in erosion volume during experiment K4 occurs after 12 h of impact. Therefore, the increase in clay quality could increase the clay erosion resistance by 50%. The wave impact duration of experiment K1 was 817 minutes, while the impact duration of experiment K4 was 1167 minutes. Comparing experiment K1 with experiment K4 shows that the increased erosion resistance, by using clay from Blija instead of clay from the

Lauwersmeerdijk-Vierhuizengat, contributes to a roughly 35% increase wave attack duration for similar erosion results.

The almost exponential increase in erosion volume occurs for both experiment K1 (low quality clay) and experiment K4 (high quality clay) after an erosion depth of 0.8 m has been reached. However, the increase in clay quality has limited effect on erosion resistance of the grass cover. Therefore, when following WBI (2017) classifying failure when an erosion depth of 0.2 m is reached, higher clay quality does not seem to yield significantly higher erosion resistance. However, the effect of stronger clay quality on erosion rate becomes significantly larger after an erosion depth of approximately 0.5 m has been reached. Consequently, grass cover quality seems to be the dominant factor for determining erosion resistance in the grass cover layer.

Comparing experiment K2 – K3 (normal grass) with experiment K5 – K6 (dried out grass) in the right plots of Figure 4-2, initially the dried grass cover does not erode faster, but after 3 h of wave impact significant difference in erosion rate is observed. The test set up for the dikes used in experiment K2 – K3 and K5 – K6 both use clay of high quality from Holwerd. The clay layer underneath the grass cover also has a higher erosion rate and is likely affected by the drought when comparing the erosion of experiment K3 with K6. Grass roots in experiment K5 seem to be significantly less erosion resistant than grass roots in experiment K2, as the grass cover erodes three times as fast (4 h vs 12 h). Lastly, and initial decrease in erosion depth at the start of experiment K3 and K6 is observed.

4.1.3 Increase in erosion depth versus erosion volume

It was noticed that the erosion depth increases faster than the erosion volume when there is hardly any erosion present in the run-up zone of the dike. The erosion depth increases faster when the erosion volume increases. This indicates that the grass cover makes it harder for erosion to spread and will therefore become deeper, eroding the more vulnerable clay layer. The erosion depth versus the erosion volume is depicted in Figure 4-3 where the difference depends on the amount of erosion. The highest amount of erosion occurred in experiment K1, where the difference between erosion depth and volume is the largest.

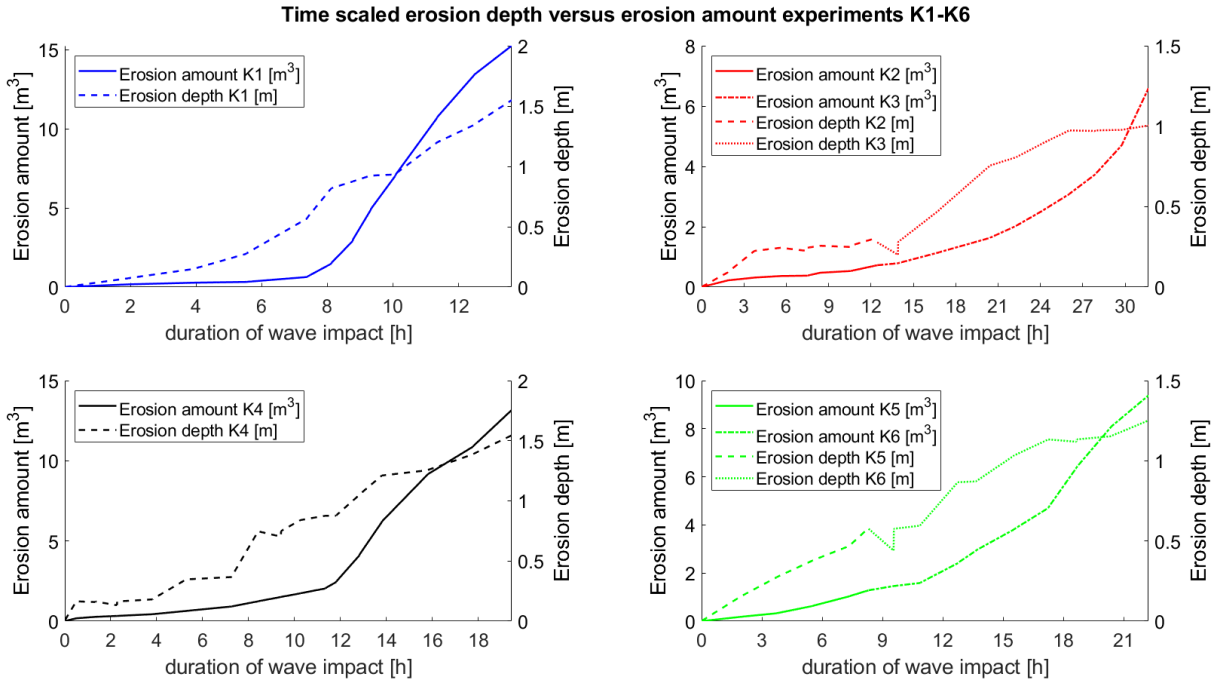

Figure 4-3 Erosion depth versus erosion volume for experiments K1, K2-K3, K4 and K5-K6 showing duration of wave impact in hours on the x-axis and the erosion depth in m and erosion volume in m^3 on the y-axis.

Figure 4-3 also shows that the development of erosion depth and volume in each experiment is similar with the same exponential increase halfway in the experiment and exponential decrease near the end. Therefore, the development of the erosion volume and depth of experiments K2 and K3 will likely be very similar to that of experiments K5 and K6 if the experiment would be prolonged. The erosion starts at the transition for all the experiments, except experiments K3 and K6 since these are continuations of experiments K2 and K5 and already have some erosion.

4.2 OpenFOAM validation

4.2.1 Wave characteristics

The OpenFOAM models of test K101 and K114 were calibrated by changing the wave height in the steering file generation of OCW3D. The wave height is the only parameter from the steering files that can be altered in OCW3D by changing the value of POT (shown in Table 4-2). The steering files contained an initial significant wave height for test K101 and K114 of 2.3 m, which has been lowered to 1.8 m to match the experimental wave height. The measured and calculated significant wave heights for simulation durations of 600 s for both OpenFOAM models, are shown in Table 4-2.

	Erosion simulation test K101 [600 s]	Erosion simulation test K114 [600s]
Hs incoming simulated [m]	1.79	1.86
Hs incoming experiment [m]	1.82	1.86
Hs reflected simulated [m]	0.59	0.68
Hs reflected experiment [m]	0.59	0.62
POT [-]	0.83	0.88

Table 4-2 Significant wave heights modelled and measured data.

Cross-correlation analysis is conducted to obtain the highest similarity between simulated and measured waves, which resulted in a sinusoidal shape that diffuses over higher lags due to lower similarity. The highest correlation for the incoming waves occurred for all simulations at a lag of approximately 5.5 – 6.5 s, leading to a probable delay between the experiment wave data and modelled wave data of 5.5 – 6.5 s.

The correlation between the simulated waves and measured waves is determined for every lag with an interval of 0.05 s. The profiles for test K101 fitted the most accurate at a lag of 127, or a model spin up time of 6.35 s. The cross-correlated incoming wave height for test K101 is shown in Figure 4-4.

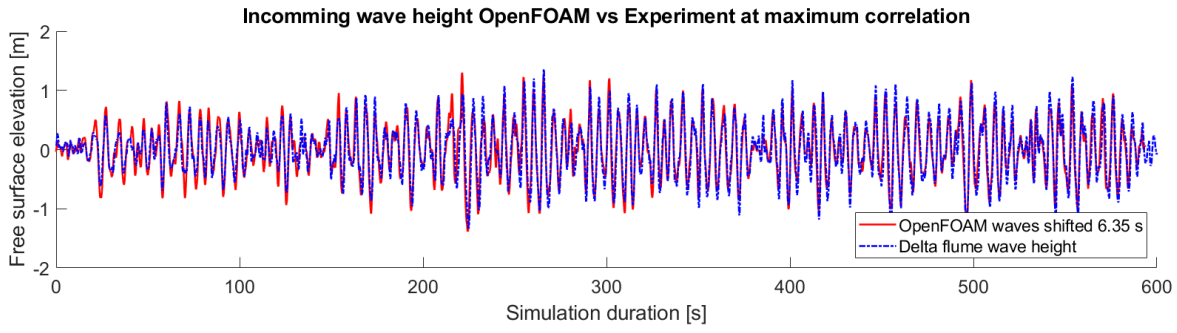

Figure 4-4 Shifted modelled incoming wave signal over experiment and wave signal from test K101.

The plot in Figure 4-4 shows the OpenFOAM wave height as the red line and the experimental wave height as the blue dashed line. The wave period of both data sets show a high level of similarity at the specific abovementioned lag. Figure 4-4 shows that the OpenFOAM model of experiment K101 generally overestimates the wave height in the first 250 s of simulation, while the wave height from the delta flume experiments is generally higher during the rest of the simulation duration. The waves in the delta flume need more time to develop than the waves in the OpenFOAM experiment. This might be caused by a slightly lower friction in the model compared to the friction in the delta flume.

The same cross-correlation has been conducted on the simulated and measured waves of experiment K114, showing highest accuracy at a lag of 108, a model spin up time of 5.9 s. The cross-correlated incoming wave height for test K114 is shown in Figure 4-5.

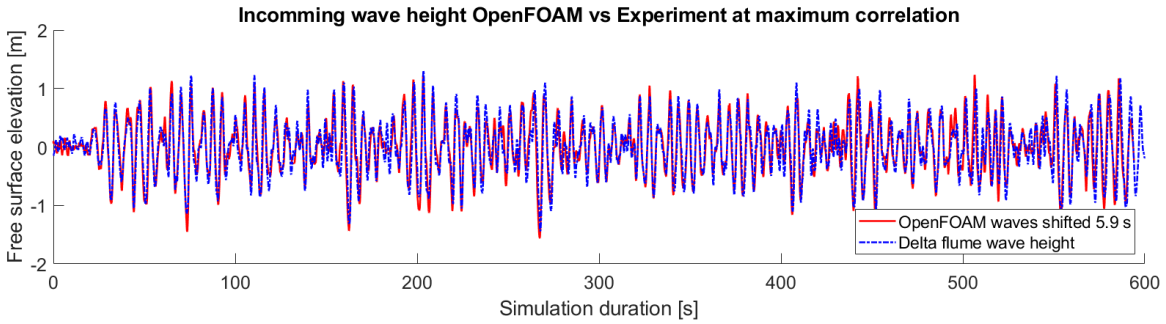

Figure 4-5 Shifted modelled incoming wave signal over experiment and wave signal from test K114.

The waves in Figure 4-5 show highest correlation at a lag of 118, a model spin up time of 5.9 s and do not seem to overestimate the waves during the first part of the simulation as occurred during the simulation of experiment K101.

The wave energy density spectrum from the model is determined to further validate the model performance. The energy density spectrum of experiment K101 and K114 is shown in Figure 4-6, where high similarity is reached between the model and experiment for the incoming waves.

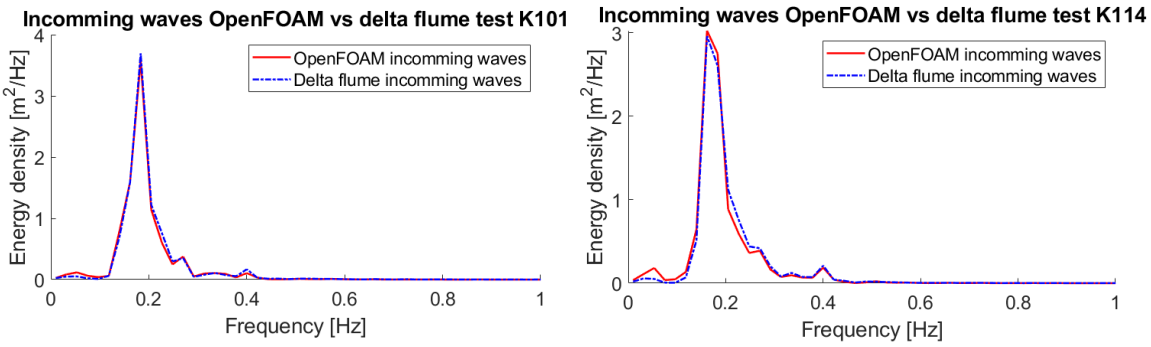

Figure 4-6 Energy density and frequency of incoming and reflected waves, OpenFOAM model K101 vs experiment K101.

4.2.2 Impact pressure

To validate the simulated impact pressures, the 10%, 5% and 2% exceedance dynamic pressures using the p_rgh and the total(p) – p pressure from the OpenFOAM model of test K101 on the dike surface against emperical relations (2.1) - (2.4) have been plotted in Figure 4-7 and Figure 4-8. The dotted black lines show the calculated maximum dynamic pressures using the emperical relations in equations (2.1) - (2.4), the red line shows the dynamic

pressure using total(p) – p and the blue line shows the dynamic pressure using the p-rgh from OpenFOAM.

The results fit better to the 10% exceedance pressures than to the top 2% and 5% of maximum pressures. The 10% exceedance pressures using the emperical relations in equations (2.1) - (2.4) are underestimating the dynamic pressures, because of the limited amount of 100 waves used as calibration data (Horstman, 2020). This is roughly the same amount of waves as used in the OpenFOAM models of test K101 and test K114. Therefore, the simulated 10% exceedance pressures are accurate to the emperical relations. The pressures in Figure 4-7 and Figure 4-8 are lower than the 2% and 5% maximum calculated values above the berm. One of the likely causes for the lower values is that the grass revetment is situated mostly above the wave impact point, not receiving the largest wave impact. The maximum impact pressure occurs at the wave impact location (Stanczak et al., 2008) which, in the models of test K101 and K114 is at the berm below the grass revetment, between 175 m and 178 m in Figure 4-7. Additionally, the emperical relations in equations (2.1) - (2.4) compute the maximum impact pressure of the wave, thus not the maximum impact pressure at every location. Therefore, it is possible that the simulated pressures are lower than the pressures calculated using the empirical equations. Secondly, the simulated pressures are possibly lower because of the limited amount of roughly 100 waves that were simulated. Simulating a larger number of waves likely results in higher 2%, 5% and 10% exceedance pressures which come closer to the values computed with equations (2.1) - (2.4).

The 2%, 5% and 10% exceedance pressure distribution over the dike slope for test K101 in Figure 4-7 shows that the maximum dynamic pressures on the grass revetment occur at the transition and decrease over the slope towards the crest. This is as expected since lower dynamic pressures occur further away from the wave impact zone (Stanczak et al., 2008).

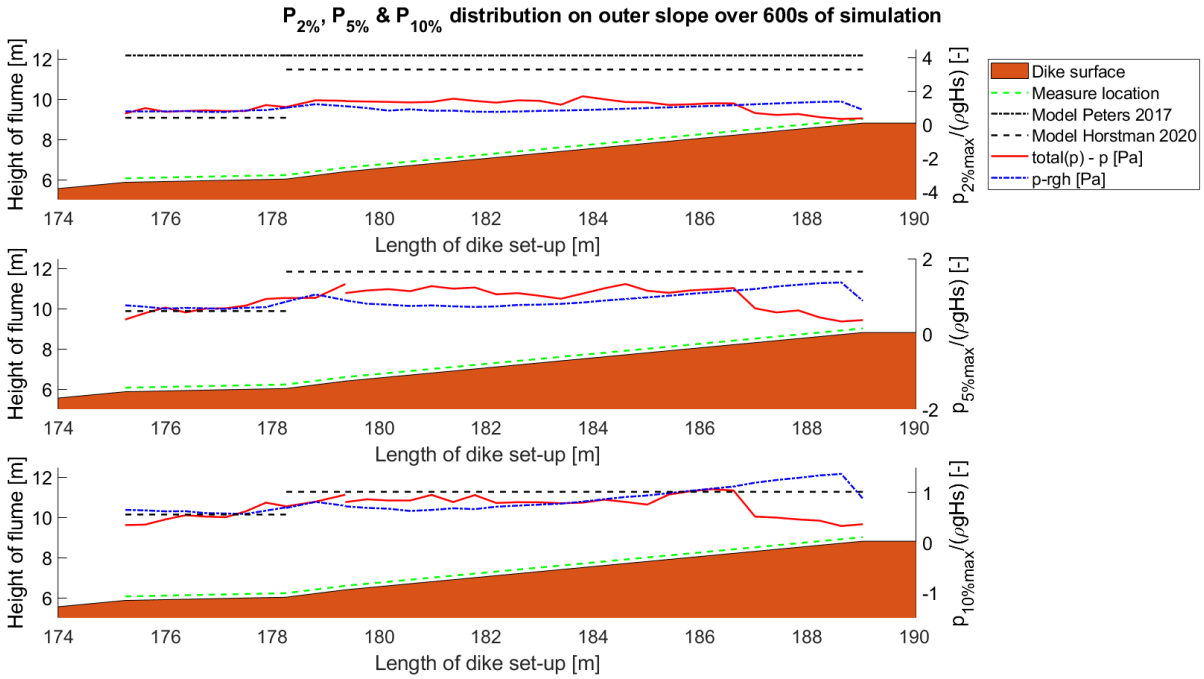

Figure 4-7 Normalized 2%, 5% and 10% exceedance impact pressures on the grass revetment surface from experiment K101 over roughly 600 s of wave impact.

The 10%, 5% and 2% exceedance dynamic pressures on same location as in test K101, have been obtained for test K114, showing similar dynamic pressures when comparing the blue lines of Figure 4-7 and Figure 4-8. The red line shows a different pressure distribution

with most dynamic pressure at the cliff between 185 m and 188 m in Figure 4-8. The grass revetment slope between 180 m and 185 m is more sheltered from erosive forces, likely due to sheltering effect of scouring hole. Therefore, dynamic pressures are not attenuated until the waves reach the cliff between 185 m and 188 m, causing higher dynamic pressures towards the crest than at the transition.

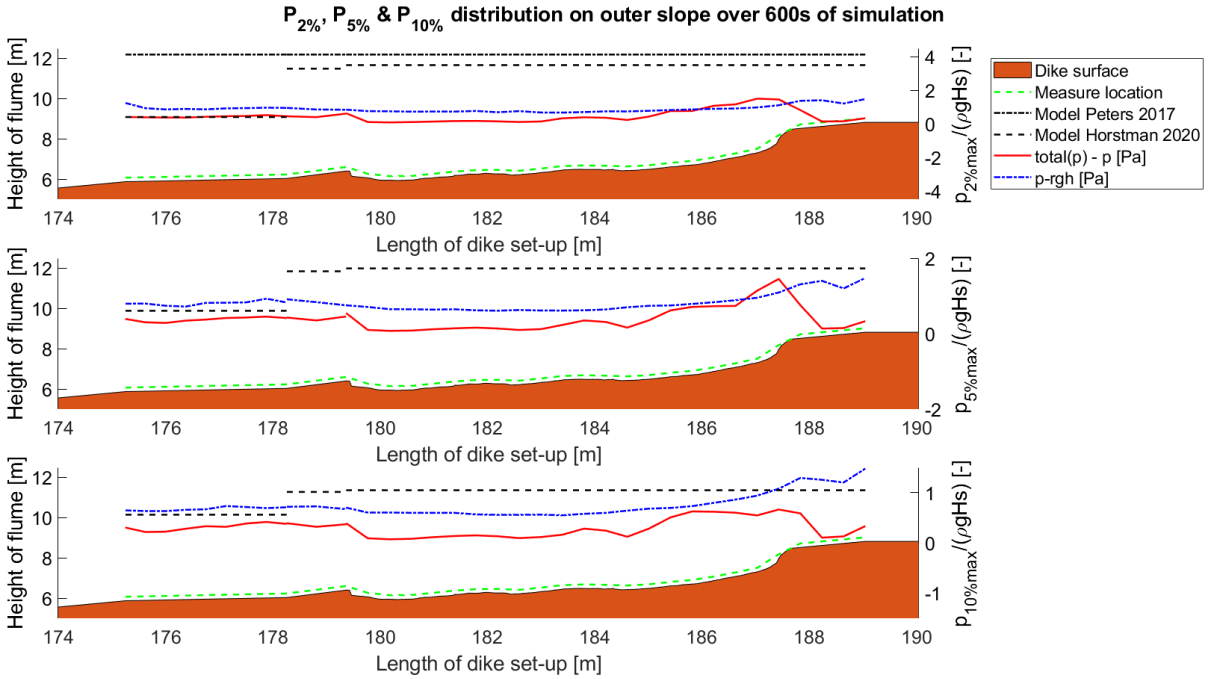

Figure 4-8 2%, 5% and 10% exceedance impact pressures on the grass revetment surface from experiment K114 over 600 s of wave impact.

4.2.3 Flow velocity

Figure 4-9 and Figure 4-10 show the velocities 0.2 m above the grass revetment surface in the top plot and the velocities over depth at the transition in the bottom plots. The black dashed lines in the top plot of Figure 4-9 and Figure 4-10 show the 2% exceedance run-up flow velocity, computed with the empirical relations described in section 2.4. The red lines show the run-up velocities and the blue lines show the run-down velocities.

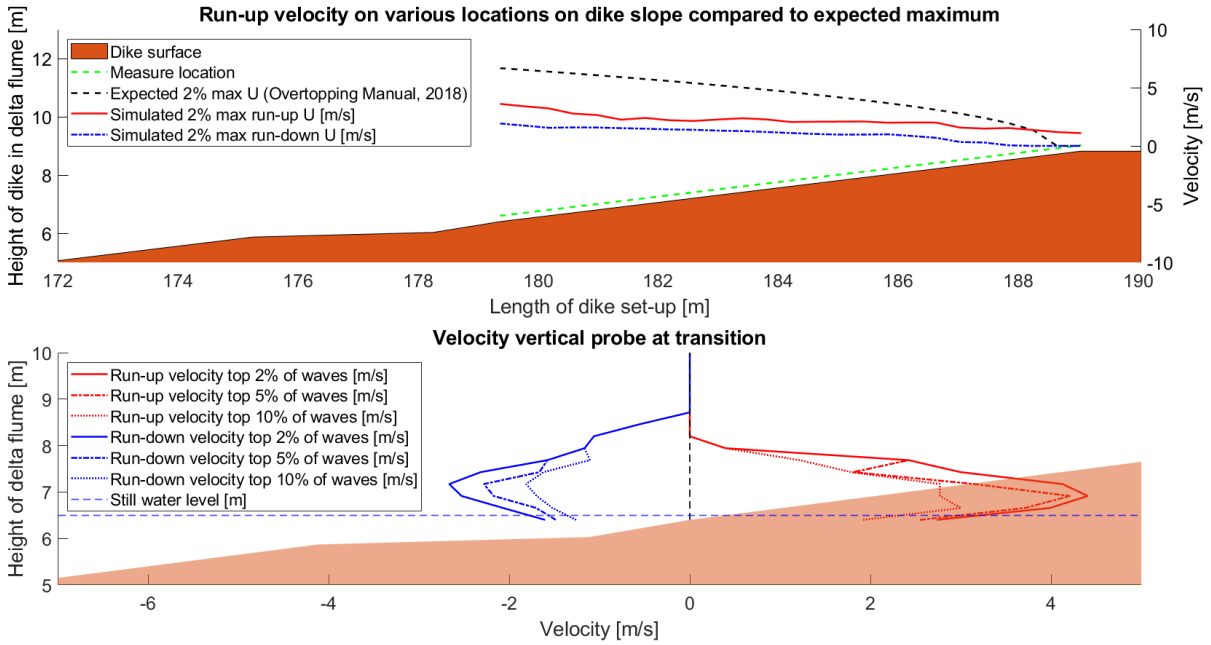

Figure 4-9 Simulated 2% exceedance flow velocity over grass revetment slope test K101 compared to calculated 2% exceedance flow velocity.

Figure 4-9 shows that the wave run-up flow velocity is higher than the run-down flow velocity, but the run-down water layer thickness is greater for experiment K101. However, the water layer thickness for the run-up and run-down velocities appear to be similar for experiment K114, although the maximum flow velocity for the run-down layer occurs at the surface due to the erosion hole. The maximum run-up flow velocity for test K101 and K114 occur near the bottom of the water layer.

The 2% exceedance flow velocity slowly decreases in magnitude when flowing over the outer slope towards the crest of the dike in test K101. However, the velocities towards the near vertical cliff in the eroded grass revetment profile of the dike in test K114 are much higher than at that location in test K101, suggesting that the forces of the wave hardly get attenuated over the eroded slope. Dynamic pressures of similar magnitude were measured in the same location suggesting high levels of erosion. Lastly, more erosion will probably be caused by wave run-down between 180 m and 182 m of test K114, because of the difference in velocities.

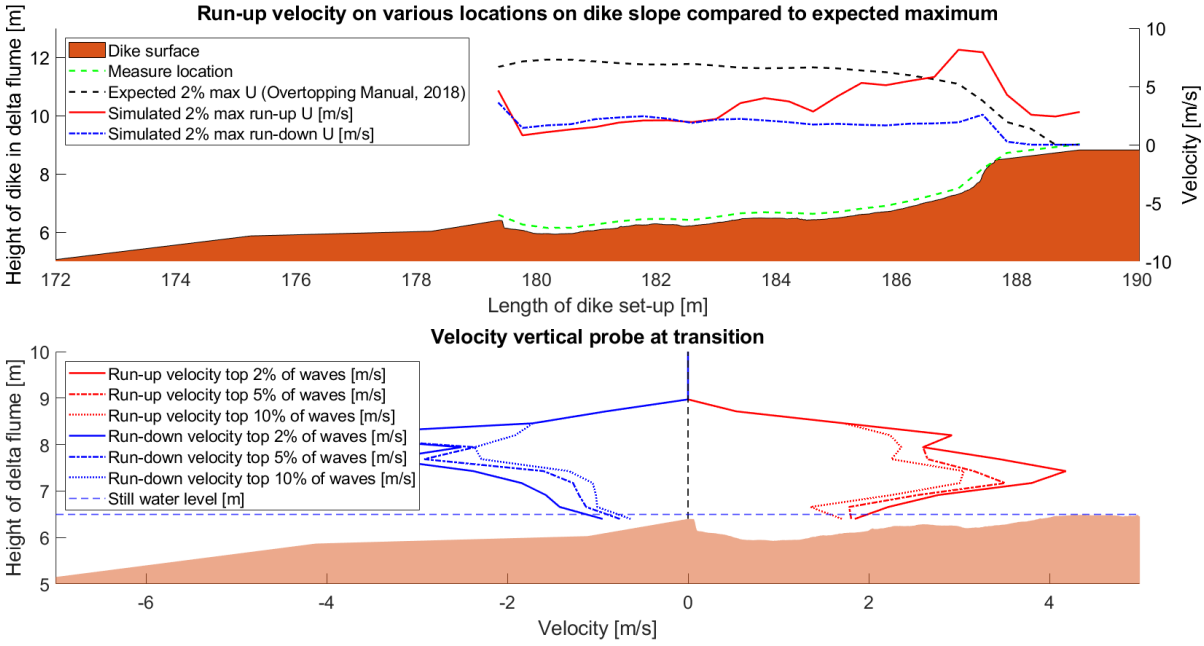

Figure 4-10 Simulated 2% exceedance flow velocity over grass revetment slope test K114 compared to calculated 2% exceedance flow velocity.

4.2.4 Effect of eroded profile on model results

The effect of the eroded grass revetment profile is determined by comparing the dynamic pressure, velocities, water depth and shear stresses on the dike surface. Comparing the 10%, 5% and 2% exceedance dynamic pressures from the OpenFOAM models of test K101 and K114 directly in Figure 4-11, shows a clear difference in pressure distribution over the outer dike slope. In general, the dynamic pressures on the dike surface of test K101 are higher, probably due to the larger water depth during experiment K114. The erosion hole in the grass revetment fills up with water during wave impact, likely resulting in a damping effect of the impacting waves. The vertical cliff is present in the grass revetment slope between 186 m and 188 m in Figure 4-11, and in combination with the absence of a damping water layer probably results in higher dynamic pressures.

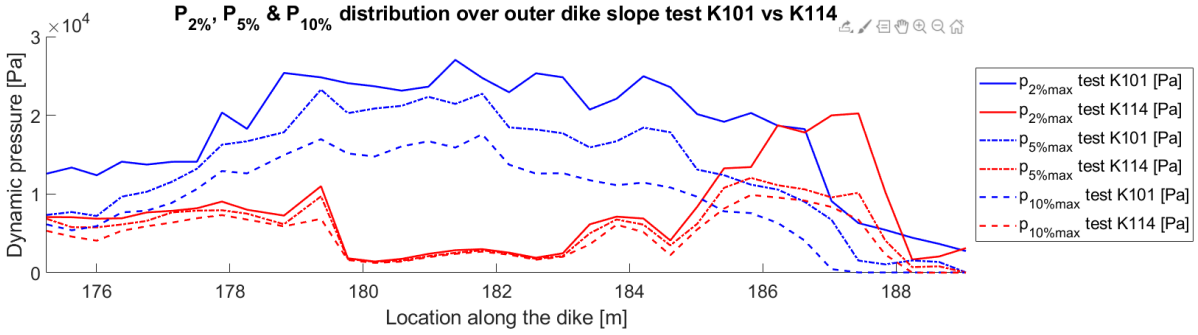

Figure 4-11 The 10%, 5% and 2% exceedance total(p) – p dynamic pressures on dike slope OpenFOAM model Lauwersmeerdijk-Vierhuizengat test K101 vs K114.

The effect of the eroded profile on the 10%, 5% and 2% exceedance flow velocity can be seen in Figure 4-12, where the velocities between the berm and transition to grass revetment are higher in test K101, while the velocities on the grass revetment area are higher during test K114. The velocities on the grass revetment surface are likely higher during test K114, due to the reduced friction because of the clay revetment even though the water depth is greater. The maximum run-up velocities of test K114 are especially high at the near vertical cliff, while run-down velocities during test K101 and K114 are similar.

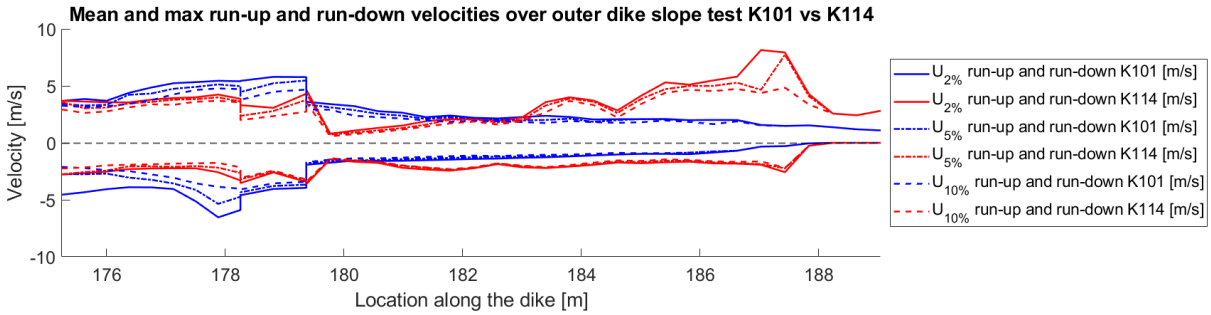

Figure 4-12 The 10%, 5% and 2% exceedance run-up and run-down flow velocities on dike slope OpenFOAM model Lauwersmeerdijk-Vierhuizengat test K101 vs K114.

The 10%, 5% and 2% exceedance shear stresses from both models, which were computed as a function of the flow velocity in OpenFOAM, visible in Figure 4-13, show a similar distribution as the run-up and run-down velocities. Again, a large shear stresses peak is visible near the cliff in test K114 and higher shear stresses are found at the berm and lower part of the grass revetment in test K101.

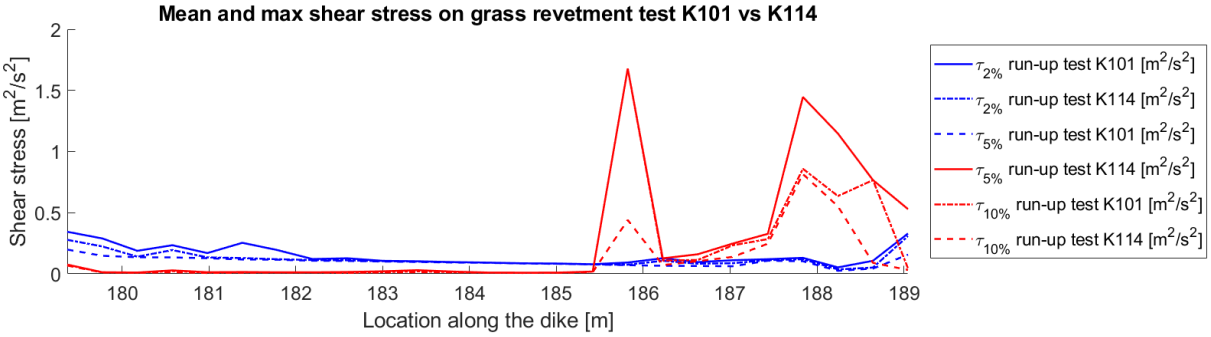

Figure 4-13 The 10%, 5% and 2% exceedance shear stresses on grass revetment OpenFOAM model Lauwersmeerdijk-Vierhuizengat test K101 vs K114.

Figure 4-14 shows a higher waterdepth in test K114 that is caused by the erosion hole which retained water, likely has a damping effect on the dynamic pressures and prevents attenuation of the run-up velocities. Therefore, lower impact pressures are present in test K114 compared to test K101 and are high maximum velocities measured at the cliff location, near the crest in test K114.

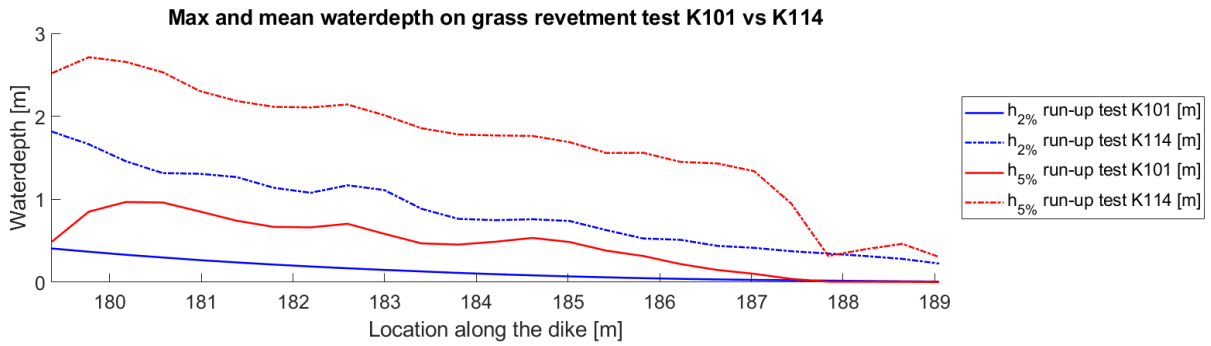

Figure 4-14 Mean and max water depth on grass revetment OpenFOAM model Lauwersmeerdijk-Vierhuizengat test K101 vs K114.

4.3 Erosion using the OpenFOAM output

The erosion was computed using the flow velocities, the pressures and the shear stresses obtained from the OpenFOAM model of experiments K101 and K114. The erosion has then been calculated using equations (2.11) - (2.31) using parameters provided in the Table 3-3.

4.3.1 Parameter calibration

The empirical parameters shown in Table 3-4 were calibrated using a multivariate sensitivity analysis. The results of the sensitivity analysis for experiment K101 can be found in Figure 4-15 showing four surfaces for each erosion relation.

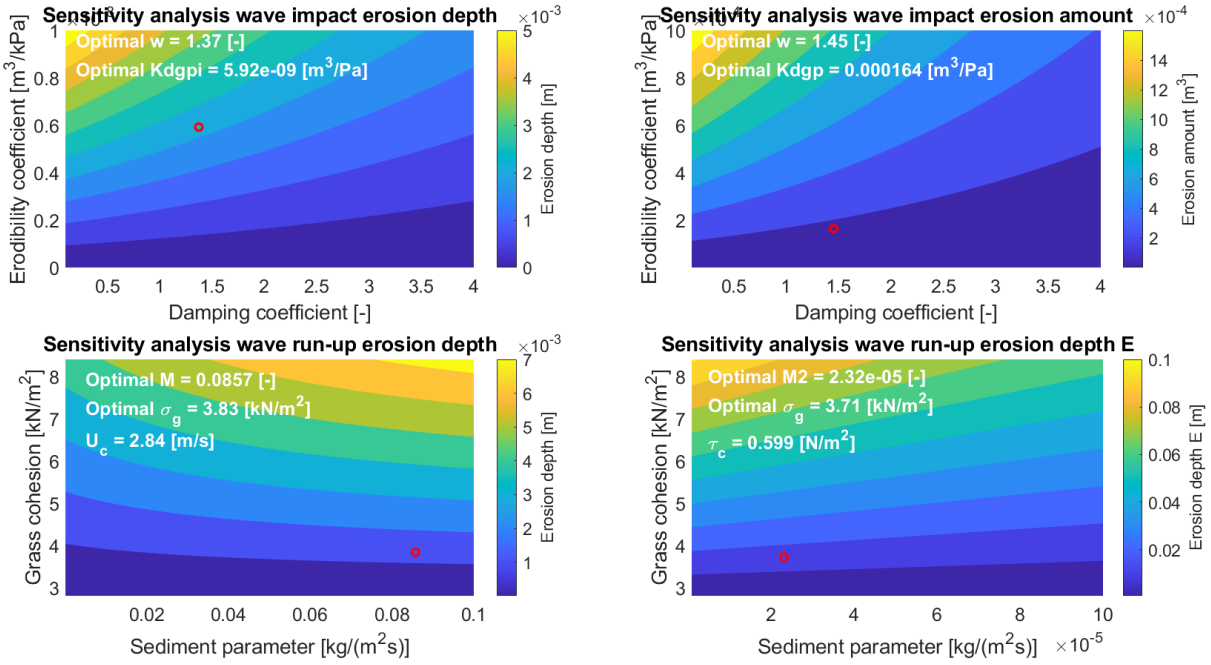

Figure 4-15 Results from multivariate sensitivity analysis on empirical parameters on wave run-up and wave impact erosion of experiment K101 (definitions found in the list of symbols).

The top two surfaces in Figure 4-15 show calibrated damping coefficients and calibrated grass erodibility coefficients. The damping coefficient (w) is in range of values found by Stanczak et al. (2007) and Stanczak et al. (2008), while the erodibility coefficients ($\mathrm{K_{dgpi}}$ and $\mathrm{K_{dgp}}$) differ significantly from the suggested ranges. Both parameters show to have significant effect on erosion results with the erodibility coefficient having more impact on the erosion results.

The two surfaces at the bottom of Figure 4-15 show the calibrated sediment parameters (M and $M2$) and grass cohesion (σ_g) from the wave impact erosion relations described in Hoffmans et al. (2008). The grass cohesion in the two bottom plots of Figure 4-15 has a larger influence on the erosion compared to the sediment parameter, indicated by the near horizonal lines in the surface plot. This means that a significantly higher or lower sediment parameter has a limited effect on the results. However, the sediment parameter for computing the erosion depth significantly differs from the sediment parameter calibrated for the erosion volume. Hoffmans et al. (2008) suggested the same sediment parameter for computing the erosion depth and volume, but it was not possible to obtain accurate results using the same value of the sediment parameter. Therefore, a new 'sediment parameter' M2 was used for computing erosion volume and computation of erosion volume and erosion depth using separately calibrated erosion parameters is suggested.

Next, the wave impact and wave run-up erosion parameters were calibrated as shown in Figure 4-16. The calibrated damping coefficient falls in the top end of the suggested range while the calibrated damping coefficient for the erosion depth is significantly larger than suggested and the damping coefficient for the erosion volume is significantly smaller than suggested by Stanczak et al. (2007) and Stanczak et al. (2008). Both the damping coefficient and the erodibility coefficient parameters have a significant effect on the erosion results in experiment K114 (Figure 4-16). The two bottom plots in Figure 4-16 show the calibrated values of the sediment parameter which are lower than the sediment parameters for the grass revetment erosion found in Figure 4-15. This is likely the result of the erosion relations being unable to describe the head cut erosion and therefore underestimating the erosion. The black line in the bottom plot of Figure 4-16 shows the erosion during experiment K114.

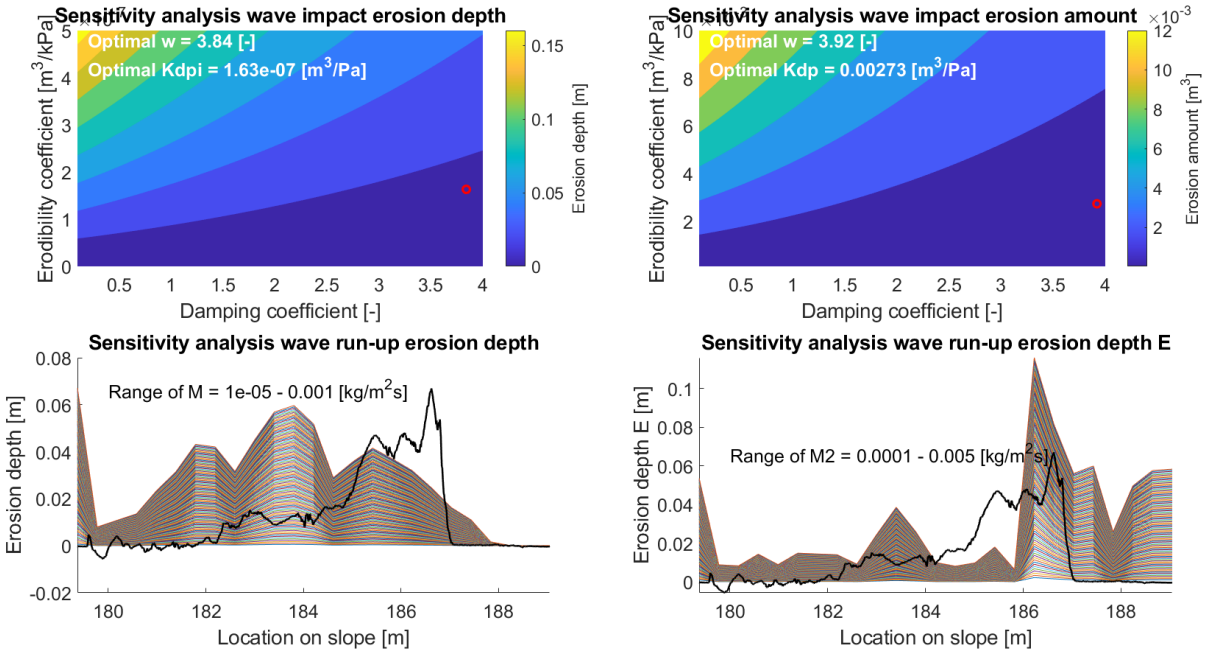

Figure 4-16 Results multivariate sensitivity analysis of wave impact erosion on empirical parameters of experiment K114 (definitions found in the list of symbols).

With the re-calibrated coefficients from equations (2.11) - (2.23), the equations read as given in Table 4-3 with a calibrated critical flow velocity of U_c = 2.84 m/s and critical shear stress of τ_c = 0.60 N/m^2 for the grass cover, suggesting that the grass is of poor/average quality. Critical flow velocity U_c = 0.12 m/s and critical shear stress τ_c = 0.38 N/m^2 for clay erosion of the poor quality clay suggest clay of very poor quality Hoffmans et al. (2008).

Applicability relation	Equation with calibrated parameters
Wave impact erosion depth grass revetment	$d_{g,i} = 5.92 \times 10^{-9} \times p_i \times e^{-1.37 h_i}$
Wave impact erosion depth poor quality clay	$d_i = 1.63 \times 10^{-7} \times p_i \times e^{-3.84 h_i}$
Wave impact erosion volume grass revetment	$R_{d,g,p} = 0.000164 \times p_{max} \times e^{-1.45 h_i}$
Wave impact erosion volume poor quality clay	$R_{d,p} = 0.00273 \times p_{max} \times e^{-3.92 h_i}$
Wave run-up erosion depth grass revetment (using U)	$y_{m,g} = (\rho_s U_c^2 (0.0857)^{-1})^{-1} \times (\alpha U_0 - U_c)^2 t$
Wave run-up erosion depth poor quality clay (using U)	$y_m = (\rho_s U_c^2 (2.2 \times 10^{-4})^{-1})^{-1} \times (\alpha U_0 - U_c)^2 t$

Wave run-up erosion depth grass revetment (using τ)	$\Delta d = \frac{2.32 \times 10^{-5} \times \Delta t}{\tau_c \times \rho_s} \times (\tau_0 - \tau_c)$
Wave run-up erosion depth poor quality clay (using τ)	$\Delta d = \frac{2.49 \times 10^{-4} \times \Delta t}{\tau_c \times \rho_s} \times (\tau_0 - \tau_c)$
Head cut model calibrated for wave impact erosion depth	$\Delta d = 6.40 \times (A - 0.146) \times \Delta t$
Head cut model calibrated for wave run-up depth erosion using U	$\Delta d = 6.37 \times (A - 0.200) \times \Delta t$
Head cut model calibrated for wave run-up erosion depth using U	$\Delta d = 6.41 \times (A - 0.129) \times \Delta t$

Table 4-3 Adapted erosion relations computing erosion depth and volume following equations (2.11) - (2.31) using calibrated parameters.

Note that these parameters have been calibrated using only one clay and grass type and can therefore only be used for determining erosion of clay and grass of poor quality.

4.3.2 Calibration head cut erosion

The erosion profile from experiment K114 could not be accurately fitted with the calibrated profiles computed using wave impact and wave run-up erosion. Therefore, the head cut erosion was computed around the cliff between 185 m and 188 m for each erosion profile of test K114. The head cut erosion was calibrated using the soil parameter $\mathrm{K_h}$ within the range of 0.01 and 0.02 to fit the erosion profile derived from the delta flume experiment, as shown in Figure 4-17.

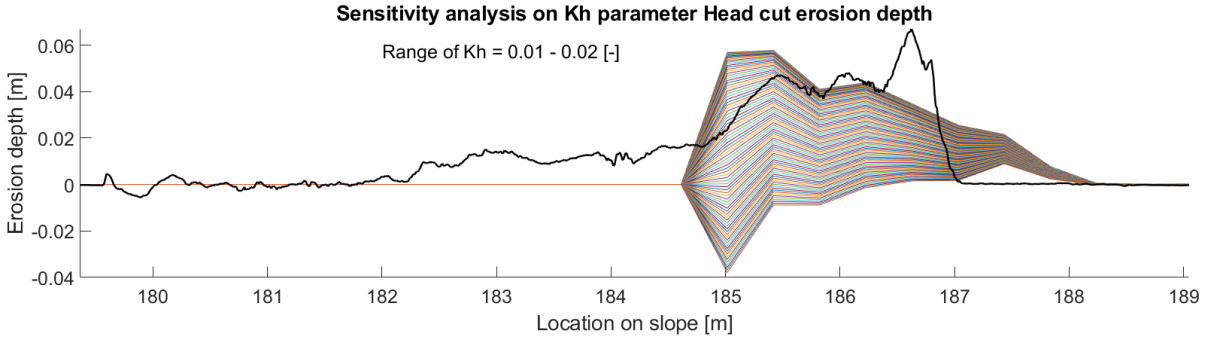

Figure 4-17 Calibration of soil parameter for computing head cut erosion with the black lines showing the erosion depth of the grass revetment after 600 s of delta flume test K114. The coloured lines show head cut erosion with different values for the soil parameter (K_h).

Figure 4-17 shows the high sensitivity of the soil parameter, which results in negative erosion when too large. This is caused by the increased value of the cliff advance threshold parameter $\mathrm{A_0}$. The erosion becomes negative when this parameter is larger than the cliff advance rate parameter A. Although not suggested by NRCS (1997) and Van Hoven (2014) lower threshold of $\mathrm{A_0} = A$ could be used to prevent negative erosion values.

4.3.3 Calibrated erosion results: wave impact

Figure 4-18 shows the erosion profile after roughly 600 s of wave impact with most erosion occurring near the transition, decreasing over the distance. The wave impact zone is generally referred to as the area of the dike between the SWL and half the significant wave height below it (Van Hoven, 2015), which would indicate that wave impact only occurs up to approximately 180 – 181 m in Figure 4-18. However, the model results are similar to the results of the experiments until 184 m in Figure 4-18. Between 184 – 189 m the difference becomes larger. Each erosion model also shows the coefficient of determination (R^2) and RMSE, indicating how well each model predicts the erosion of the delta flume experiments.

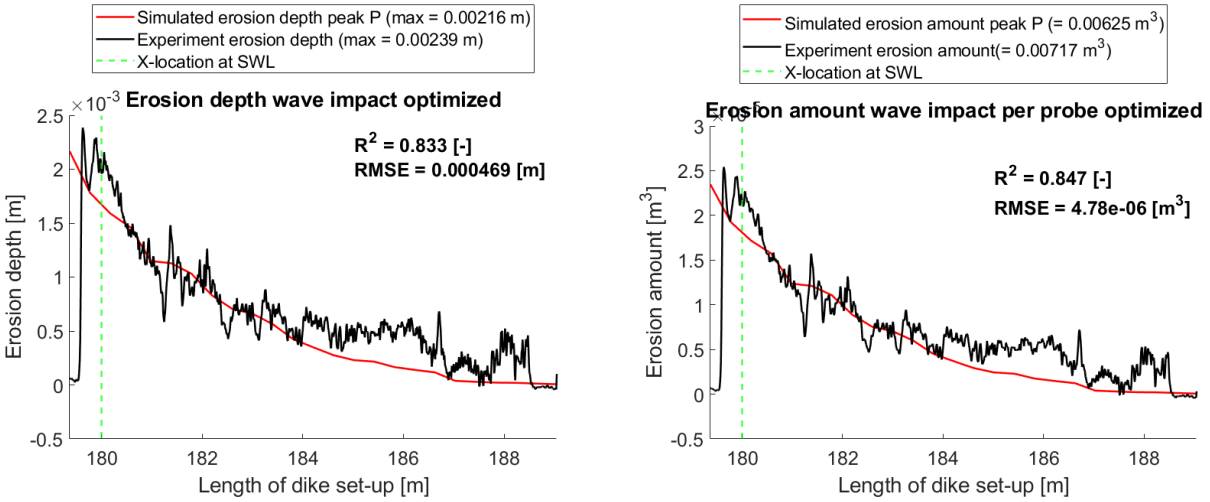

Figure 4-18 Erosion depth and volume using peak dynamic pressures (P) from OpenFOAM model following calibrated wave impact erosion relations showed as the red line and the erosion from the first 600 s of test K101 is shown as the black line. The goodness of the model is measured by the coefficient of determination and RMSE, also included in the figure.

The maximum erosion depth due to wave impact during experiment K114 is 10 times higher than during experiment K101. The location of maximum erosion depth has also shifted to 183.5 m in Figure 4-19, which is below the SWL due to the eroded profile causing the SWL to be shifted to 185.1 m in Figure 4-19. The dike slope between 180 m and 182 m experience comperatively little erosion, which is likely caused by a sheltering effect due to the steep drop directly at the transition, visible between 179 and 180 m in Figure 3-8. However, the profile does not fit well with the erosion from the experiment shown with the black line.

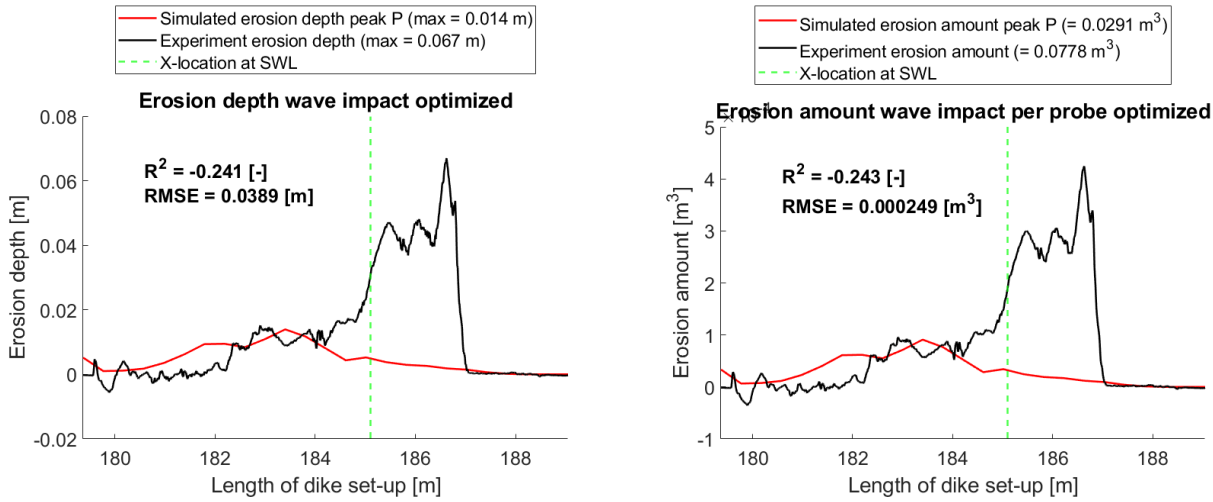

Figure 4-19 Erosion depth and volume using peak dynamic pressures (P) from OpenFOAM model following calibrated wave impact erosion relations showed as the red line and the erosion from the first 600 s of test K114 is shown as the black line. The goodness of the model is measured by the coefficient of determination and RMSE, also included in the figure.

4.3.4 Calibrated erosion results: wave run-up

The calibrated wave run-up erosion of experiment K101 is visible in Figure 4-20. The erosion depth due to wave run-up and run-down in the left plot shows a sharp increase near the SWL and transition as also observed in the delta flume experiments. However, the erosion depth computed using shear stress, shown in the right plot of Figure 4-20 shows to increase by a similar volume on the entire grass revetment dike slope, giving very different results than the

erosion depth increase in the left plot of Figure 4-20. Additionally, for increase in erosion depth the wave run-down seems to be dominant while for increase in erosion depth E the wave run-up shows to be more influential in Figure 4-20.

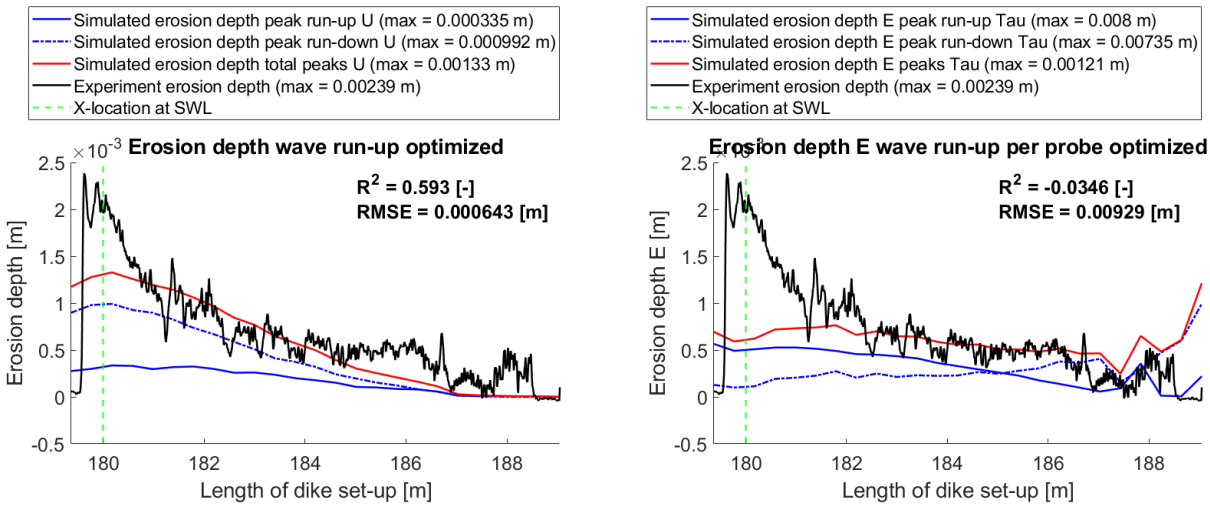

Figure 4-20 Wave run-up and run-down erosion depth using flow velocity (U) and shear stress (τ) from OpenFOAM model following calibrated wave run-up erosion relations showed as the red and blue lines, the erosion from the first 600 s of test K101 is shown as the black line. The goodness of the model is measured by the coefficient of determination and RMSE, also included in the figure.

The erosion due to wave run-up for experiment K114 is shown Figure 4-21. The profile for erosion depth increase is similar to the profiles found in Figure 4-19 due to wave impact. However, the profile showing increase in erosion depth using data from the experiment, shows most erosion occuring at the end of the eroded grass revetment profile between 186 – 188 m instead of in the middle between 182 – 185 m.

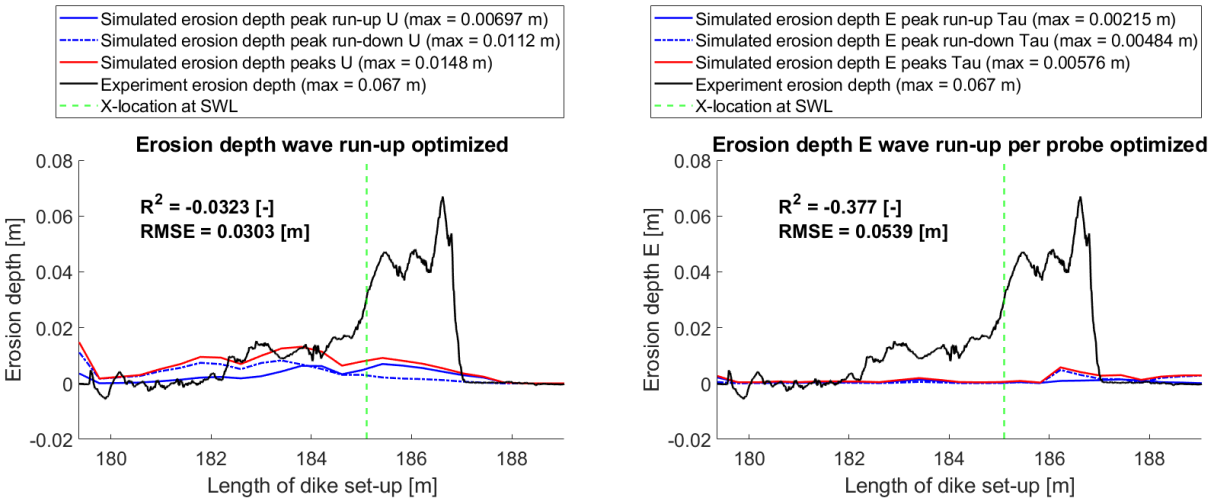

Figure 4-21 Wave run-up and run-down erosion depth using flow velocity (U) and shear stress (τ) from OpenFOAM model following calibrated wave run-up erosion relations showed as the red and blue lines, the erosion from the first 600 s of test K114 is shown as the black line. The goodness of the model is measured by the coefficient of determination and RMSE, also included in the figure.

4.3.5 Calibrated erosion results: head cut

The amount of head cut erosion was calibrated to the wave impact erosion and the wave run-up and run-down erosion as shown in Figure 4-22. The profiles with head cut erosion fit the data from the experiment (black line in Figure 4-22) significantly better. However, the

largest peaks are not accurately represented and erosion also occurs closer to the crest than in the experiment.

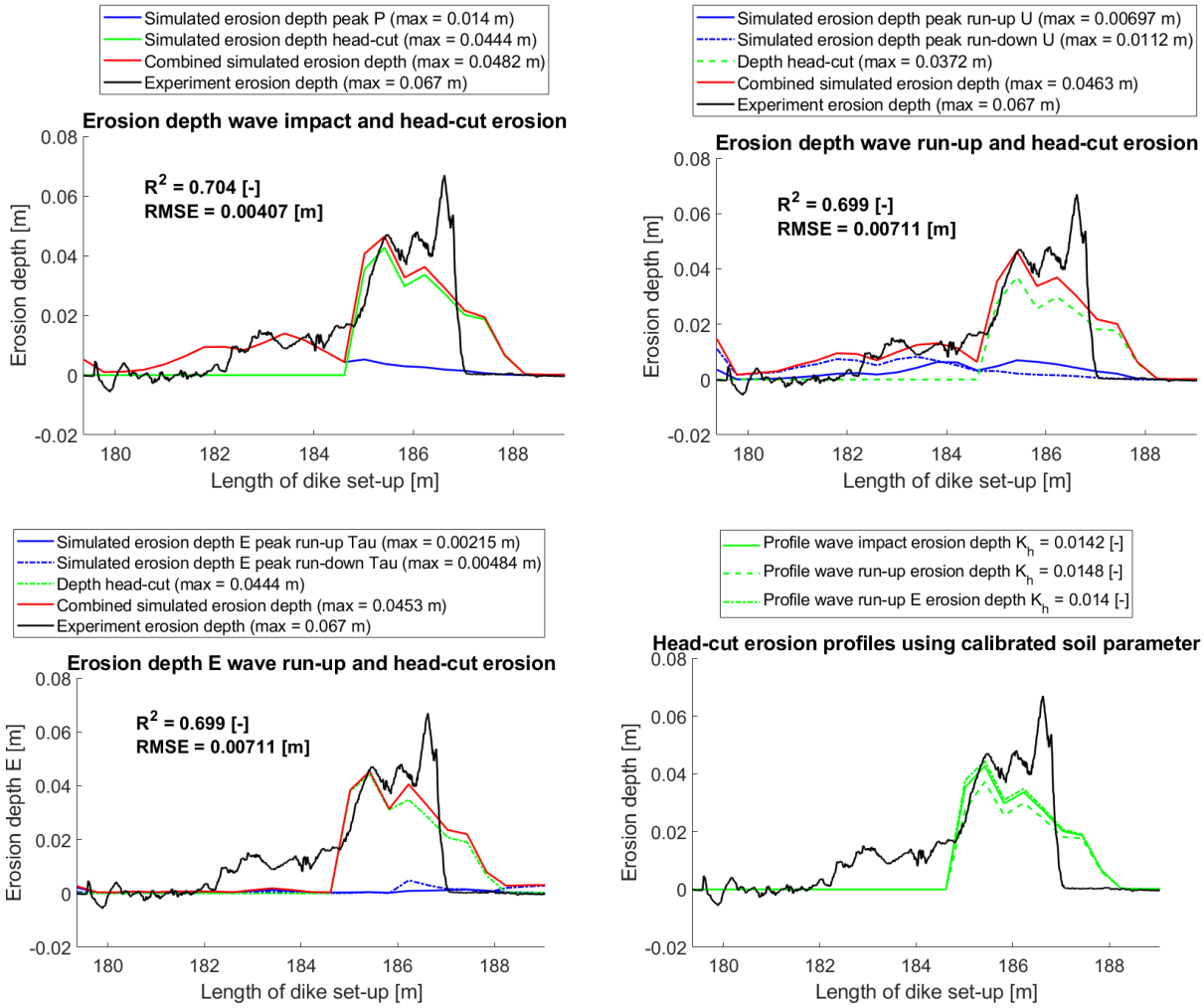

Figure 4-22 Wave run-up, run-down and wave impact erosion depth using calibrated erosion relations with individually calibrated head cut erosion data shown as the red lines, the erosion from the first 600 s of test K114 is shown as the black line. The lower right subplot shows the amount of head cut erosion with the calibrated soil parameters for the three erosion models used for computing run-up, run-down and impact erosion depth.

From applying the wave impact, wave run-up and head cut erosion relations, it can be concluded that the wave impact relations can predict the erosion most accurately when looking at the coefficient of determination and RMSE. Moreover, head cut erosion relations are required to compute the erosion during test K114. Therefore, wave impact erosion appears to be dominant during the initial grass cover erosion. A combination of wave impact and head cut erosion is dominant when a large part of the grass cover and clay layer is eroded and a cliff is present in the erosion profile. As the erosion progresses and the erosion cliff becomes larger, head cut erosion appears to become more dominant for determining erosion depth and volume than wave run-up or wave impact erosion.

5 Discussion

In this chapter the relevance of the results will be discussed. The results show that a change in grass or clay quality has a significant influence on the erosion resistance of the outer dike slope and that erosion can be rather accurately predicted using the dynamic pressures on the dike slope. First, the significance of the results is discussed. Second, the applicability of the research findings is discussed.

5.1 Insights and limitations of this study

The results of this report are divided into three parts used for answering the 4 research questions. In the first part, the data from the delta flume experiments were analysed to investigate the effect of clay and grass quality on erosion rate which will be used to answer the first research question. In the second part, the OpenFOAM model of the Lauwersmeerdijk-Vierhuizengat is validated and the effect of an eroded profile on the model results is determined to answer the second research question. In the third part, erosion relations were used to compute the erosion from the delta flume experiments using OpenFOAM model data. The empirical erosion relations were calibrated to fit the erosion occurring during the delta flume experiments and subsequently answer the third research question. The calibrated erosion relations in combination with the accuracy quantification by the coefficient of determination and RMSE were used to answer the fourth and last research question. All of the aforementioned results are discussed in this section as well as the model description.

5.1.1 Effect of clay and grass quality on erosion rate

The erosion during the delta flume experiments is measured using a FARO3D laser scanner which measures the erosion profile of the grass revetment after each test. However, the erosion in between each test is not measured. Therefore, it is not possible to determine the erosion progression during the experiment using the FARO3D data. The erosion data from the FARO3D laser scanner likely also contains some errors in the measurements effecting the accuracy of the results. In the results the erosion was scaled to the duration of each test and the erosion per minute was derived by assuming linear erosion, which is not necessarily the case. The time scaled erosion lines presented in the results are therefore not completely accurate.

During the first five experiments K1 – K5, artificial damage was created in some of the earlier tests to accelerate the erosion progress. Therefore, the grass cover likely eroded significantly faster, affecting the erosion profiles presented in the results. However, the grass revetment landward of the artificial damage erodes slower as lots of energy is dissipated in the artificial damage spot. The artificial damage was different for every experiment and applied at different stages. Consequently, it is difficult to account for the effect of artificial damage when comparing the experiments to determine the effect of clay and grass quality on erosion rate. Additionally, the quality of clay and grass was also not consistent for the entire profile during each experiment (Klein Breteler, 2021). For example, in experiment K6 a deep erosion hole arose in a spot with weak quality clay which had to be filled in order to not compromise the remainder of the experiment. Consequently, the erosion rate of similar experiments could vary due to the quality of the clay and grass blocks.

5.1.2 OpenFOAM model mesh and post-processing of results

The computational time of simulating 600 s of wave impact using the OpenFOAM models was almost a week. To limit the computational time, the mesh was optimized to contain as few as possible cells without sacrificing model accuracy. Therefore, a cut off of the refinement surface landward of x = 165 m is tested resulting in a reduction of the computational time by approximately 30% compared to an extension to the dike surface for experiment K114. The mesh with the long refinement surface adds approximately 3000 extra cells, increasing the computational time. However, a more efficient mesh setting was tested, but it was shown that the long-refinement mesh was essential for accurate results. Consequently, the mesh with a long refinement surface is used for simulation of the experiment K101 and K114.

Probes were added in the OpenFOAM model to obtain variables that were post-processed into pressures and velocities used for computing the erosion. Probes have been placed at various locations in order to determine the ideal locations to measure the dynamic pressures. From calibration, it was found that the highest dynamic pressures were measured at a height of 20 cm above the dike surface in case the probes were placed above the SWL and around the water level in case the probes were placed below the SWL. Furthermore, it was observed that the waves generally break at the berm (around x = 175 m). Therefore, measuring probes were placed starting at the berm until the crest of the dike. More detailed information on the probe calibration making use of dynamic pressures is found in appendix 3. Only one line of probing locations on the waterside slope between x = 175 m and x = 189 m at an interval of approximately 40 cm have been used to measure the data in order to reduce the amount of data points. However, due to varying run-up water layer thickness, it is possible that the maximum flow velocity occurred at a higher or lower depth than measured using the probes leading to a possible underestimation of the flow velocity.

The roughness of the grass revetment was modelled based on the calibrated roughness height of Van Bergeijk (2020) and the clay friction was computed following Marriott & Jayaratne (2010). However, the fricion was not calibrated and validated because no data was available for calibration of the pressures, velocities and shear stresses, which might influences the model results.

5.1.3 OpenFOAM model validation

Model results show that the incoming waves were well reproduced compared to the measured ones in terms of wave propagation and wave characteristics.

Two different dynamic pressures from OpenFOAM have been analysed, p_rgh and total(p) – p, where the pressures using total(p) – p more variability in the dynamic pressures and a clear difference between test K101 and test K114. The dynamic pressures predicted by the variable p_rgh are more constant and less accurate compared to the modelled and measured pressures on seaside slopes in other studies (Horstman, 2020; Mous, 2010). The water depth used for computing p_rgh is determined by the vertical height of the cell from a reference height of 0 m. The dynamic pressure using p_rgh is only equal to total(p) – p when the free surface is at 0 m (Davidson et al., 2015). Therefore, p_rgh gives inconsistent results over the grass revetment slope with the maximum p_rgh occurring near the crest. The total(p) - p dynamic pressures show lower maximum pressures higher up the slope. This is more logical than the p-rgh pressures since the impact forces of the wave are mostly attenuated at the top of the slope resulting in lower pressures. Therefore, the dynamic pressure obtained using total(p) – p were used for the computation of the erosion.

The simulated velocities and dynamic pressures are lower than the empirical relations suggested by previous research (Peters, 2017, Overtopping manual, 2018 and Horstman,

2020). This is likely caused by the limited simulation duration of 100 waves and usually around 500 - 1000 waves are required to determine the exceedance values, suggested in the EurOtop overtopping manual (2018) and in experiments by Chen et al. (2020a) and Chen et al. (2020b). However, simulating 500 – 1000 waves would result in a computational time in excess of a month and was therefore not feasible. Additionally, lower roughness values could be used in the OpenFOAM model which would increase the flow velocities to possibly be more in line with the empirical relations. Moreover, the friction along the grass revetment slope is constant in the OpenFOAM model while varying in the experiment, which could have affected the run-up/run-down flow velocities.

5.1.4 Erosion estimation using the OpenFOAM output

The results have shown that the erosion along the dike profile can be computed using existing erosion formulas and the modelled pressures and run-up velocities. However, the addition of a head cut erosion model is required for experiment K114 to compute the additional erosion due to the presence of a cliff. Consequently, the wave impact and wave run-up/run-down do not solely explain the acceleration of erosion when a vertical cliff is present in the eroded dike profile. Additionally, the minimum height of the cliff at which a head cut erosion model is required to compute erosion is not determined in this study.

The large erosion volume from experiment K114 is not accurately displayed using the hydraulic variables from the OpenFOAM model for computing wave run-up and wave impact erosion. It is possible that the erosion occurred during a later stage in experiment K114 which has not been modelled. Another possibility is that the waves become higher during the latter part of the experiment, causing more erosion to the grass revetment near the crest. However, the wave height after the period that was modelled in OpenFOAM, which is determined using the incoming wave data from the delta flume experiment, is not significantly higher than during the simulation period. The large erosion peak occurs at the cliff at the end of the erosion hole (between x = 185 m and x = 188 m) which might cause the soil to erode more quickly. However, changes in the erosion rate due to spatial differences in clay quality cannot be calculated because uniform erosion parameters were adopted for the whole profile. Consequently, a head cut erosion model was used to account for the aforementioned head cut erosion (Van Hoven, 2014).

The empirical parameter in the run-up and wave impact erosion relations (Stanczak et al., 2007, Stanczak et al., 2008 and Hoffmans et al., 2008) had to be calibrated significantly above the proposed ranges by the aforementioned authors. Only a few publications describing grass cover erosion were determined, using smaller scale experiments (Stanczak et al., 2007, Husrin, 2007 and Hoffmans et al., 2008). Therefore, computing the erosion for a 1:1 scale dike cover likely caused the grass detachability coefficient to be significantly greater than proposed values by the authors. Only one value for the sediment parameter is determined by Hoffmans et al. (2008). However, the two erosion relations for the wave run-up erosion depth depend on the parameter and no accurate results, when comparing the erosion using modelled results and erosion from the experiments, could be obtained when using one value for the sediment parameter. Therefore, a second parameter M2 is used which is calibrated separately for wave run-up erosion due to shear stress. The calibration has shown that changing the sediment parameter has a limited effect on the erosion depth which could explain why the sediment parameter is calibrated outside of the suggested range. The damping coefficient has also been calibrated but within the range suggested by Stanczak et al. (2007). The damping coefficient for test K114 is higher than for test K101, but the water depth is also larger for that test explaining the larger damping coefficient.

5.2 Applicability of this research

Comparing the erosion from the delta flume experiments has shown that the quality of clay and grass have a significant effect on the erosion rate (Van Bergeijk et al., 2021 and Sprangers, 1999). During dike cover safety assessment, it might be important to consider the large impact dried out grass has on erosion rate during extreme storms. However, many dikes will likely not comply to safety regulations when assessed dike covers assuming dried out grass. Therefore, it might be interesting to consider more erosion resistant dike covers to prevent significant reduction of strength during long periods of drought. In a study by Scheres et al. (2020) different dike covers were tested for erosion resistance where was concluded that grass dominated vegetations are most erosion resistant. Scheres et al. (2020) found that erosion is most often initiated at weak spots and the erosion due to wave impact decreases exponentionally with increasing root density and root length for unreinforced soils. Regular sowing of grass to maintain a grass dominated dike cover and periodic maintenance to prevent weak spots could make the dike more erosion resistant after long droughts. Soil reinforcement using Geogrid lattice fabric could also be used to significantly increase the erosion resistance (Scheres et al., 2020). Using a higher quality clay, when designing or renovating the outer slope of dikes might also be a worthy consideration.

The effect that an eroded dike profile has on the distribution and magnitude of erosive forces on the outer slope of the dike is significant. The eroded area of the profile is partly sheltered, enduring lower erosive forces on the seaward half, while the landward half endures larger flow velocities and shear stresses when compared to a dike slope without erosion. The dynamic pressures are lower in the seaward half of the eroded profile and the landward part endures equal pressures as the dike slope without erosion. Additionally, the erosion rate increases rapidly when a cliff is formed in the dike cover.

Results of the erosion computed using the OpenFOAM model output and empirical relations, show that wave run-up and wave impact erosion relations are capable of predicting the erosion in the delta flume experiments. Cliff erosion present in the profile of experiment K114 can be computed using a head cut erosion model. The erosion calculated using the modelled wave impact pressures produce the most accurate results and are able to accurately model the variability in erosion along the profile. The run-up flow velocity can also be used to compute the erosion but will give slightly less accurate results. The erosion relations using shear stress did not accurately represent the erosion profile. However, earlier studies suggest that hydraulic variables such as (shear) velocities, pressure, normal stress and shear stress are all important variables to understand dike failure by cover erosion (Zhang et al., 2017; Chen et al., 2015 and Ponsioen et al., 2019). This indicates that the erosion relation used for computing erosion using shear stress is not suitable for computing wave run-up erosion.

The flow velocity and water depth on the outer slope are also important variables since these are required for computing cliff erosion. This study also showed that some parameters require calibration outside of suggested ranges to produce meaningful results. The parameters in this report were calibrated specifically for the OpenFOAM model with a grass revetment on the wave run-up zone of an outer dike slope and likely require recalibration when applied to other cases.

6 Conclusion and Recommendations

6.1 Conclusion

This research aims to assess the wave impact and wave run-up erosion on the outer slope of sea dikes. Erosion data from delta flume experiments have been obtained and analysed to determine the effect of clay and grass quality on erosion rate. An OpenFOAM model was created of the Lauwersmeerdijk-Vierhuizengat (experiment K1) and hydraulic load on the grass revetment surface was simulated on a grass covered dike without erosion (delta flume test K101) and a dike with significant erosion (delta flume test K114). The erosion was computed using the model output and was compared to the measured erosion during the experiments to determine if and what empirical relations can be used to determine grass cover erosion. The four sub-questions and main research question are answered in this chapter.

1. *How is the dynamics of the grass cover and clay layer erosion in the delta flume experiments affected by the clay and grass quality?*

The erosion dynamics for each experiment was similar, where the erosion depth showed a linear increase during the whole experiment and the erosion volume showed an exponential increase. The location where the highest erosion depth occurred, moved from near the transition from hard to grass revetment towards the crest during each experiment. Clay quality appeared to have a very limited effect on the erosion rate of the grass cover, while having a significant effect on erosion rate once the grass cover was eroded. The increased erosion resistance, achieved by using clay from Blija instead of clay from the Lauwersmeerdijk-Vierhuizengat, contributes to a roughly 35% increase in wave attack duration for similar erosion results. The grass quality has a large effect on the erosion rate during the first hours of wave attack. The results show that the grass cover with dried out grass erodes three times as fast as a similar grass cover that is watered. However, the specific grass quality parametrization was not available, causing some uncertainties in the results. The clay layer beneath the dried and watered grass layer seemed to erode at equal rate. Therefore, the quality of the grass cover has a massive effect on the grass cover erosion rate but does not seem to significantly affect the erosion rate of the underlying clay layer.

2. *How does an eroded dike profile affect the simulated dynamic pressures and run-up velocities in the OpenFOAM model?*

An OpenFOAM model has been set-up and successfully validated. The simulation of the eroded profile showed that erosion causes a shift in dynamic pressures and velocities on the grass revetment slope compared to the initial profile. The maximum dynamic pressures of test K101 are higher compared to test K114 and occur closer to the transition from hard to grass revetment. There is a vertical cliff directly downward at the transition to grass revetment of test K114, resulting in a sheltering effect with low velocities and pressures on the dike cover between the transition and 5 m landward of the transition. The high pressures occur at the almost vertical cliff in test K114, where the steep slope causes high dynamic pressures and flow velocities. However, the simulated dynamic pressures at the cliff location in test K114 are equally large as those at the same location in test K101. The eroded profile of test K114 causes a significant decrease in dynamic pressures over the grass revetment slope. The flow velocities of test K114 between the transition and 5 m landward of the transition are lower compared to test K101 but are hardly attenuated because of the larger water depth present in the eroded profile. Therefore, the velocities when impacting the cliff

are much higher compared to test K101. The distribution of the shear stresses over the grass revetment slope of both profiles is similar to the distribution of the flow velocities.

3. *How accurately can the erosion as a result of wave run-up, wave impact and head cut be predicted using the existing empirical equations and OpenFOAM model results?*

The erosion has been calculated using empirical relations for the wave impact erosion depth and volume using the numerically modelled dynamic pressures, and the wave run-up erosion depth using the modelled velocities and the modelled shear stresses. Several empirical parameters describing clay and grass cover strength were calibrated in order to obtain realistic results. Additionally, a head cut erosion model is used to account for the cliff erosion during test K114, with the eroded profile. The cliff erosion has been calibrated separately and combined with the wave impact and run-up erosion models, showing that the erosion can be predicted with a head cut erosion model with a Root Mean Square Error (RMSE) of 0.00407 [m] and a coefficient of determination (R^2) of 0.70 [-]. This study shows that wave impact and run-up erosion relations can individually be used to predict erosion for test K101, while for test K114 an additional head cut erosion is necessary to simulate the cliff erosion at the end of the eroded area. Accuracy of the erosion models is determined using the RMSE and R^2. Computing erosion depth using modelled dynamic pressures gave the most accurate results, with a RMSE of 0.000469 [m] and a R^2 of 0.84 [-]. Computing erosion depth using the modelled shear stresses is the least accurate method for determining erosion depth on a grass cover without erosion, with a RMSE of 0.00929 [m] and a R^2 of -0.0346 [-]. The erosion relations using the dynamic pressures also most accurately predict erosion for grass covers with significant erosion. Wave impact relations are therefore likely the best predictors for outer slope erosion during the whole erosion process.

4. *For which part of the dike slope can wave impact be used to predict erosion and for what part of the dike slope are wave run-up or head cut erosion models applicable?*

The dynamic pressures can be used to accurately predict erosion for the whole grass revetment profile of test K101. However, from roughly 5 m landward of the transition until the crest, the dynamic pressures underestimate the erosion and the run-up erosion model fits more accurately. Consequently, in order to predict erosion of the initial grass revetment slope most accurately, wave impact and run-up erosion should both be considered. Wave impact erosion using dynamic pressures for test K101 can be used until roughly $0.6H_s$ above the Still Water Level (SWL), the remaining part of the outer slope experiences wave run-up erosion. Hardly any difference in erosion due to wave impact or run-up is observed for test K114. Therefore, wave run-up or wave impact relations can both be used to predict erosion of the entire eroded grass revetment profile of test K114. Additionally, a head cut erosion model was required to compute the erosion during test K114 between 2 m seaward and 1 m landward of the vertical cliff present in the eroded grass revetment profile. Lastly, artificial damage does not have an effect on the model results because no artificial damage was created before or during test K101 and K114.

With the answers to the sub-questions, the main research question can be answered:

"How does the grass revetment on the seaside slope of a dike erode and what influences the erosion process and the erosion rate?"

This study shows that the clay and grass quality have a significant effect on the erosion resistance of grass revetment on the wave impact and run-up zone of the dike. The erosion depth of the grass revetment increases linearly with the maximum depth moving towards the crest. The erosion volume increases exponentially, especially once an erosion depth of approximately 0.5 m is reached. The distribution of hydraulic variables such as dynamic

pressures, flow velocities and shear stresses on an undamaged dike profile vary significantly from those of a dike profile with significant erosion, which likely prevents erosion occurring at the same location during the erosion process. The results from the OpenFOAM model show that the erosion can be computed using the dynamic pressures, flow velocities and shear stresses and that using dynamic pressures to compute erosion provides the most accurate results. Therefore, the dynamic pressures have the largest effect on determining the erosion rate in combination with water depth and the flow velocity in case of an erosion cliff. Consequently, dynamic pressures which originate from wave impact appear to be the dominant factor in dike cover erosion and consequently dike failure.

6.2 Recommendations

This section provides recommendations for determining grass cover erosion on the outer dike slope and recommendations for further research.

6.2.1 Grass cover erosion

The erosion data from the experiments show the large impact of the grass quality on the grass cover erosion rate. Any grass cover could be weakened by the effect of a dry summer, possibly resulting in rapid dike failure. It is therefore recommended to design the grass cover in such a way that it is resistant to failure when not fully recovered from the effects of a dry summer, or to guarantee dike cover recovery before the start of the storm season. The erosion resistance can be improved by using Geogrid, periodic sowing and maintenance to prevent weak spots, which usually initiate erosion (Scheres et al., 2020) as also mentioned in section 5.2. The clay quality has a significant effect on the erosion rate of the clay layer but has only a limited effect on the erosion rate of the grass cover, as also concluded by Sprangers (1999). The effect of clay quality on failure is limited because the grass cover fails when 20 cm of erosion depth was reached, following the failure definition of the Dutch safety assessment (Van Hoven, 2015). The quality of the grass cover also has a large influence on the erosion rate at the transition from the smoother hard revetment to grass revetment with higher roughness, which increases scour potential (Aguilar-López et al., 2018). High grass quality along the entire grass revetment slope presents much lower dike failure probabilities than lower ‘realistic’ grass quality (Aguilar-López et al., 2018). Therefore, it is recommended to focus on the strength of the grass cover layer with reduced erosion resistance, when accessing the failure probability of a dike with a grass revetment in the wave run-up zone.

Dynamic pressures, shear stresses and run-up velocities can all be used for determining dike erosion. However, computing erosion using the dynamic pressures produces the most accurate results. Determining erosion with a combination of wave impact and wave run-up has not shown to improve the results significantly. Wave run-up erosion relations underestimate the erosion below the SWL in this study and are therefore not recommended to be used for computing erosion below the SWL. The modelled erosion using the shear stress deviates the most from the erosion profile of the Lauwersmeerdijk-Vierhuizengat in experiment K1 and is therefore not recommended for determining the wave run-up erosion.

6.2.2 Further research

This study focussed on the erosion of the Lauwersmeerdijk-Vierhuizengat which was tested in the delta flume as experiment K1. An OpenFOAM model has been created specifically for simulating the waves generated in the delta flume. Validation of the modelled dynamic pressures and modelled flow velocities showed that the modelled variables are underestimated compared to the empirical relations. The modelled hydraulic variables could only be validated against empirical relations because hydraulic variables were not measured

during the delta flume experiments. OpenFOAM simulations should be ran for a longer duration to determine if the model results become more accurate and closer to the values determined using the empirical relations (Overtopping manual, 2018, Peters, 2017 and Horstman, 2020). The empirical erosion formulas (Stanczak et al., 2007, Stanczak et al., 2008 and Hoffmans et al., 2008) have also been specifically calibrated for computing erosion of experiment K1. The hydraulic loading and computed erosion using the OpenFOAM simulation results of the other experiments still remain unknown. Data from simulating the other experiments could be used to re-calibrate the erosion parameters to suggest a range of empirical parameters for computing erosion with varying clay and grass cover strength.

This study has shown that an eroded dike profile has a large impact on the distribution and magnitude of wave impact pressures, run-up flow velocities, shear stresses and water layer thickness on the dike slope. However, how the distribution of the aforementioned variables changes as the grass revetment erodes is not defined. Therefore, obtaining a relation between the eroding grass revetment profile and changes in distribution of the hydraulic variables could be useful to better predict grass cover and clay erosion of sea dikes.

7 References

Aguilar-López, J. P., Warmink, J. J., Bomers, A., Schielen, R. M., & Hulscher, S. J. M. H. (2018). Failure of Grass Covered Flood Defences with Roads on Top Due to Wave Overtopping: A Probabilistic Assessment Method. *Marine Science and Engineering, 6, 74, https://doi.org/10.3390/jmse6030074*.

Barnston, A. G. (1992). Correspondence among the Correlation, RMSE, and Heidke Forecast Verification Measures; Refinement of the Heidke Score. *Climate Analys Center, NMC/NWS/NOAA, Washington D.C.*, 699-709.

Berberović, E., Hinsberg, N. P., Jakirlić, S., Roisman, V. I., & Tropea, C. (2009). *Drop impact onto a liquid layer of finite thickness: Dynamics of the cavity evolution.* Physical Review E - Statistical, Nonlinear, and Soft Matter Physics 79 (3), Art.no: 036306.

Breteler, M. K. (2020). *Erosie van kleibekleding met gras op boventalud van Lauwersmeerdijk. Meetverslag Deltagootproeven voor dijktraject Lauwersmeerdijk-Vierhuizergat.* Delft, The Netherlands: Deltares, 11204841-006-HYE-0001.

Breteler, M. K. (2020). *Erosie van kleibekleding met gras op buitentalud van zee- en meerdijken, plan van aanpak.* Delft, The Netherlands: Deltares.

Breteler, M. K. (2021). *Erosie van kleibekleding met gras op boventalud van Waddenzeedijken.* Delft, The Netherlands: Deltares, 11204841-006-HYE-0004.

Chen, W., Gent, M. R., Warmink, J. J., & Hulscher, S. J. M. H. (2020a). The influence of a berm and roughness on the wave overtopping at dikes. *Coastel Engineering 156, https://doi-org.ezproxy2.utwente.nl/10.1016/j.coastaleng.2019.103613*.

Chen, W., Marconi, A., Gent, M. R., Warmink, J. J., & Hulscher, S. J. M. H. (2020b). Experimental Study on the Influence of Berms and Roughness on Wave Overtopping at Rock-Armoured Dikes. *Marine Science and Engineering, 8, 446, https://doi.org/10.3390/jmse8060446*.

Chen, W., Warmink, J. J., Gent, M. V., & Hulscher, S. J. M. H. (2021). Numerical modelling of wave overtopping at dikes using OpenFOAM. *Coastal Engineering (under review)*.

Chen, X., Hofland, B., Altomare, C., Suzuki, T., & Uijttewaal, W. (2015). Forces on a vertical wall on a dike crest due to overtopping flow. *Coastal Engineering, 95, https://doi.org/10.1016/j.coastaleng.2014.10.002*, 94-104.

Chow, V. (1959). *Open channel hydraulics.* McGraw Hill.

Davidson, J., Cathelain, M., Gullemet, L., Huec, T. L., & Ringwood, J. V. (2015). Implementation of an OpenFOAM Numerical Wave Tank For Energy Experiments . *European Wave and Tidal Energy Conference, ISSN 2309-1983* , 09B1-1-1 - 09B1-1-10.

De Waal, J. P. (2016). *Basisraport WBI 2017.* Delft, The Netherlands: Deltares.

D'Eliso, C. (2007). *Breaching of sea dikes initiated by wave overtopping. A tiered and modular approach, Ph.D-Thesis.* University of Florence, https://doi.org/10.24355/dbbs.084-200708270200-0.

Deltares. (2021). *Delta flume*. Retrieved from www.deltares.nl: https://www.deltares.nl/nl/faciliteiten/delta-flumedeltagoot/

Draper, N. R., & Smith, H. (1966). *Applied regression analysis.* John Wiley & Sons Ltd., New York, 407 p.

Fischerinch, C. (2001). *Stability thresholds for stream restoration materials. Technical Note: ERDC TN-EMRRP-SR-29.* US Army Corps of Engineers Research and Development Center. Vicksburg, Mississippi, USA. 10p.

Higuera, P., L. Lara, J., & J. Losada, I. (2013). *Realistic wave generation and active wave absorption for Navier–Stokes modelsApplication to OpenFOAM®.* Coastal Engineering 71, (2013), 102-118; https://doi.org/10.1016/j.coastaleng.2012.07.002.

Higuera, P., L. Lara, J., & J. Losada, I. (2013). *Simulating coastal engineering processes with OpenFOAM®.* Coastal Engineering 71, 119-134; https://doi.org/10.1016/j.coastaleng.2012.06.002.

Horstman, M. (2020). *Feasibility assessment of a grass cover dike in a coastal wetland setting towards a design tool.* MSc thesis, University of Twente.

Husrin, S. (2007). *Laboratory Experiments on the Erosion of Clay Revetment of Sea Dike due to Breaking Wave Impacts. MSc Thesis WSE-HE-CEPD-07.03.* Delft, The Netherlands: Delft: UNESCO, Institute for Water Education.

HWBP. (2020). *HoogWaterBeschermingsProgramma* . Retrieved from https://www.hoogwaterbeschermingsprogramma.nl/

Jacobsen, N. G. (2017). *waves2Foam manual.* v. 0.9 (DRAFT) - SVN Revision 2113.

Jacobsen, N. G., & Fredsøe, J. (2014). *Cross-Shore Redistribution of Nourished Sand Near a Breaker Bar.* Journal of Waterway, Port, Coastal and Ocean Engineering 140 (2), 125-134; https://doi.org/10.1061/(ASCE)WW.1943-5460.0000233.

Jacobsen, N. G., Fuhrman, D. R., & Fredsøe, J. (2012). *A Wave Generation Toolbox for the Open-Source CFD Library: OpenFoam.* International Journal for Numerical Methods in Fluids 70 (9), 1073-1088; https://doi.org/10.1002/fld.2726.

Jensen, B., Jacobsen, N. G., & Christensen, E. D. (2014). Investigations on the porous media equations and resistance coefficients for coastal structures. *Coastal Engineering, Volume 84; https://doi.org/10.1016/j.coastaleng.2013.11.004*, 56-72.

Larsen, B. E., Fuhrman, D. R., & Roenby, J. (2019). Performance of interFoam on the simulation of progressive waves. *Coastal Engineering Journal, Volume 61*, 380-400.

M.J.Marriott, & R.Jayaratne. (2010). *Hydraulic roughness – links between Manning's coefficient, Nikuradse's equivalent sand roughness and bed grain size.* London: School of Computing, Information Technology and Engineering, University of East London.

Mansard, E., & Funke, E. (1980). *The measurement of incident and reflected spectra using a least squares method.* ASCE - Texas Digital Library.

Meyer, L. (1964). *Mechanics of soil erosion by rainfall and runoff as influenced by slope length, slope steepness, and particle size.* Ph.D. thesis, Purdue University Library, W. Lafeyette, IN.

Mous, B. C. (2010). *Wave impact on grass covered outer slopes, MSc-thesis.* Delft, The Netherlands: Delft University of Technology.

Neumann, B., Vafeidis, A. T., Zimmermann, J., & Nicholls, R. J. (2015). Future Coastal Population Growth and Exposure to Sea-Level Rise and Coastal Flooding - A Global Assessment. *PLOS ONE 10(6): e0131375. https://doi.org/10.1371/journal.pone.0131375*.

NRCS. (1997). *National Engineering Handbook part 628 Dams. chapter 51 Earth Spillway Erosion Model and Chapter 52 Field Procedures Guide for the Headcut Erodability index.* Natural Resources Conservation Service. 210-vi-NEH.

Paulsen, B. T., Bredmose, H., Bingham, H. B., & Jacobsen, N. G. (2014). *Forcing of a bottom-mounted circular cylinder by steep regular water waves at finite depth.* Journal of Fluid Mechanics 755, 1-34; https://doi.org/10.1017/jfm.2014.386.

Peters, D. (2017). *Design of Pattern-placed Revetments ISBM 9709055841745.* https://doi.org/10.4233/uuid:0b67a0dd-a951-46f3-bbaa-86270e546c4e.

Ponsioen, L., van Damme, M., Hofland, B., & Peeters, P. (2019). Relating grass failure on the landside slope to wave overtopping induced excess normal stresses. *Coastal Engineering, 148, https://doi.org/10.1016/j.coastaleng.2018.12.009*, 49-56.

Saidia, M. S., Rismaniana, M., Monjezia, M., Zendehbadb, M., & Fatehiboroujeni, S. (2014). Comparison between Lagrangian and Eulerian approaches in predicting motion of micron-sized particles in laminar flows. *Atmospheric Environment, 89, https://doi.org/10.1016/j.atmosenv.2014.01.069*, 199-206.

Scheres, B., & Schüttrumpf, H. (2020). Investigating the Erosion Resistance of Different Vegetated Surfaces for Ecological Enhancement of Sea Dikes. *Marine Science and Engineering, 8, 519, https://doi.org/10.3390/jmse8070519*.

Sprangers, H. (1999). *Vegetation dynamics and erosion resistance of seadyke grass-land.* Wageningen, The Netherlands: Ph.D.-Thesis, Landbouwuniverseit Wageningen.

Stanczak, G., Oumeraci, H., & Kortenhaus, A. (2007). *Laboratory Tests on the Erosion of Clay Revetment of Sea Dike With and Without a Grass Cover Induced by Breaking Wave Impact.* Floodsite, LWI REPORT NR 935.

Stanczak, G., Oumeraci, H., & Kortenhaus, A. (2008). *Breaching of sea dikes initiated from the seaside by breaking wave impacts.* FLOODsite, University of Braunschweig – Institute of Technology.

Temple, D., & Hanson, G. (1994). *Headcut development in vegetated earth spillways.* Applied Engineering in Agriculture, 10, pp. 677-682.

Temple, D., Robinson, K., Ahring, R., & Davis, A. (1987). *Stability design of grass-lined open channels.* USDA Agricultural Handbook. No. 667.

Van Bergeijk, V. M., Verdonk, V. A., Warmink, J. J., & Hulscher, S. J. M. H. (2021). The Cross-Dike Failure Probability by Wave Overtopping over Grass-Covered and damaged dikes. *Water 2021, 13(5), 690; https://doi.org/10.3390/w13050690*.

Van Bergeijk, V. M., Warmink, J. J., & Hulscher, S. J. M. H. (2020). Modelling of wave overtopping flow over complex dike geometries: Case study of the afsluitdijk. *Coastal Engineering Proceedings (36v), papers.52.; https://doi.org/10.9753/icce.v36v.papers.52*.

Van der Meer, J. A. (2018). *EurOtop, Manual on wave overtopping of sea defences and related structures. An overtopping manual largely based on European research, but for worldwide application.* www.overtopping-manual.com.

Van Hoven, A. (2014). *Residual dike strength after macro-instability, WTI 2017.* Delft, The Netherlands: Deltares.

Van Hoven, A. (2015). *WTI2017 Faalmechanismebeschrijving grasbekleding.* Delft: Deltares.

Woolhiser, D., Smith, R., & Goodrich, D. (1990). *KINEROS, A Kinematic Runoff and Erosion Model.* USDA-ARS, ARS 77.

Zhang, Y., Chen, G., Hu, J., Chen, X., Yang, W., Tao, A., & Zheng, J. (2017). Experimental study on mechanism of sea-dike failure due to wave overtopping. *Applied Ocean Research, 68, https://doi.org/10.1016/j.apor.2017.08.009*, 171-181.

A Appendix 1: Erosion data obtained from FARO3D laser

A.1 Data delta flume experiments

The data obtained from processing the FARO3D laser data of experiments K1 – K6 is summarized in the tables below. The experiment data for experiment K1 is summarized in Table A-1.

Test nr	Erosion depth [m]	Erosion amount [m^3]	Test duration [h]	Scaled hourly erosion depth [m]	Scaled hourly erosion amount [m^3]	Wave height Hs [m]	Wave period Tp [s]
K101	0.000	0.000	0.250	0.000	0.000	1.964	5.493
K103	0.074	0.172	1.961	0.038	0.088	2.025	5.547
K104	0.151	0.277	2.000	0.075	0.138	1.996	5.501
K105	0.276	0.326	1.620	0.171	0.201	2.012	5.505
K107	0.569	0.636	1.870	0.304	0.340	1.943	5.632
K108	0.817	1.476	0.750	1.090	1.968	1.948	5.501
K109	0.874	2.902	0.670	1.305	4.331	2.003	5.557
K110	0.924	4.861	0.560	1.649	8.681	2.030	5.571
K111	0.933	7.022	0.760	1.228	9.239	2.016	5.549
K112	1.196	10.670	1.290	0.927	8.271	1.996	5.553
K113	1.343	13.391	1.150	1.168	11.644	1.941	5.528
K114	1.549	15.261	1.170	1.324	13.044	1.967	5.529

Table A-1 Erosion and experiment data per test of experiment K1, with data from the delta flume experiments (supplied by Klein Breteler, 2020).

The experiment data for experiment K2 is summarized in Table A-2

Test nr	Erosion depth [m]	Erosion amount [m^3]	Test duration [h]	Scaled hourly erosion depth [m]	Scaled hourly erosion amount [m^3]	Wave height Hs [m]	Wave period Tp [s]
K201	0.000	0.000	0.250	0.000	0.000	2.000	5.525
K202	0.092	0.222	2.000	0.046	0.111	2.000	5.525
K203	0.225	0.314	2.000	0.112	0.157	2.000	5.525
K204	0.244	0.367	2.000	0.122	0.183	1.924	5.489
K205	0.225	0.379	2.000	0.112	0.189	1.959	5.487
K206	0.238	0.475	1.000	0.238	0.475	2.016	5.532
K207	0.230	0.532	2.300	0.100	0.231	1.931	5.491
K208	0.280	0.723	2.000	0.140	0.361	2.000	5.525

Table A-2 Erosion and experiment data per test of experiment K2, with data from the delta flume experiments (supplied by Klein Breteler, 2020).

The experiment data for experiment K3 is summarized in Table A-3.

Test nr	Erosion depth [m]	Erosion amount [m^3]	Test duration [h]	Scaled hourly erosion depth [m]	Scaled hourly erosion amount [m^3]	Wave height Hs [m]	Wave period Tp [s]
K301	0.280	0.000	2.040	0.137	0.000	1.933	5.468
K302	0.201	0.066	1.580	0.127	0.042	1.840	5.621
K303	0.401	0.429	3.110	0.129	0.138	1.914	5.528
K304	0.678	0.909	3.830	0.177	0.237	1.945	5.519
K305	0.730	1.309	2.000	0.365	0.655	1.942	5.513
K306	0.816	1.814	2.000	0.408	0.907	1.944	5.502
K307	0.897	2.358	2.000	0.448	1.179	1.941	5.503
K308	0.893	3.023	2.000	0.447	1.512	1.948	5.505
K309	0.897	3.989	2.000	0.448	1.994	1.939	5.503
K310	0.924	5.865	2.000	0.462	2.933	1.950	5.518

Table A-3 Erosion and experiment data per test of experiment K3, with data from the delta flume experiments (supplied by Klein Breteler, 2020).

The experiment data for experiment K4 is summarized in Table A-4.

Test nr	Erosion depth [m]	Erosion amount [m^3]	Test duration [h]	Scaled hourly erosion depth [m]	Scaled hourly erosion amount [m^3]	Wave height Hs [m]	Wave period Tp [s]
K401	0.000	0.000	0.350	0.000	0.000	1.915	5.549
K402	0.165	0.177	0.520	0.317	0.340	2.097	5.522
K403	0.159	0.268	0.840	0.189	0.319	2.042	5.550
K404	0.127	0.325	0.960	0.132	0.339	2.040	5.529
K405	0.144	0.433	1.560	0.092	0.277	2.009	5.503
K406	0.310	0.636	1.490	0.208	0.427	2.016	5.515
K407	0.330	0.915	2.000	0.165	0.457	2.062	5.534
K408	0.711	1.238	1.170	0.607	1.058	2.044	5.551
K409	0.666	1.504	1.000	0.666	1.504	2.066	5.521
K410	0.759	1.733	0.860	0.883	2.015	2.025	5.551
K411	0.796	2.036	1.100	0.724	1.851	2.008	5.531
K412	0.797	2.443	0.500	1.593	4.885	1.670	5.033
K413	0.968	4.092	1.010	0.959	4.051	2.051	5.536
K414	1.130	6.185	1.000	1.130	6.185	2.057	5.534
K415	1.174	9.132	2.000	0.587	4.566	2.055	5.534
K416	1.307	10.879	2.000	0.653	5.440	2.006	5.504
K417	1.465	13.162	1.700	0.862	7.743	2.081	5.507

Table A-4 Erosion and experiment data per test of experiment K4, with data from the delta flume experiments (supplied by Klein Breteler, 2020).

The experiment data for experiment K5 is summarized in Table A-5.

Test nr	Erosion depth [m]	Erosion amount [m^3]	Test duration [h]	Scaled hourly erosion depth [m]	Scaled hourly erosion amount [m^3]	Wave height Hs [m]	Wave period Tp [s]
K501	0.000	0.000	0.330	0.000	0.000	1.983	5.513
K502	0.148	0.173	2.000	0.074	0.086	2.047	5.537
K503	0.274	0.328	2.000	0.137	0.164	2.043	5.537
K504	0.377	0.626	1.890	0.199	0.331	2.075	5.564
K505	0.470	1.037	2.000	0.235	0.519	2.052	5.522
K506	0.579	1.280	1.000	0.579	1.280	2.050	5.536

Table A-5 Erosion and experiment data per test of experiment K5, with data from the delta flume experiments (supplied by Klein Breteler, 2020).

The experiment data for experiment K6 is summarized in Table A-6.

Test nr	Erosion depth [m]	Erosion amount [m^3]	Test duration [h]	Scaled hourly erosion depth [m]	Scaled hourly erosion amount [m^3]	Wave height Hs [m]	Wave period Tp [s]
K601	0.579	0.000	1.750	0.331	0.000	1.991	5.484
K602	0.440	0.178	1.350	0.326	0.132	2.023	5.497
K603	0.459	0.308	1.420	0.324	0.217	1.534	4.820
K604	0.730	1.127	2.000	0.365	0.564	2.044	5.534
K605	0.736	1.663	1.000	0.736	1.663	2.044	5.530
K606	0.896	2.530	2.000	0.448	1.265	2.002	5.494
K607	0.998	3.425	1.830	0.545	1.871	2.005	5.496
K608	0.983	5.096	1.500	0.655	3.397	1.967	5.504
K609	1.003	6.785	1.830	0.548	3.708	1.942	5.503
K610	1.101	8.100	2.000	0.551	4.050	1.952	5.492

Table A-6 Erosion and experiment data per test of experiment K6, with data from the delta flume experiments (supplied by Klein Breteler, 2020).

B Appendix 2: Experiment artificial damage

Initial erosion of the grass and clay revetment of the first experiment K1 was very low. Therefore, an artificial damage hole was created after the third test with dimensions 20x20x5 cm. However, the erosion rate was still insufficient (Klein Breteler, 2020) and the hole was enlarged to the dimensions of 40x40x14 cm after the fourth test. The resulting increase in erosion rate due to artificial damage is visible in Figure 4-1 after the third test. After the fourth tests the erosion volumes become much higher, with a linear increase in each test (not compensated for the duration of the tests). This is an indication that the grass cover is highly important for erosion resistance in case the clay quality of a dike is poor, since the removal of the grass cover resulted in large amounts of erosion after prolonged wave impact.

The high initial percentage increase in erosion depth and volume during experiment K2 is explained by the artificial damage created to increase erosion rate. The second experiment represented the Lauwersmeerdijk-Vierhuizengat with higher quality clay from Blija. The dike proved to be very erosion resistance as after almost 14 h of wave impact less than 1 m^3 of erosion was measured compared to 16 m^3 after 11 h of impact in the first experiment. The artificial damage that was created after the first test of experiment K2 consisting of a hole with dimensions 20x20x5 cm, did not seem to increase the erosion rate. Therefore, the size of the artificial damage hole was increased after the second test to 40x40x14 cm. Lastly, an artificial cliff with a depth of 20 cm was created after the seventh test since hardly any erosion was measured still. The erosion process of experiment K2 is best observed in Figure 4-1 where three major increases in maximum erosion depth and volume are observed after the 2nd , 3rd and 8th test. After these tests, only minor increases in erosion were observed, showing that the dike is very erosion resistant compared to experiment K1 indicating the potentially large influence of the clay quality on erosion.

The erosion process of experiment K3 is a continuation of experiment K2 and similar to K1 regarding the percentage increase (Figure 4-1). Between experiment K2 and K3 the berm has been lowered by approximately 15 cm to increase the run-up erosion (Klein Breteler, 2020). After the second test an artificial hole was created in the grass revetment with a maximum depth of 34 cm and unknown width and length. The lowering of the berm height resulting in an increase in water level likely has a major influence because there was significantly more erosion in experiment K3 compared to experiment K2.

Initial erosion during experiment K4 was significant, due to the apparent lower quality of grass compared to experiment K1 (Klein Breteler, 2021). Therefore, no artificial erosion was created during experiment K4. On the contrary, an 80 cm deep erosion hole arose during the 8th test of experiment K4, which was filled in to a depth of 35 cm. The erosion hole likely arose due to poor quality clay that was locally present and was filled in order to not influence the rest of the experiment. The effect of the aforementioned erosion is visible as the rapid increase in erosion depth between test 7 and 8 in the top left plot of Figure 4-1.

A low level of erosion occurred during the first test of experiment K5 and therefore an erosion hole was created, which was expanded after the second test of experiment K5 (Klein Breteler, 2021). The size of the artificial erosion hole is the same as created and expanded after the 2nd and 3rd of experiment K2. The effect of the artificial erosion is not directly visible in the erosion depth and erosion volume in the figures shown in the results.

No significant artificial damage was created during experiment K6, although some crevasses between the clay blocks were filled in after several tests to prevent the crevasses from influencing the erosion rate.

The significant artificial damage from the experiments K1 – K6 is summarized in Table B-1.

Test number	Erosion type
K103	Hole created with size 20x20x5 cm^3
K104	Hole size increased to 40x40x15 cm^3
K202	Hole created with size 20x20x5 cm^3
K203	Hole size increased to 40x40x15 cm^3
K301	Lowered berm in front of grass revetment by 15 cm
K302	Hole with 35 cm depth
K408	Filled up deep erosion hole to reduce depth to 35 cm
K501	Hole created with size 20x20x5 cm^3
K502	Hole size increased to 40x40x15 cm^3

Table B-1 Summary of artificial damage during wave impact experiments (after: Klein Breteler, 2021).

C Appendix 3: Erosion profiles and surfaces

Erosion profiles obtained from FARO 3D laser scanner data of Deltares delta flume experiments were obtained for each test. However, not all profiles are included in the appendix due to the large amount of tests. Therefore, only the profiles with significant erosion change are included.

C.2 Erosion surface experiment K1

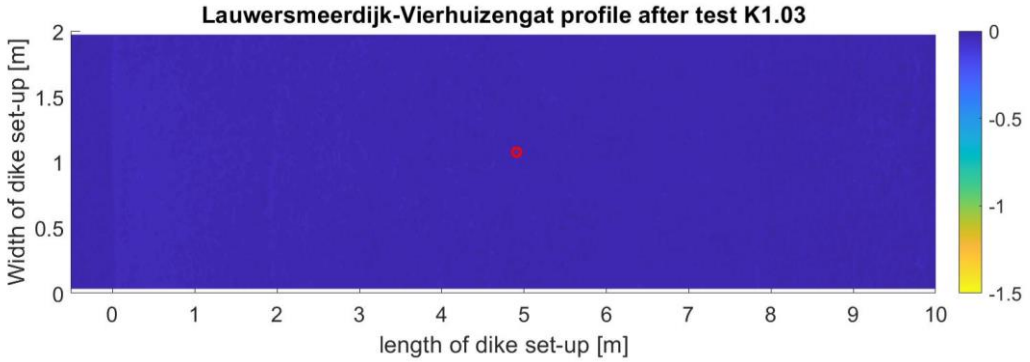

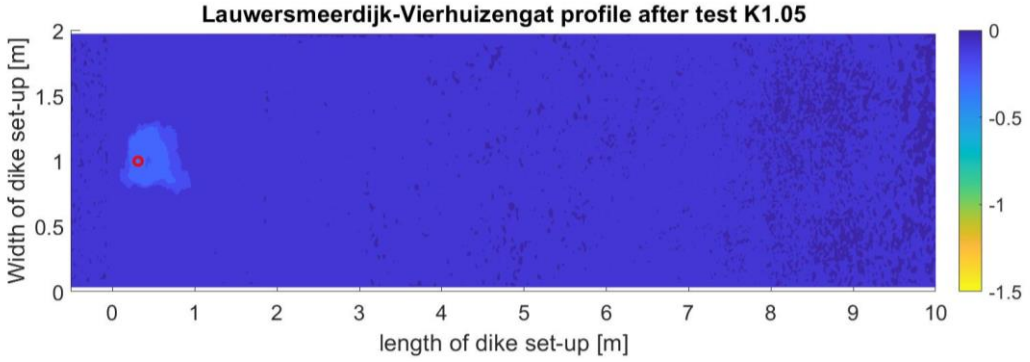

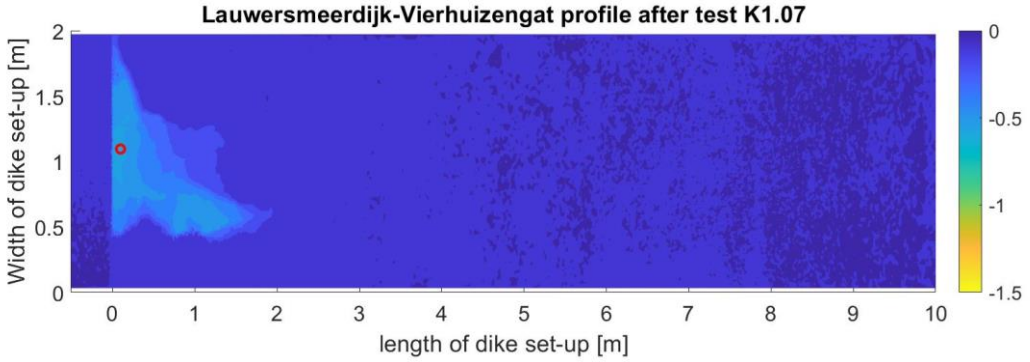

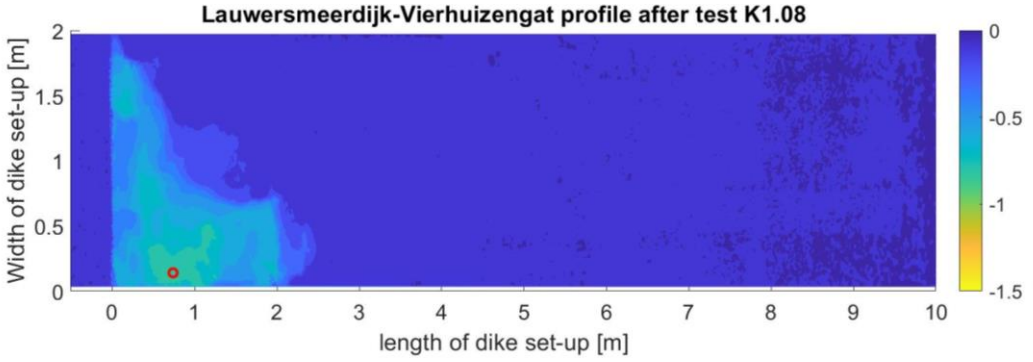

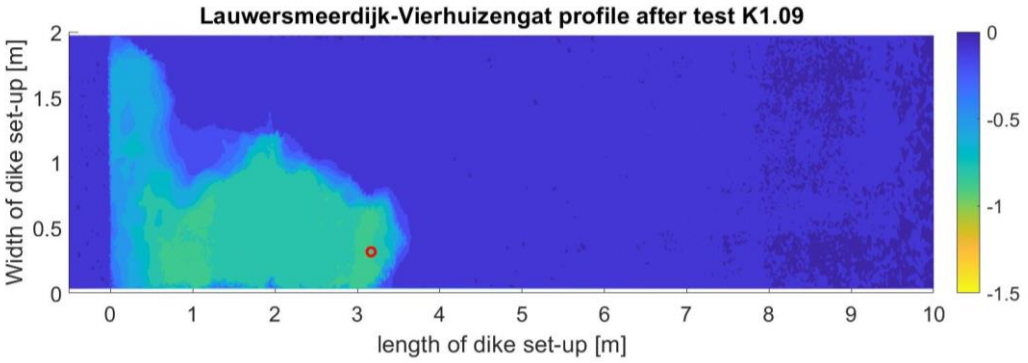
Lauwersmeerdijk-Vierhuizengat profile after test K1.09
Width of dike set-up [m]
length of dike set-up [m]
0
0.5
1
1.5
2
0
1
2
3
4
5
6
7
8
9
10
0
-0.5
-1
-1.5

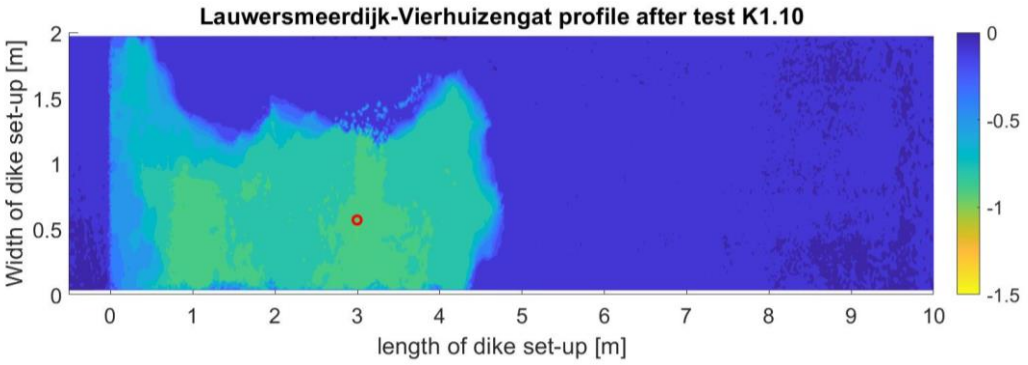
Lauwersmeerdijk-Vierhuizengat profile after test K1.10
Width of dike set-up [m]
length of dike set-up [m]
0
0.5
1
1.5
2
0
1
2
3
4
5
6
7
8
9
10
0
-0.5
-1
-1.5

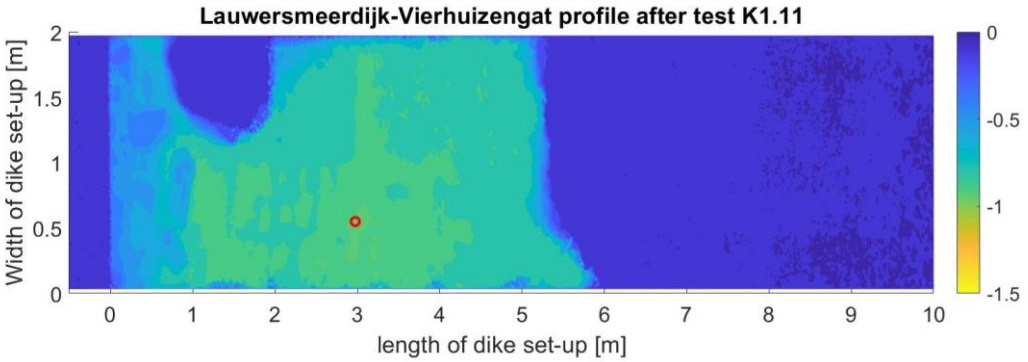
Lauwersmeerdijk-Vierhuizengat profile after test K1.11
Width of dike set-up [m]
length of dike set-up [m]
0
0.5
1
1.5
2
0
1
2
3
4
5
6
7
8
9
10
0
-0.5
-1
-1.5

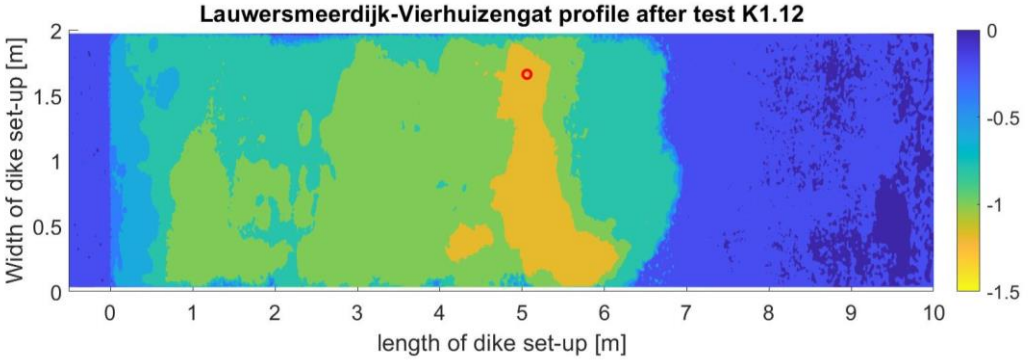
Lauwersmeerdijk-Vierhuizengat profile after test K1.12
Width of dike set-up [m]
length of dike set-up [m]
0
0.5
1
1.5
2
0
1
2
3
4
5
6
7
8
9
10
0
-0.5
-1
-1.5

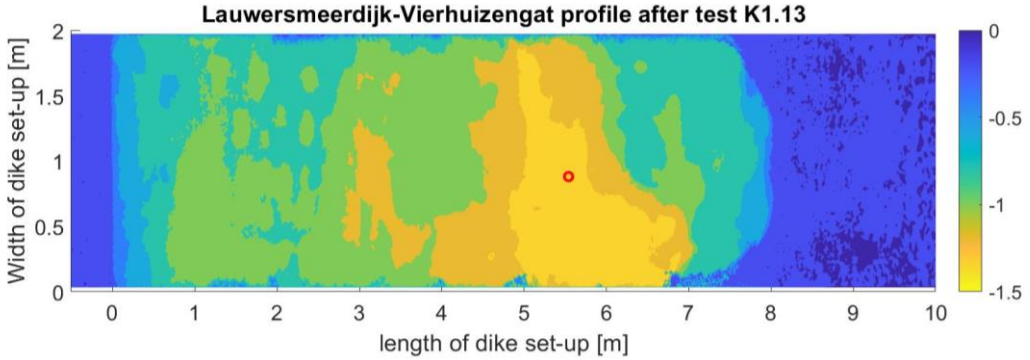

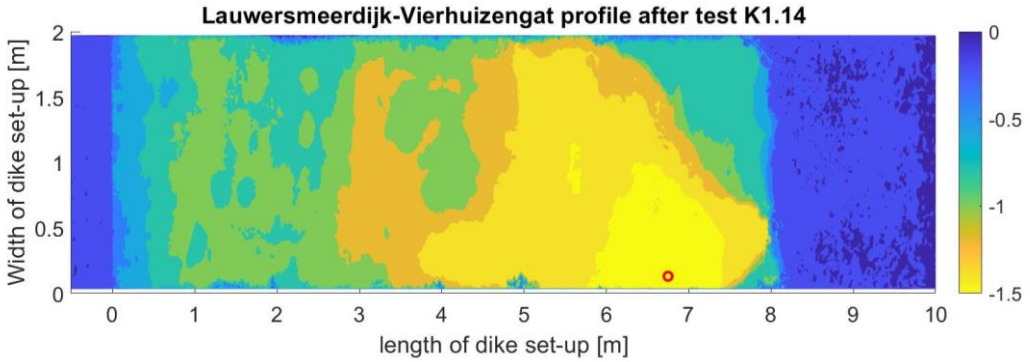

C.3 Erosion cross-sections experiment K1

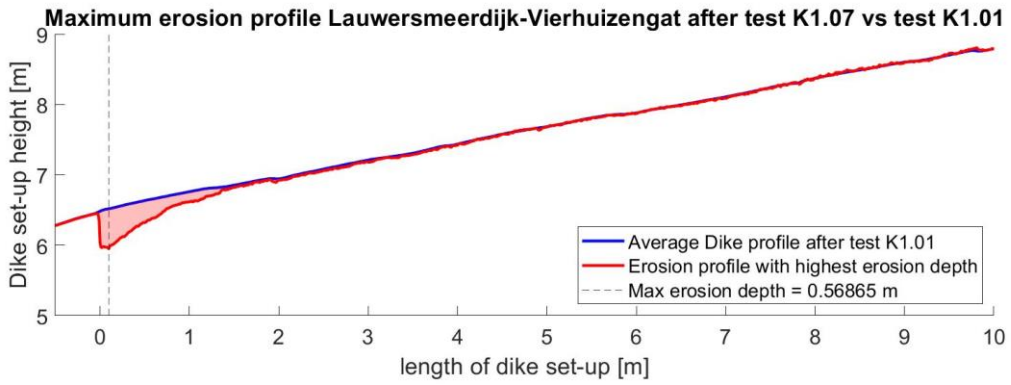

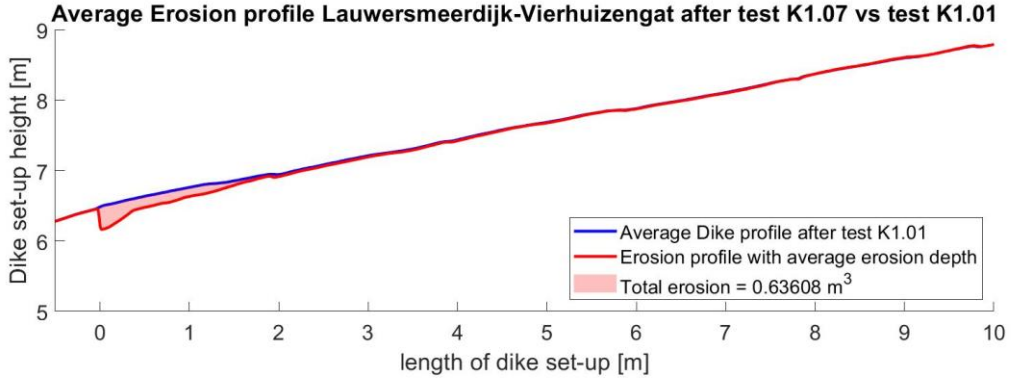

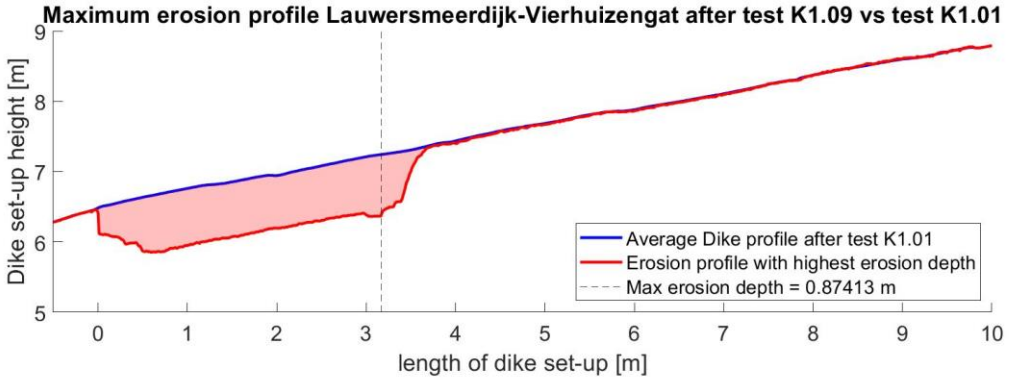
Maximum erosion profile Lauwersmeerdijk-Vierhuizengat after test K1.09 vs test K1.01
Dike set-up height [m]
length of dike set-up [m]
Average Dike profile after test K1.01
Erosion profile with highest erosion depth
Max erosion depth = 0.87413 m

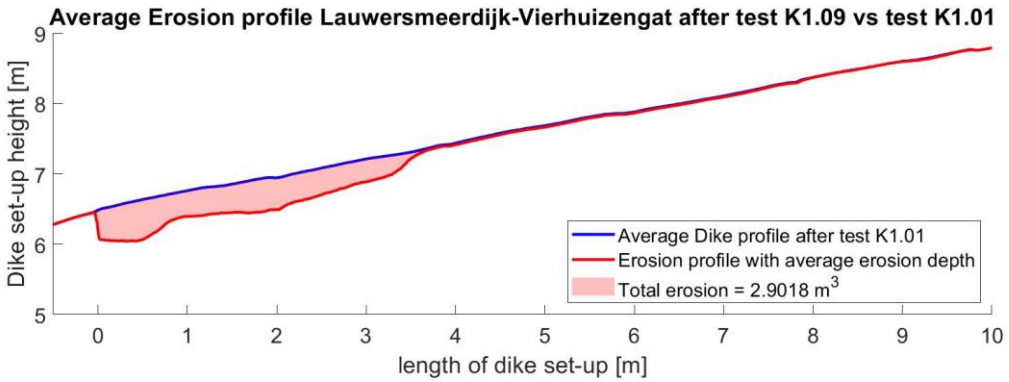
Average Erosion profile Lauwersmeerdijk-Vierhuizengat after test K1.09 vs test K1.01
Dike set-up height [m]
length of dike set-up [m]
Average Dike profile after test K1.01
Erosion profile with average erosion depth
Total erosion = 2.9018 m3

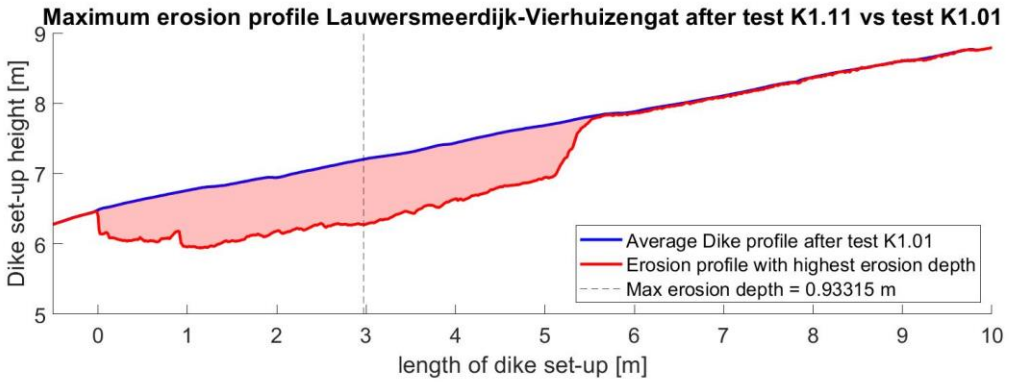
Maximum erosion profile Lauwersmeerdijk-Vierhuizengat after test K1.11 vs test K1.01
Dike set-up height [m]
length of dike set-up [m]
Average Dike profile after test K1.01
Erosion profile with highest erosion depth
Max erosion depth = 0.93315 m

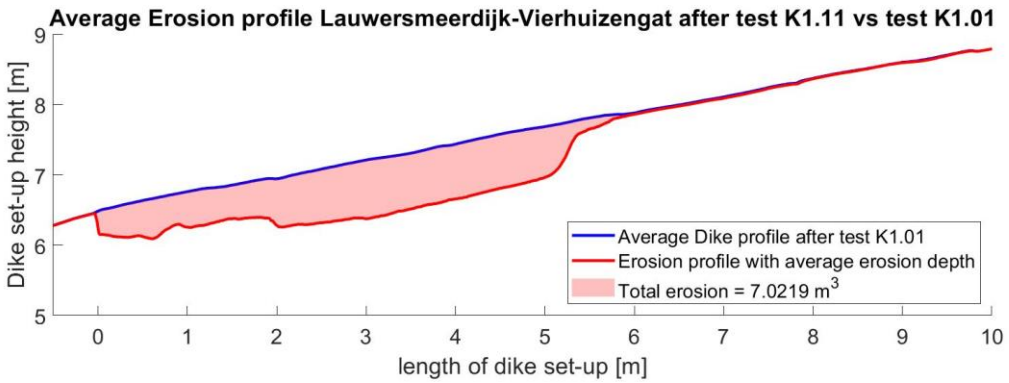
Average Erosion profile Lauwersmeerdijk-Vierhuizengat after test K1.11 vs test K1.01
Dike set-up height [m]
length of dike set-up [m]
Average Dike profile after test K1.01
Erosion profile with average erosion depth
Total erosion = 7.0219 m3

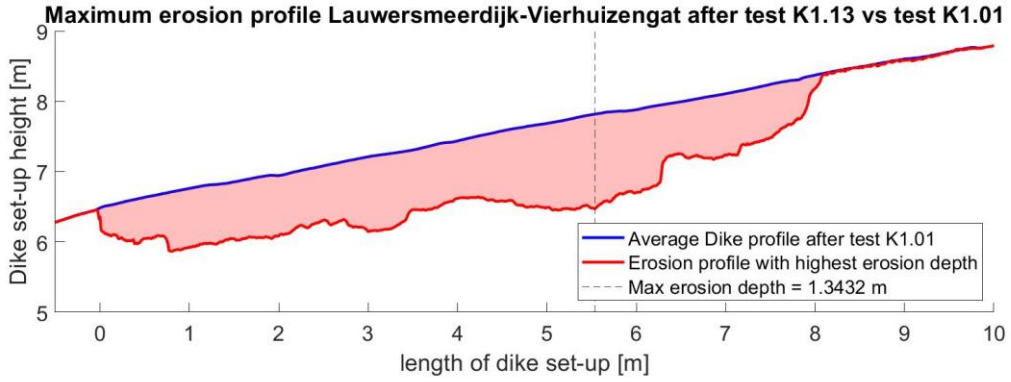
Maximum erosion profile Lauwersmeerdijk-Vierhuizengat after test K1.13 vs test K1.01
Dike set-up height [m]
length of dike set-up [m]
Average Dike profile after test K1.01
Erosion profile with highest erosion depth
Max erosion depth = 1.3432 m

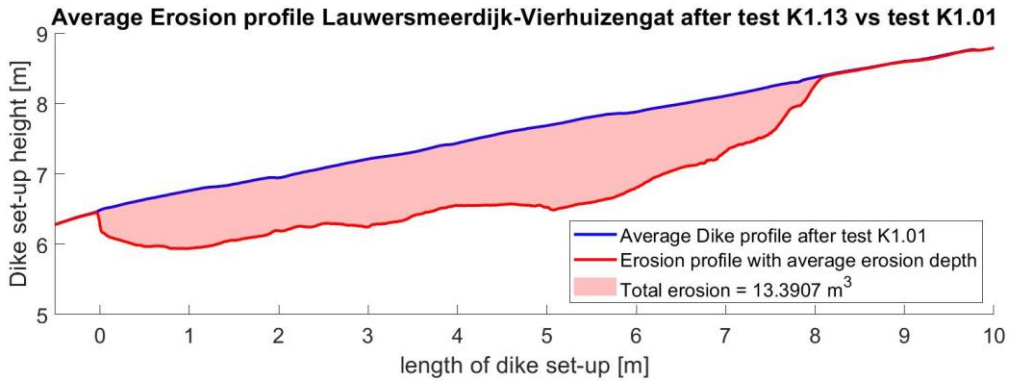
Average Erosion profile Lauwersmeerdijk-Vierhuizengat after test K1.13 vs test K1.01
Dike set-up height [m]
length of dike set-up [m]
Average Dike profile after test K1.01
Erosion profile with average erosion depth
Total erosion = 13.3907 m3

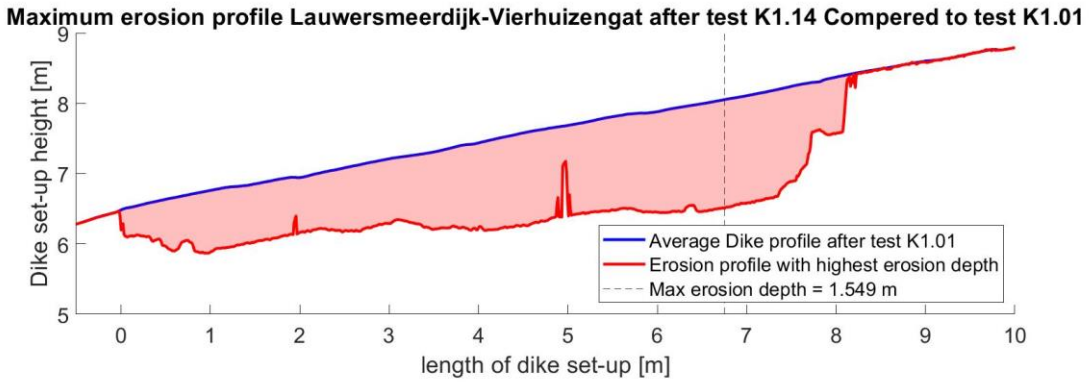
Maximum erosion profile Lauwersmeerdijk-Vierhuizengat after test K1.14 Compered to test K1.01
Dike set-up height [m]
length of dike set-up [m]
Average Dike profile after test K1.01
Erosion profile with highest erosion depth
Max erosion depth = 1.549 m

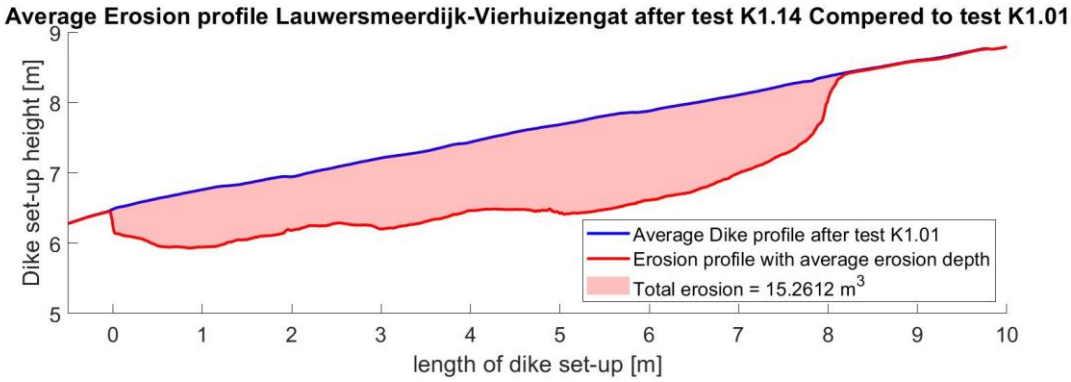
Average Erosion profile Lauwersmeerdijk-Vierhuizengat after test K1.14 Compered to test K1.01
Dike set-up height [m]
length of dike set-up [m]
Average Dike profile after test K1.01
Erosion profile with average erosion depth
Total erosion = 15.2612 m3

C.4 Erosion surface experiment K2

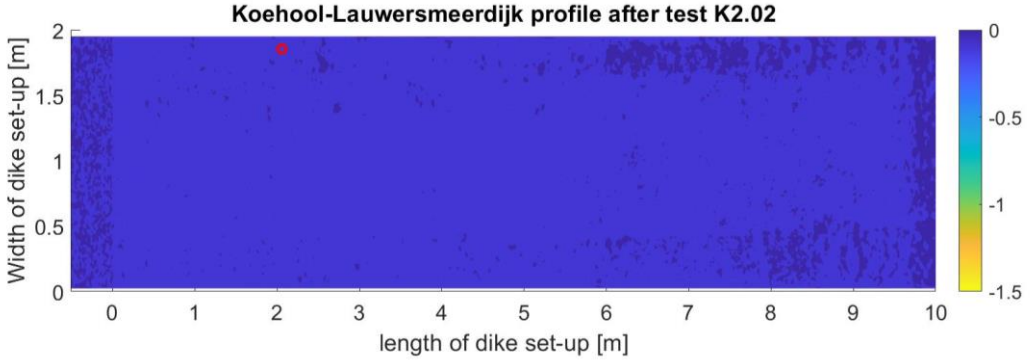

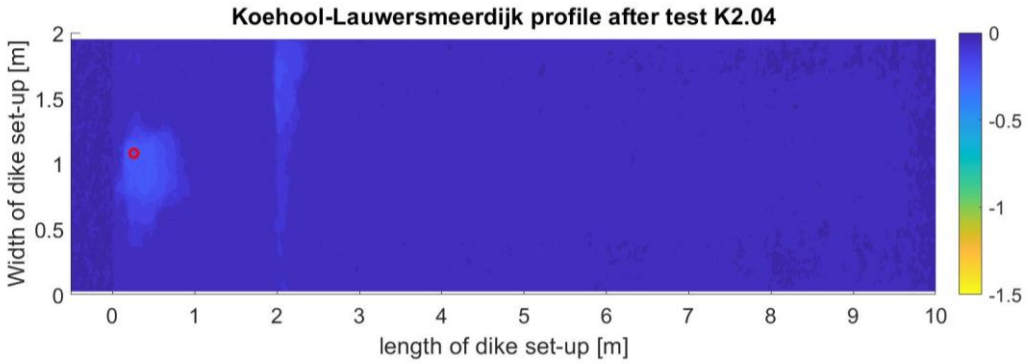

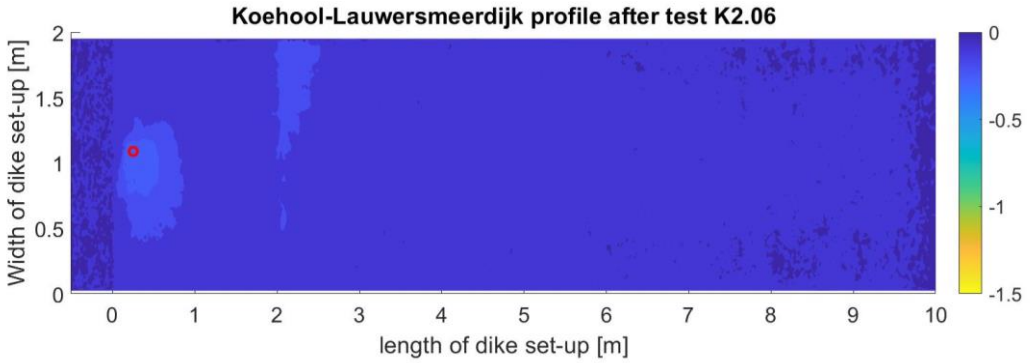

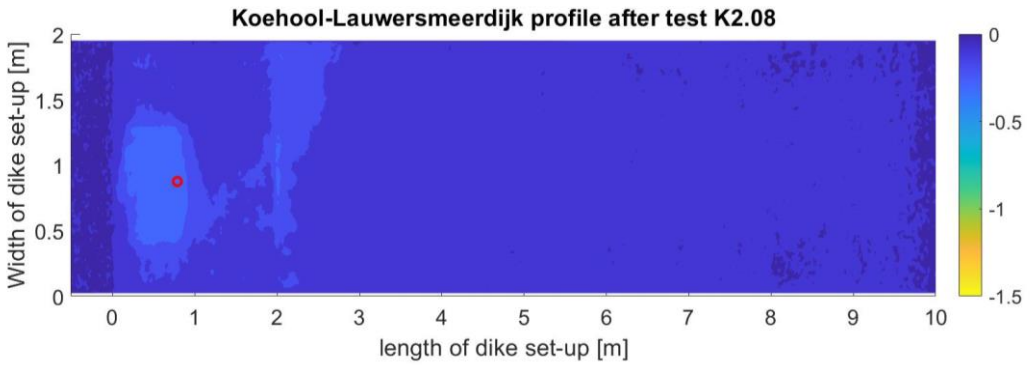

C.5 Erosion cross-section experiment K2

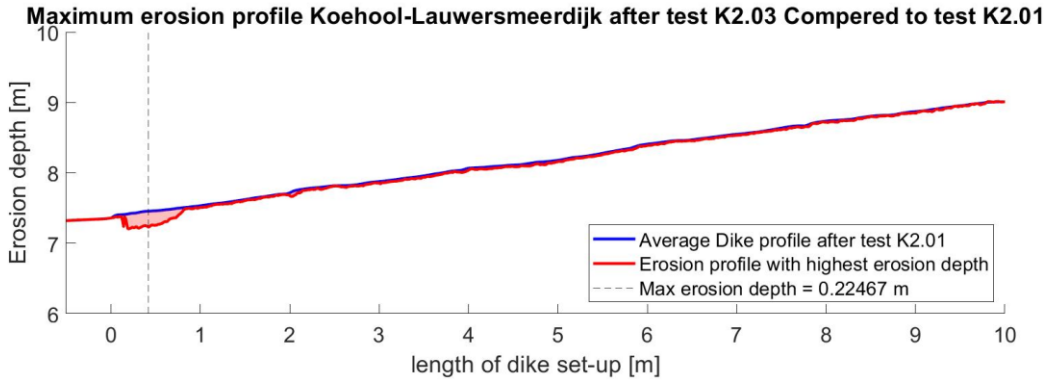

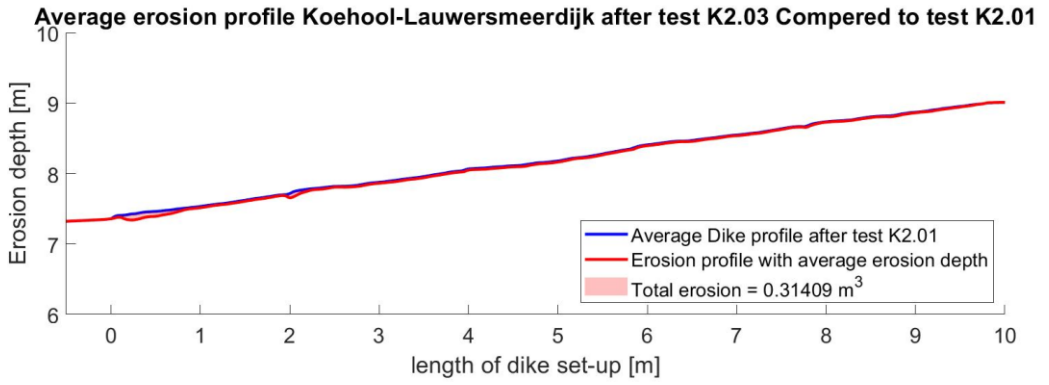

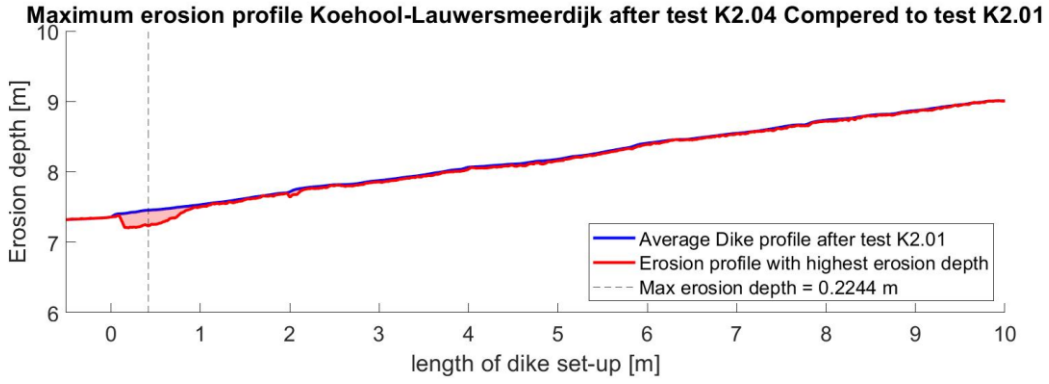

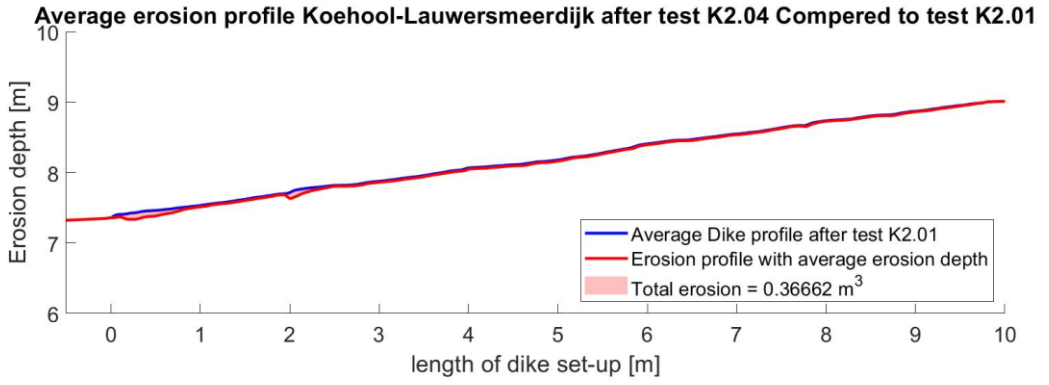

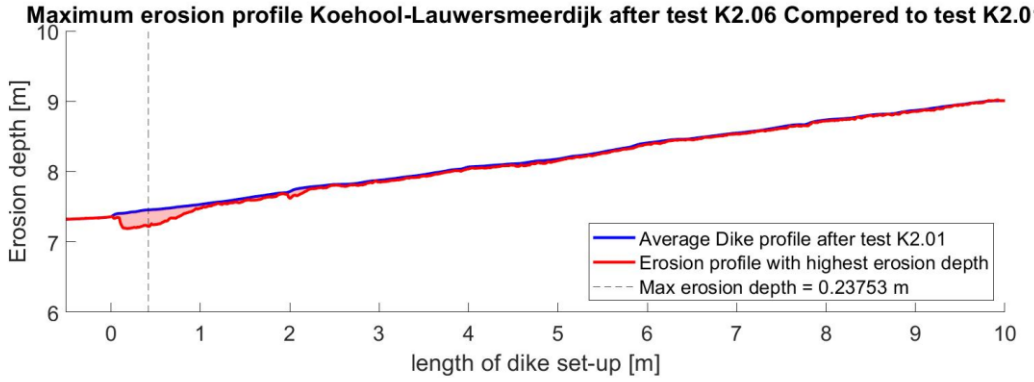
Maximum erosion profile Koehool-Lauwersmeerdijk after test K2.06 Compered to test K2.01
Erosion depth [m]
length of dike set-up [m]
Average Dike profile after test K2.01
Erosion profile with highest erosion depth
Max erosion depth = 0.23753 m

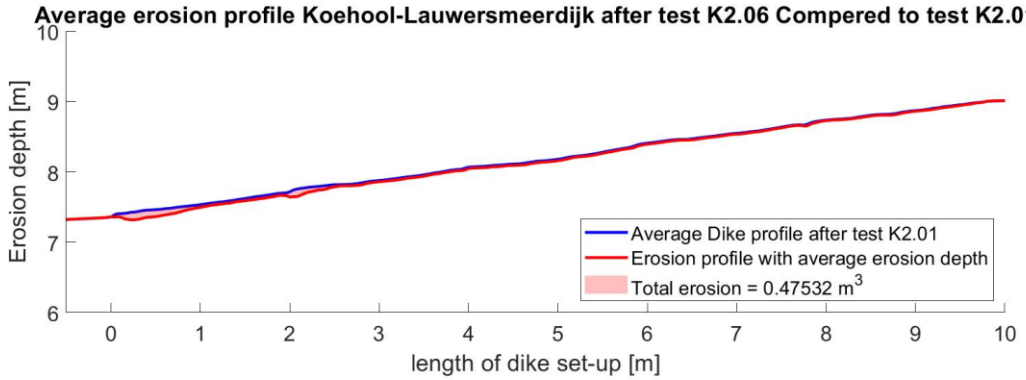
Average erosion profile Koehool-Lauwersmeerdijk after test K2.06 Compered to test K2.01
Erosion depth [m]
length of dike set-up [m]
Average Dike profile after test K2.01
Erosion profile with average erosion depth
Total erosion = 0.47532 m3

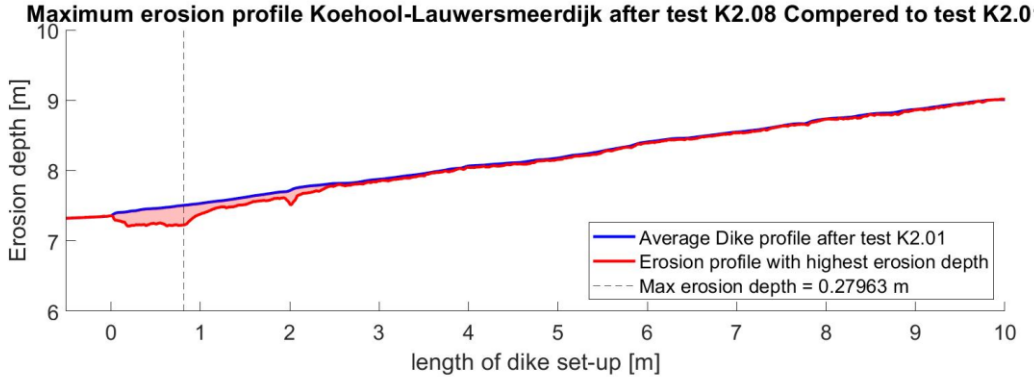
Maximum erosion profile Koehool-Lauwersmeerdijk after test K2.08 Compered to test K2.01
Erosion depth [m]
length of dike set-up [m]
Average Dike profile after test K2.01
Erosion profile with highest erosion depth
Max erosion depth = 0.27963 m

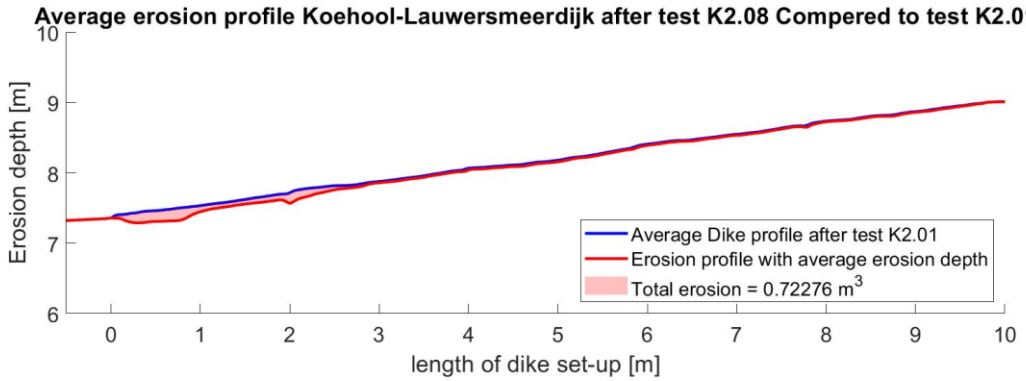
Average erosion profile Koehool-Lauwersmeerdijk after test K2.08 Compered to test K2.01
Erosion depth [m]
length of dike set-up [m]
Average Dike profile after test K2.01
Erosion profile with average erosion depth
Total erosion = 0.72276 m3

C.6 Erosion surface experiment K3

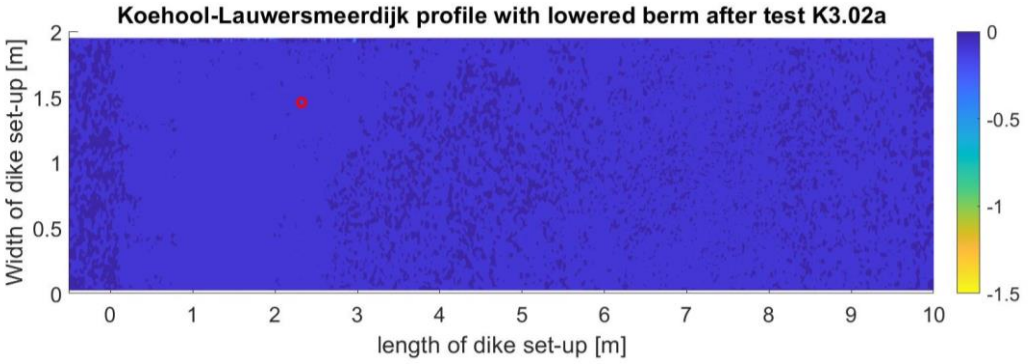

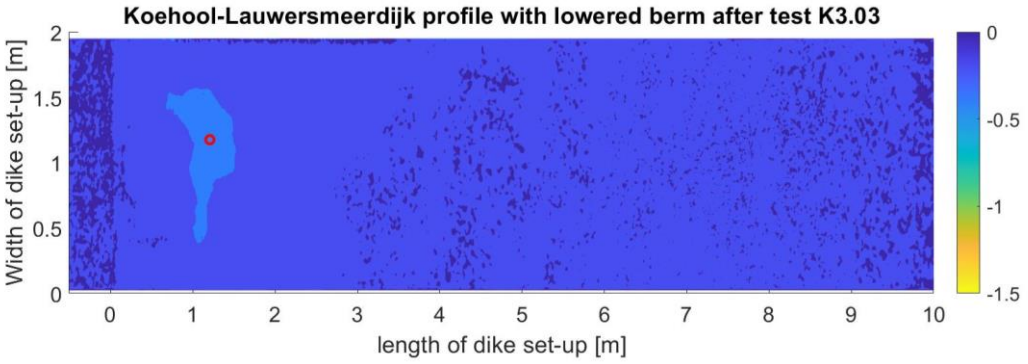

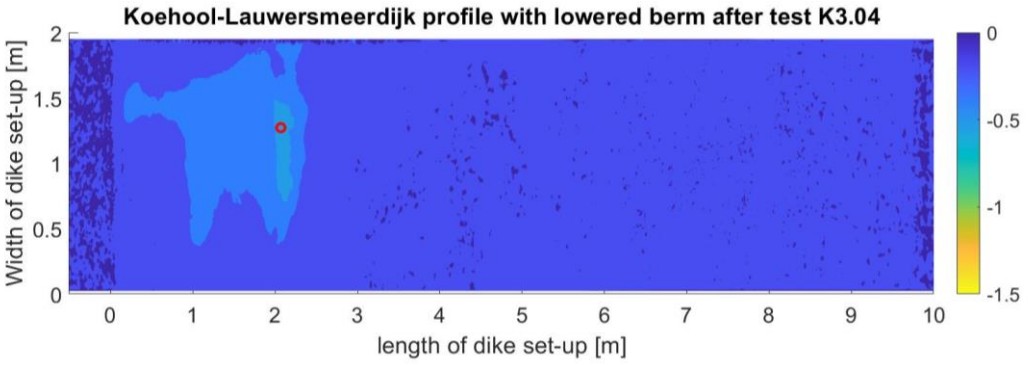

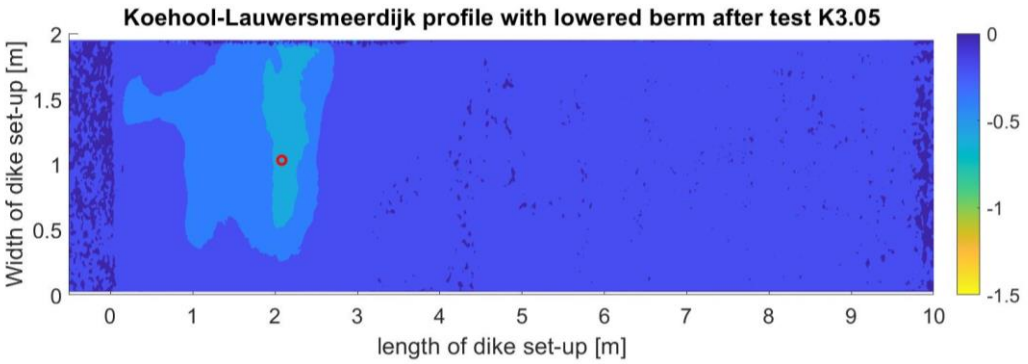

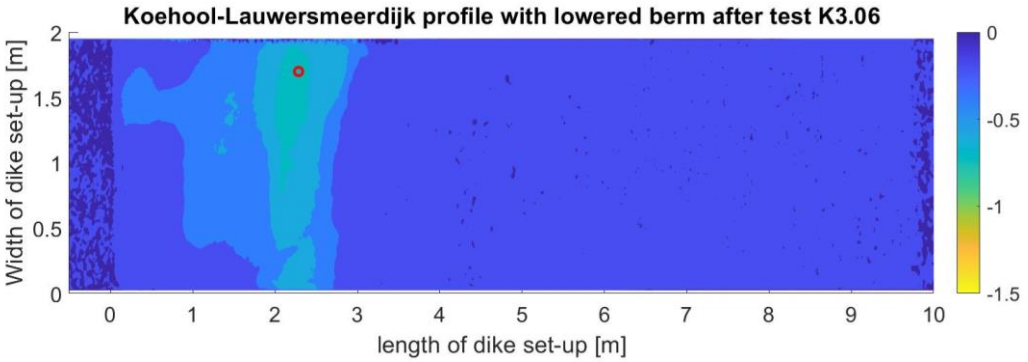
Koehool-Lauwersmeerdijk profile with lowered berm after test K3.06
Width of dike set-up [m]
length of dike set-up [m]
0
0.5
1
1.5
2
0
1
2
3
4
5
6
7
8
9
10
0
-0.5
-1
-1.5

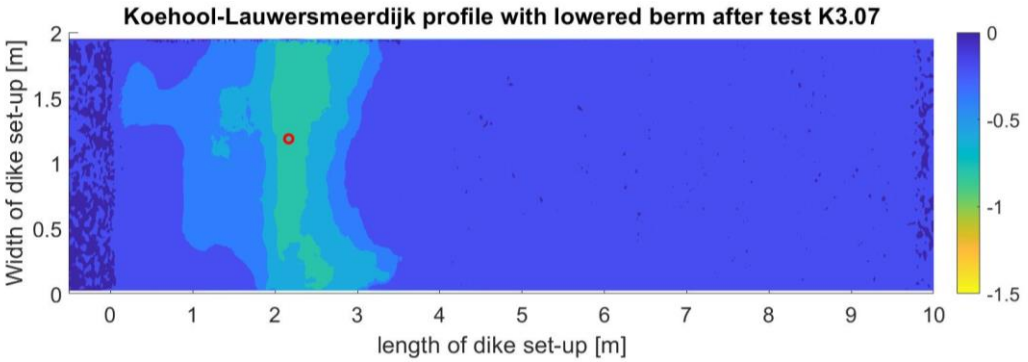
Koehool-Lauwersmeerdijk profile with lowered berm after test K3.07
Width of dike set-up [m]
length of dike set-up [m]
0
0.5
1
1.5
2
0
1
2
3
4
5
6
7
8
9
10
0
-0.5
-1
-1.5

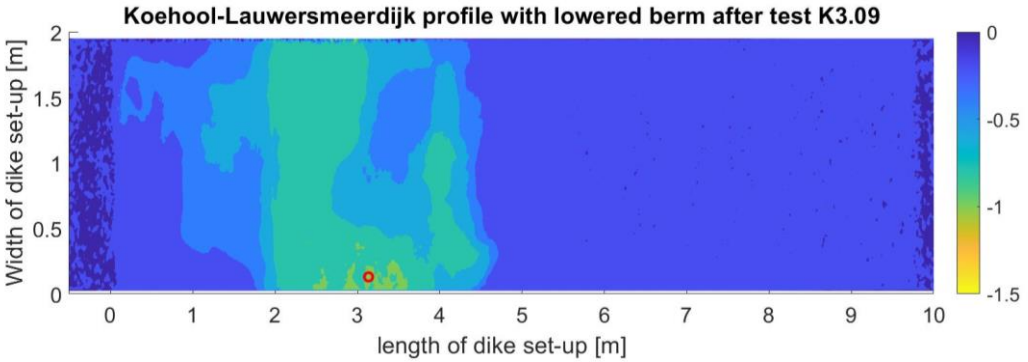
Koehool-Lauwersmeerdijk profile with lowered berm after test K3.09
Width of dike set-up [m]
length of dike set-up [m]
0
0.5
1
1.5
2
0
1
2
3
4
5
6
7
8
9
10
0
-0.5
-1
-1.5

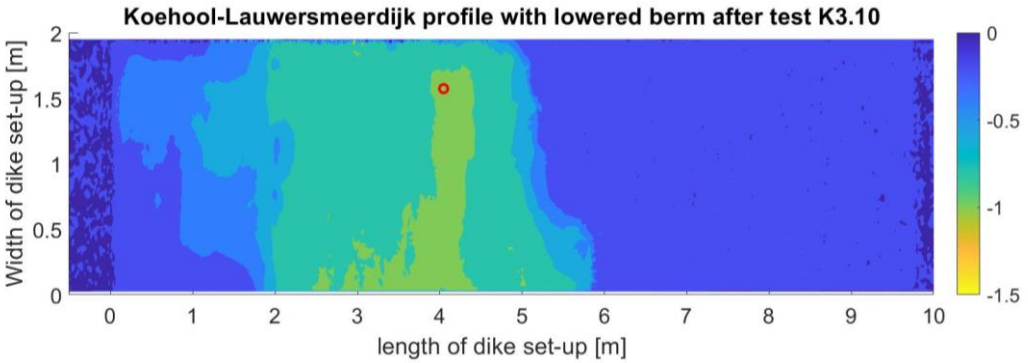
Koehool-Lauwersmeerdijk profile with lowered berm after test K3.10
Width of dike set-up [m]
length of dike set-up [m]
0
0.5
1
1.5
2
0
1
2
3
4
5
6
7
8
9
10
0
-0.5
-1
-1.5

C.7 Erosion cross-section experiment K3

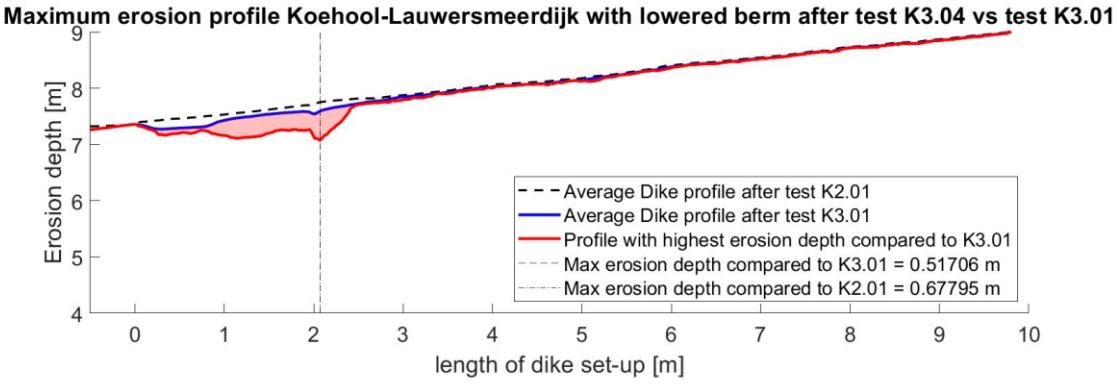

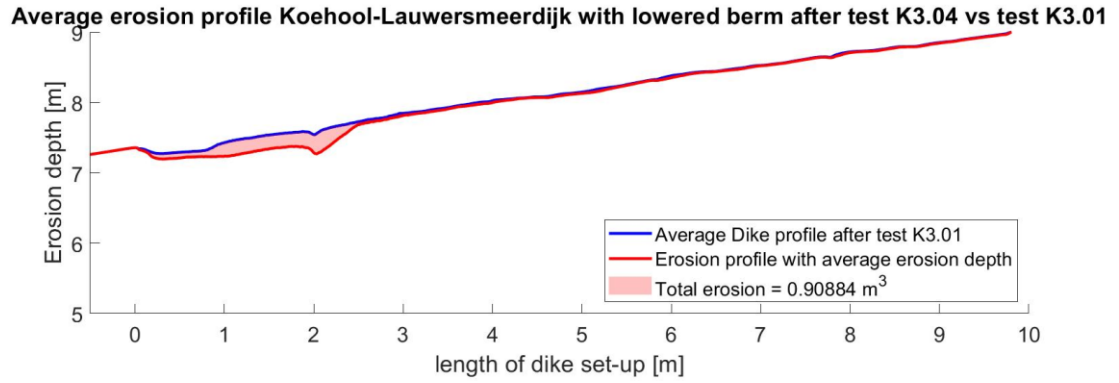

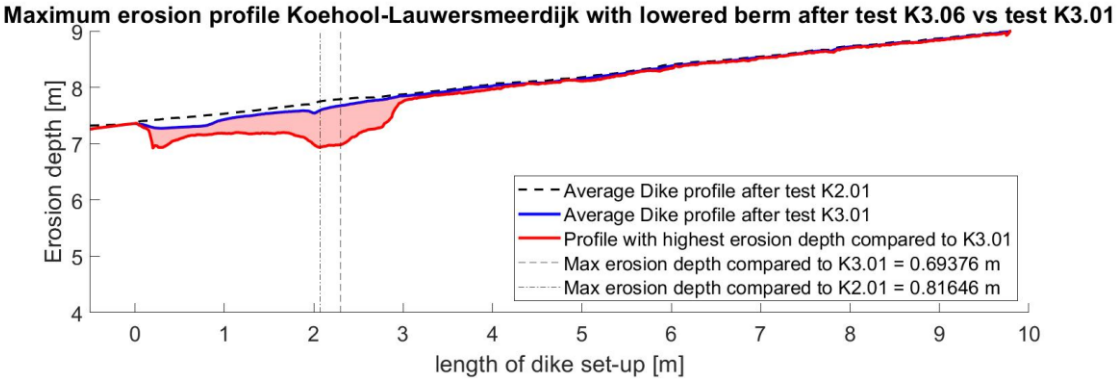

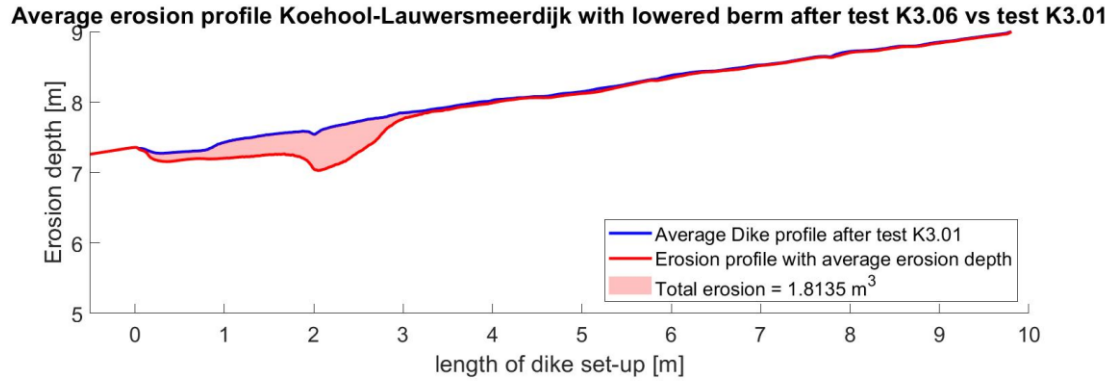

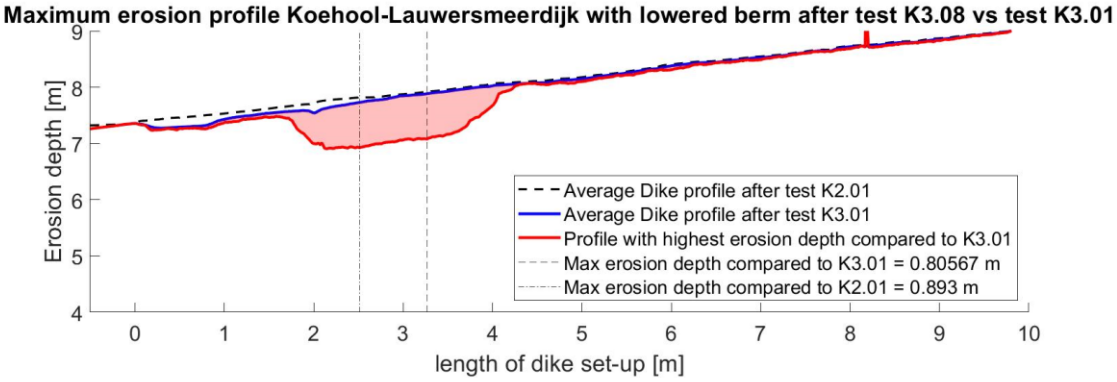
Maximum erosion profile Koehool-Lauwersmeerdijk with lowered berm after test K3.08 vs test K3.01
Erosion depth [m]
length of dike set-up [m]
Average Dike profile after test K2.01
Average Dike profile after test K3.01
Profile with highest erosion depth compared to K3.01
Max erosion depth compared to K3.01 = 0.80567 m
Max erosion depth compared to K2.01 = 0.893 m

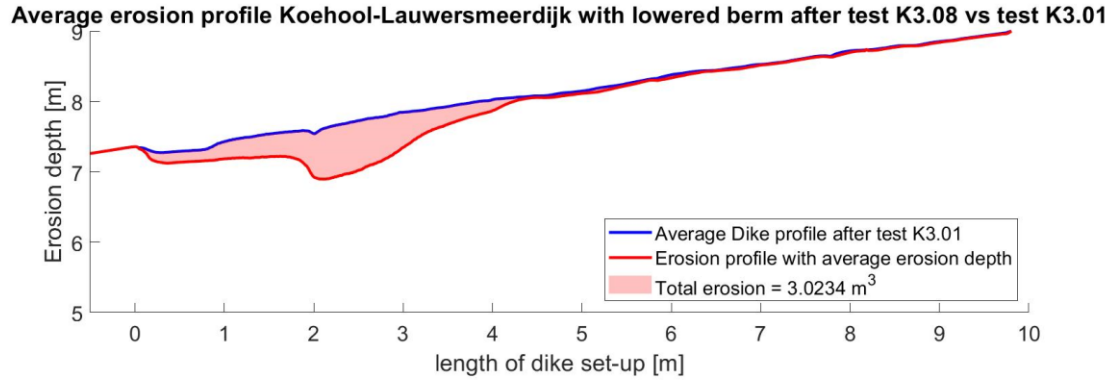
Average erosion profile Koehool-Lauwersmeerdijk with lowered berm after test K3.08 vs test K3.01
Erosion depth [m]
length of dike set-up [m]
Average Dike profile after test K3.01
Erosion profile with average erosion depth
Total erosion = 3.0234 m3

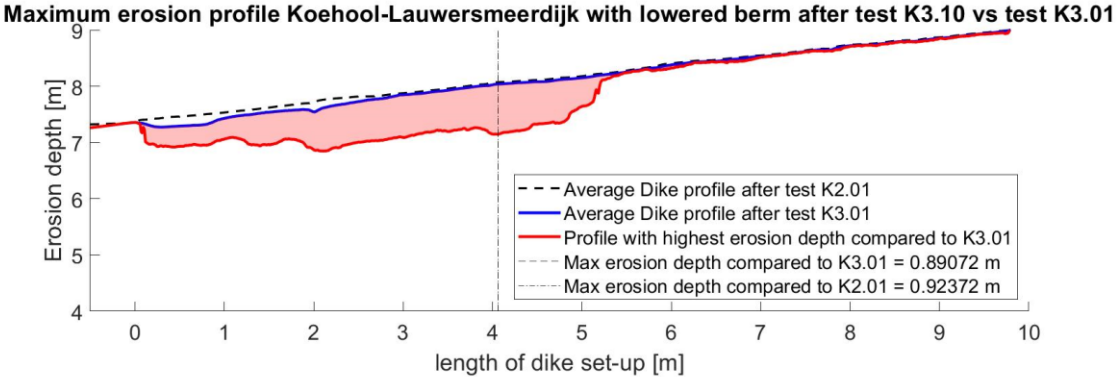
Maximum erosion profile Koehool-Lauwersmeerdijk with lowered berm after test K3.10 vs test K3.01
Erosion depth [m]
length of dike set-up [m]
Average Dike profile after test K2.01
Average Dike profile after test K3.01
Profile with highest erosion depth compared to K3.01
Max erosion depth compared to K3.01 = 0.89072 m
Max erosion depth compared to K2.01 = 0.92372 m

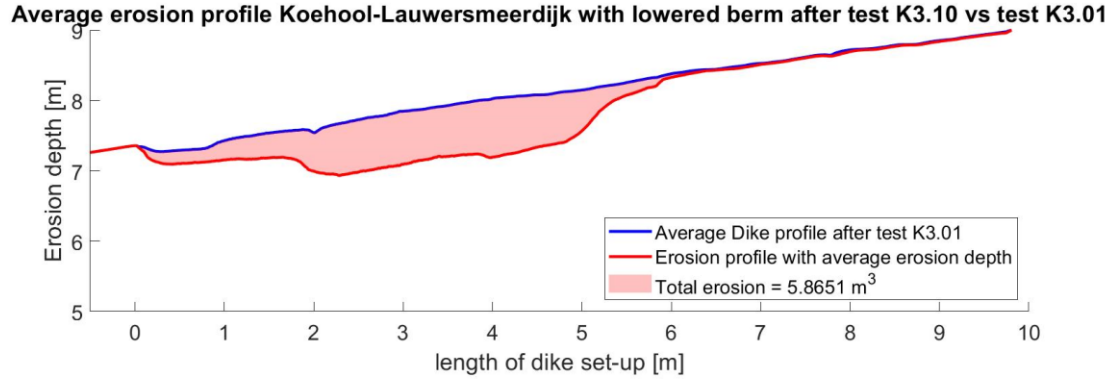
Average erosion profile Koehool-Lauwersmeerdijk with lowered berm after test K3.10 vs test K3.01
Erosion depth [m]
length of dike set-up [m]
Average Dike profile after test K3.01
Erosion profile with average erosion depth
Total erosion = 5.8651 m3

C.8 Erosion surface experiment K4

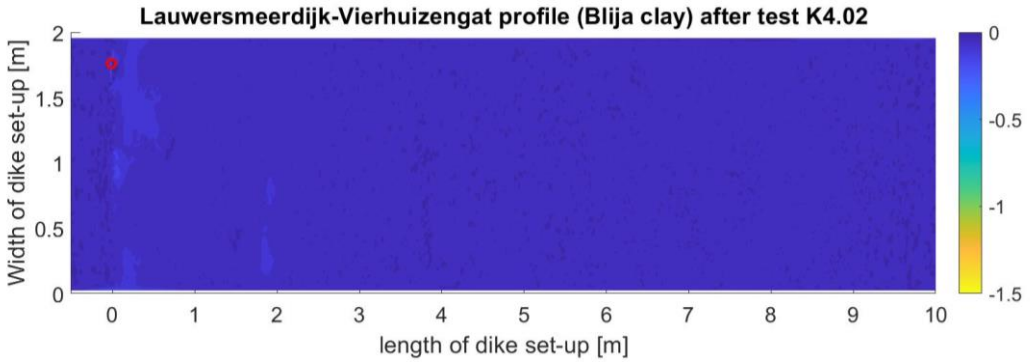

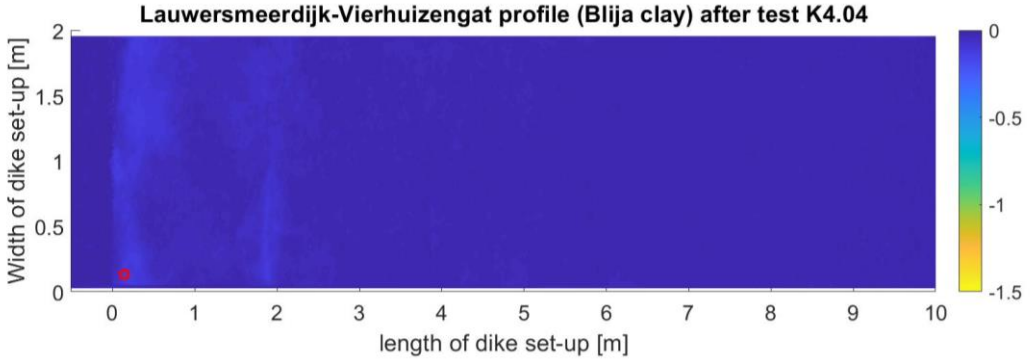

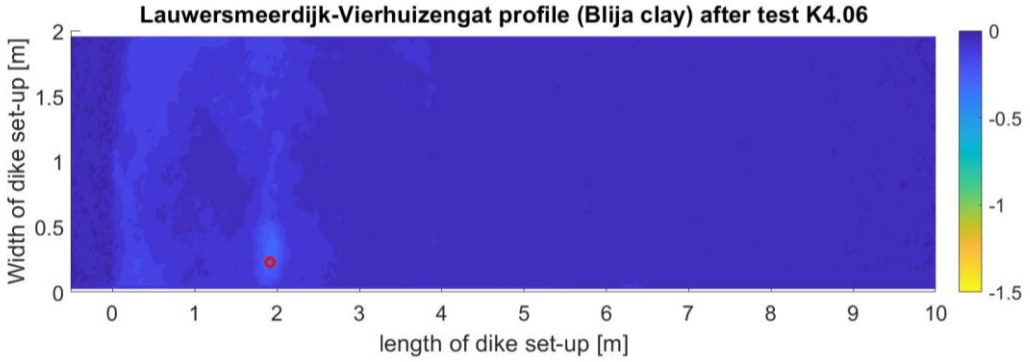

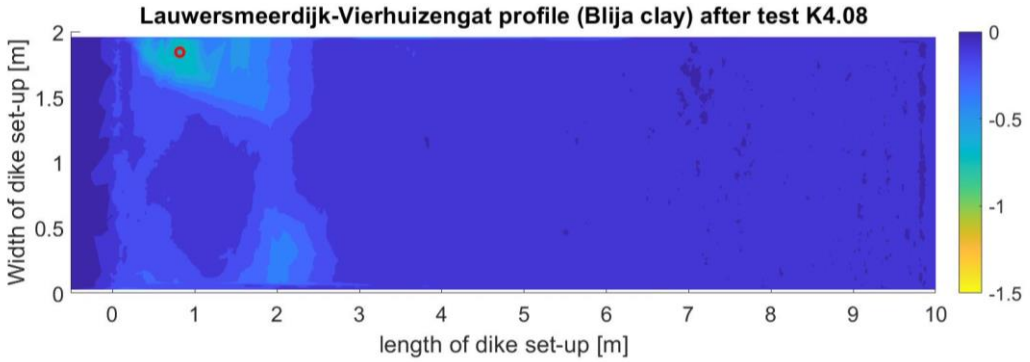

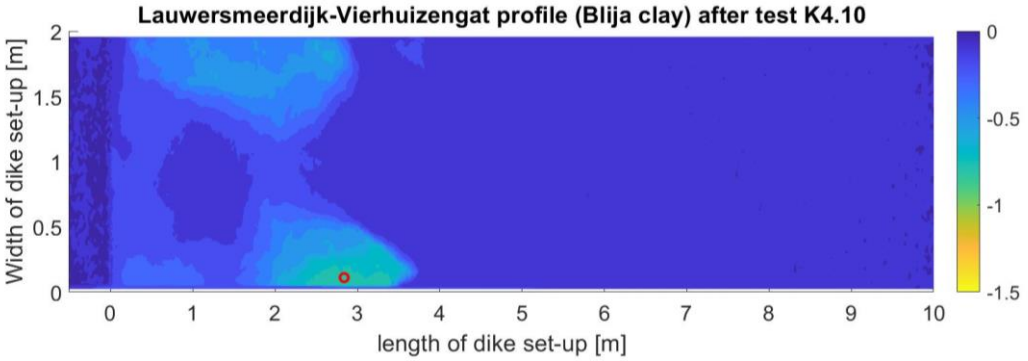
Lauwersmeerdijk-Vierhuizengat profile (Blija clay) after test K4.10
Width of dike set-up [m]
length of dike set-up [m]
0
0.5
1
1.5
2
3
4
5
6
7
8
9
10
-0.5
-1
-1.5

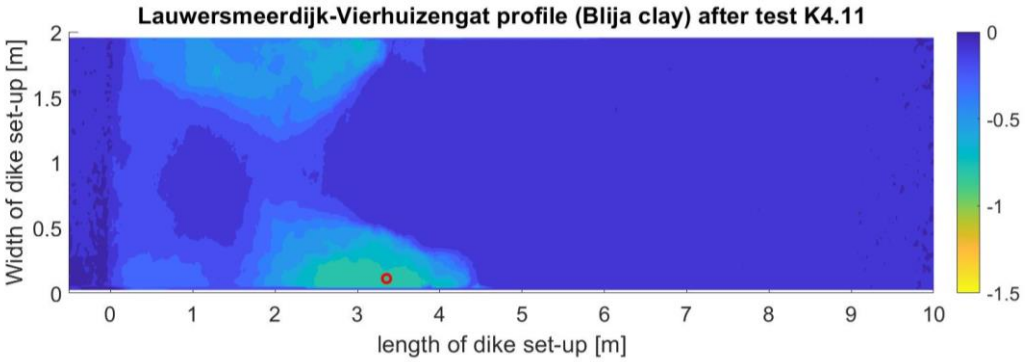
Lauwersmeerdijk-Vierhuizengat profile (Blija clay) after test K4.11
Width of dike set-up [m]
length of dike set-up [m]
0
0.5
1
1.5
2
3
4
5
6
7
8
9
10
-0.5
-1
-1.5

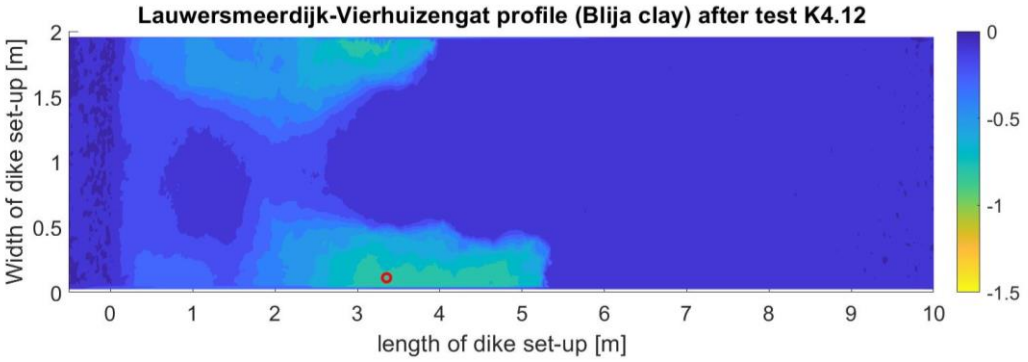
Lauwersmeerdijk-Vierhuizengat profile (Blija clay) after test K4.12
Width of dike set-up [m]
length of dike set-up [m]
0
0.5
1
1.5
2
3
4
5
6
7
8
9
10
-0.5
-1
-1.5

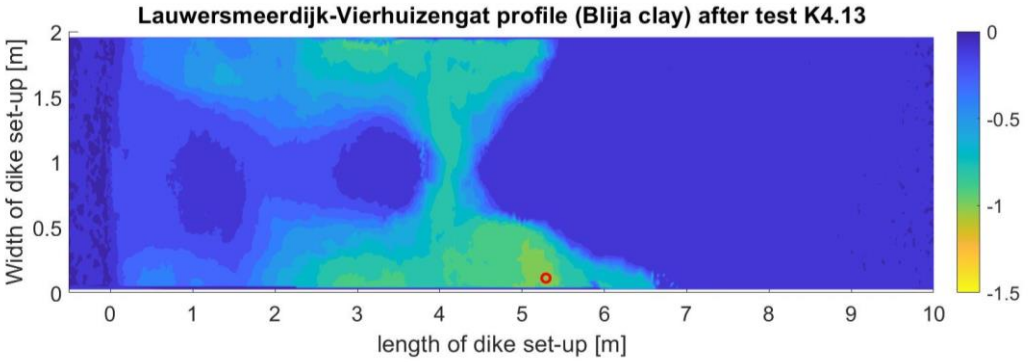
Lauwersmeerdijk-Vierhuizengat profile (Blija clay) after test K4.13
Width of dike set-up [m]
length of dike set-up [m]
0
0.5
1
1.5
2
3
4
5
6
7
8
9
10
-0.5
-1
-1.5

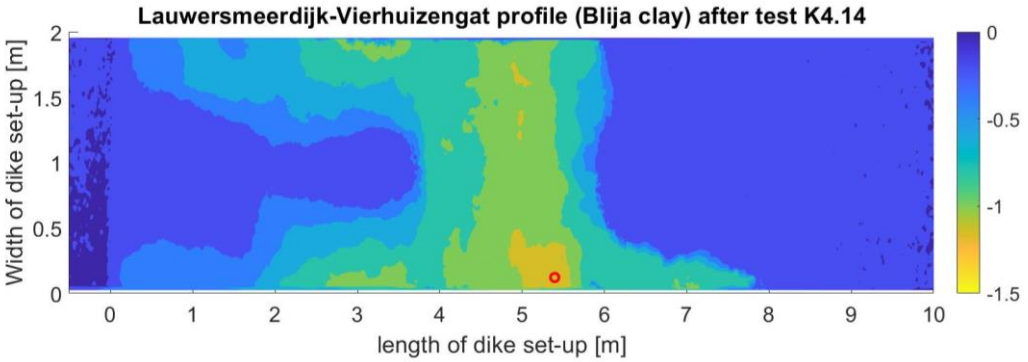
Lauwersmeerdijk-Vierhuizengat profile (Blija clay) after test K4.14
Width of dike set-up [m]
length of dike set-up [m]

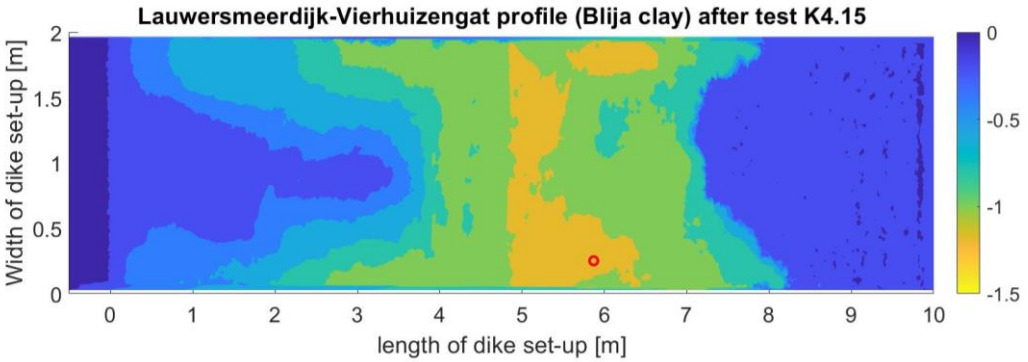
Lauwersmeerdijk-Vierhuizengat profile (Blija clay) after test K4.15
Width of dike set-up [m]
length of dike set-up [m]

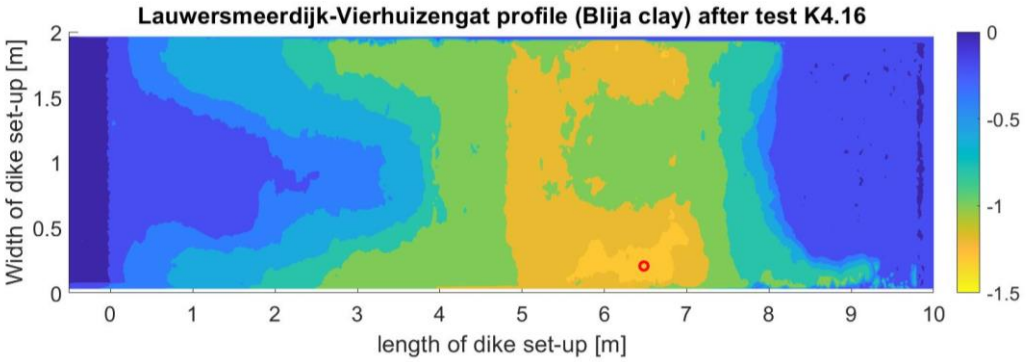
Lauwersmeerdijk-Vierhuizengat profile (Blija clay) after test K4.16
Width of dike set-up [m]
length of dike set-up [m]

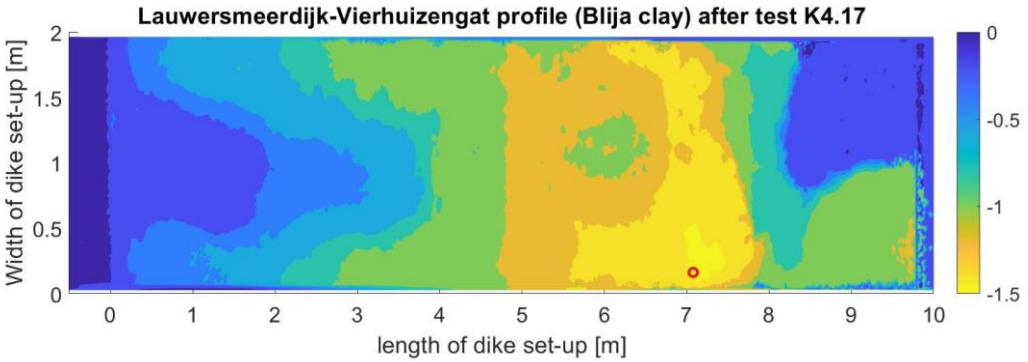
Lauwersmeerdijk-Vierhuizengat profile (Blija clay) after test K4.17
Width of dike set-up [m]
length of dike set-up [m]

C.9 Erosion cross-section experiment K4

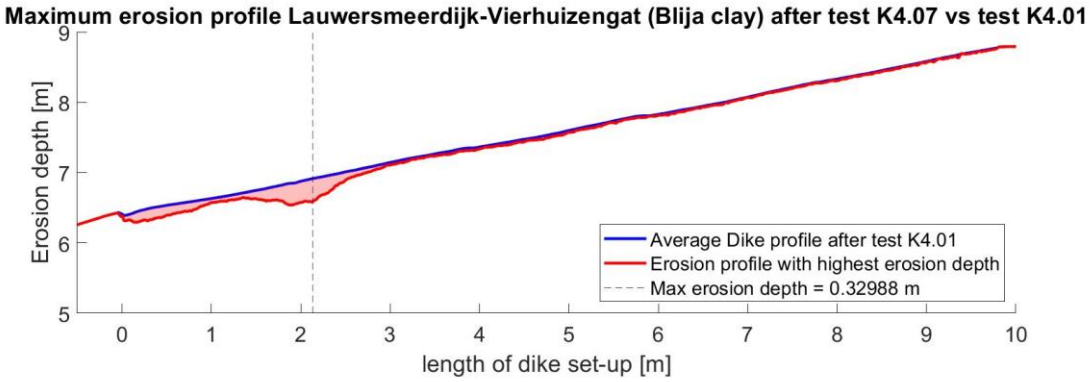

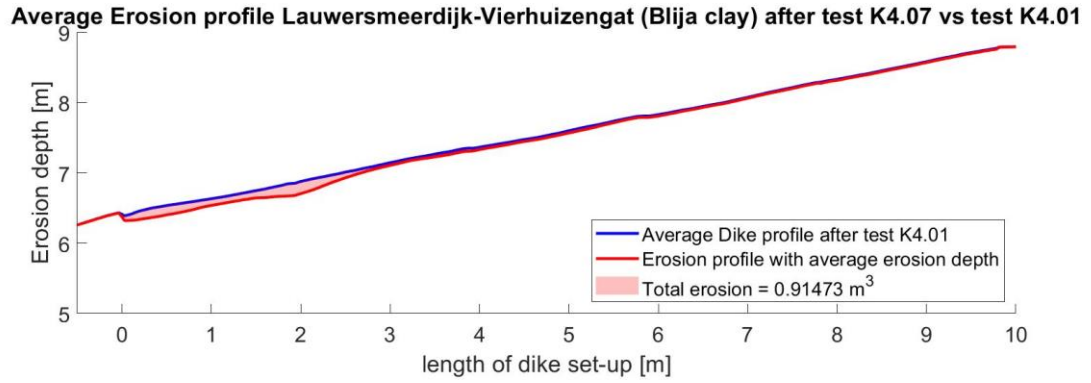

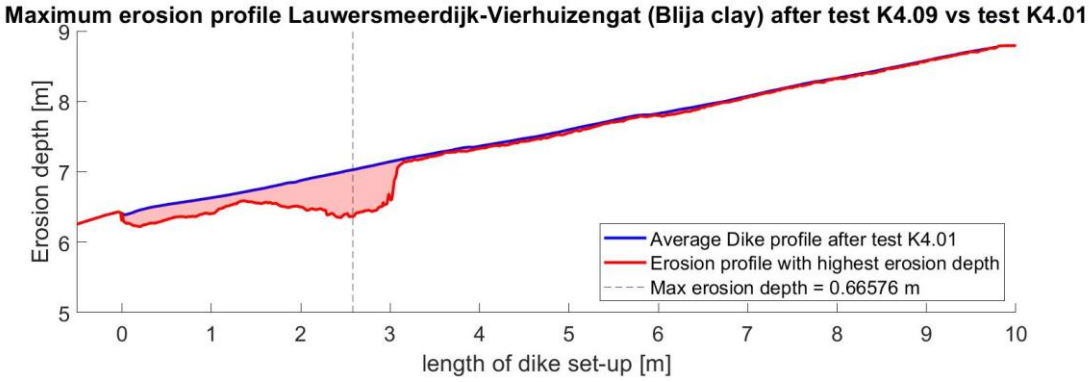

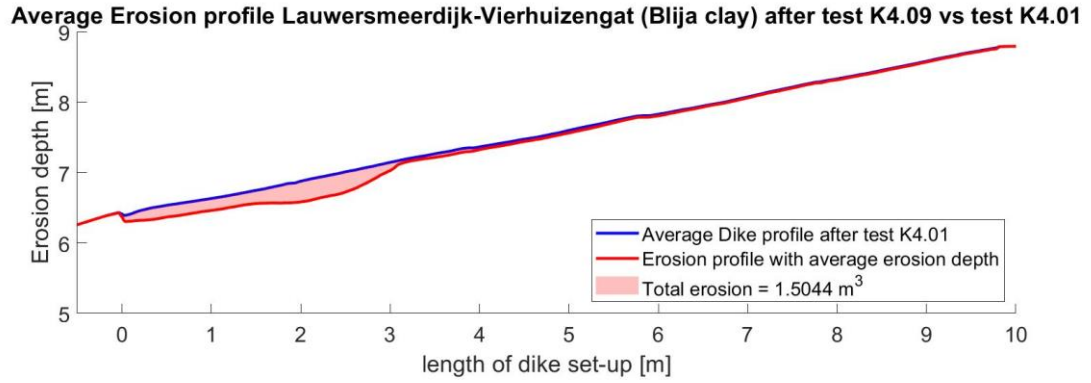

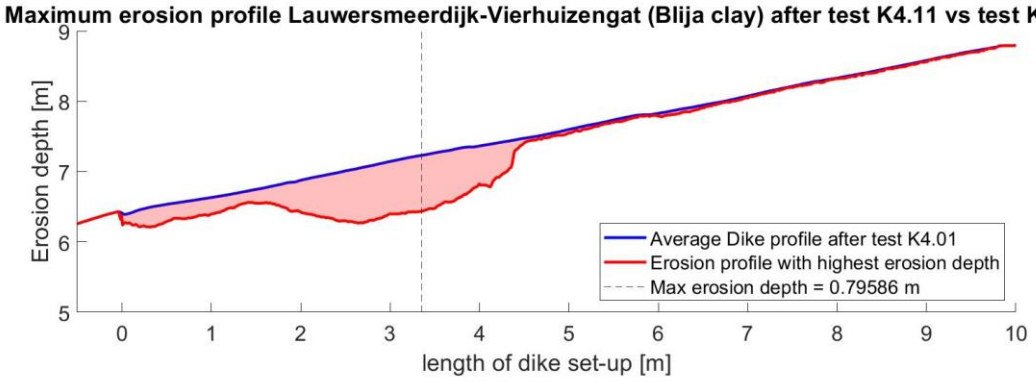
Maximum erosion profile Lauwersmeerdijk-Vierhuizengat (Blija clay) after test K4.11 vs test K4.01
Erosion depth [m]
length of dike set-up [m]
Average Dike profile after test K4.01
Erosion profile with highest erosion depth
Max erosion depth = 0.79586 m

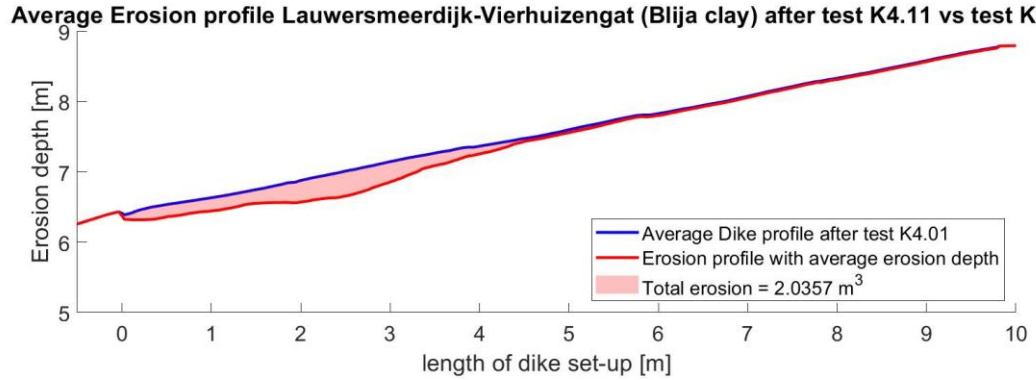
Average Erosion profile Lauwersmeerdijk-Vierhuizengat (Blija clay) after test K4.11 vs test K4.01
Erosion depth [m]
length of dike set-up [m]
Average Dike profile after test K4.01
Erosion profile with average erosion depth
Total erosion = 2.0357 m3

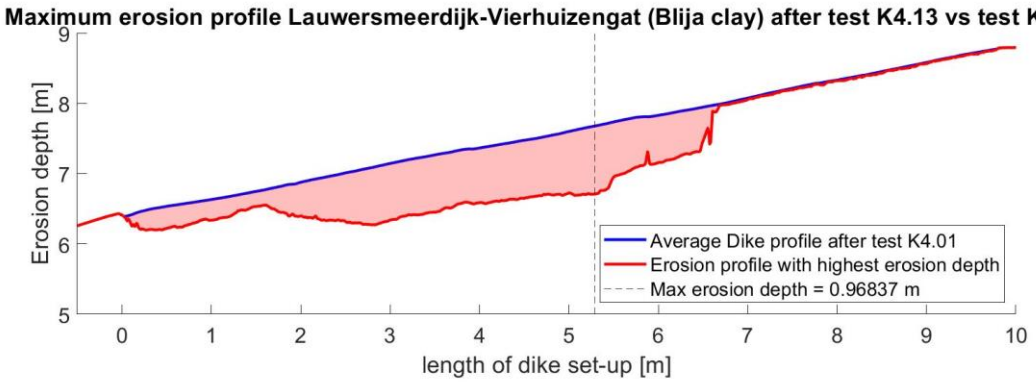
Maximum erosion profile Lauwersmeerdijk-Vierhuizengat (Blija clay) after test K4.13 vs test K4.01
Erosion depth [m]
length of dike set-up [m]
Average Dike profile after test K4.01
Erosion profile with highest erosion depth
Max erosion depth = 0.96837 m

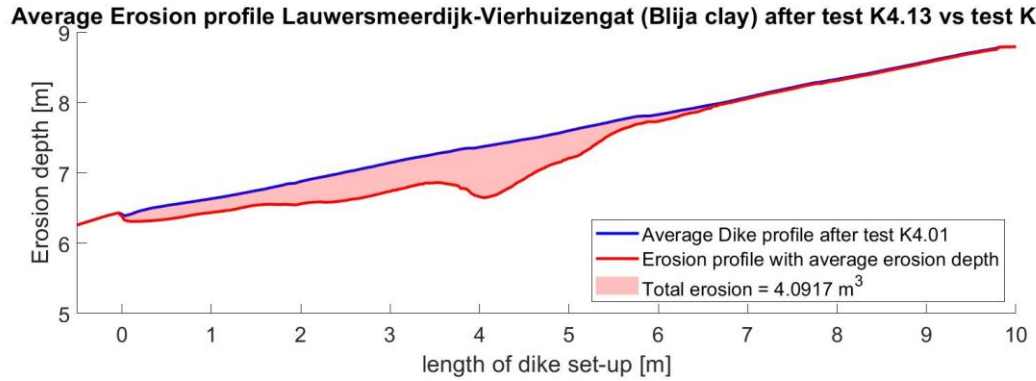
Average Erosion profile Lauwersmeerdijk-Vierhuizengat (Blija clay) after test K4.13 vs test K4.01
Erosion depth [m]
length of dike set-up [m]
Average Dike profile after test K4.01
Erosion profile with average erosion depth
Total erosion = 4.0917 m3

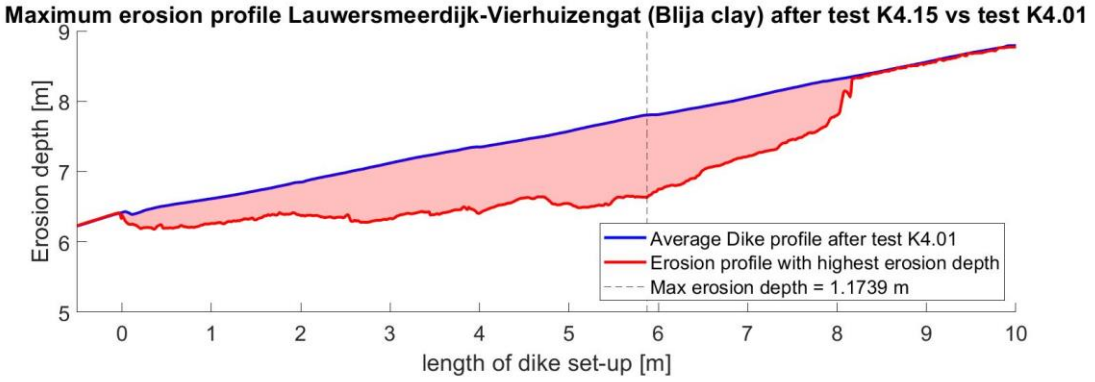
Maximum erosion profile Lauwersmeerdijk-Vierhuizengat (Blija clay) after test K4.15 vs test K4.01
Erosion depth [m]
length of dike set-up [m]
Average Dike profile after test K4.01
Erosion profile with highest erosion depth
Max erosion depth = 1.1739 m

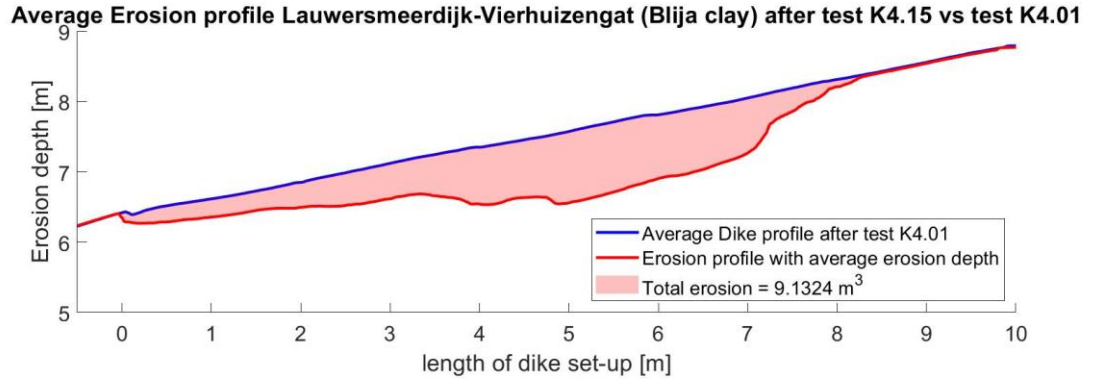
Average Erosion profile Lauwersmeerdijk-Vierhuizengat (Blija clay) after test K4.15 vs test K4.01
Erosion depth [m]
length of dike set-up [m]
Average Dike profile after test K4.01
Erosion profile with average erosion depth
Total erosion = 9.1324 m3

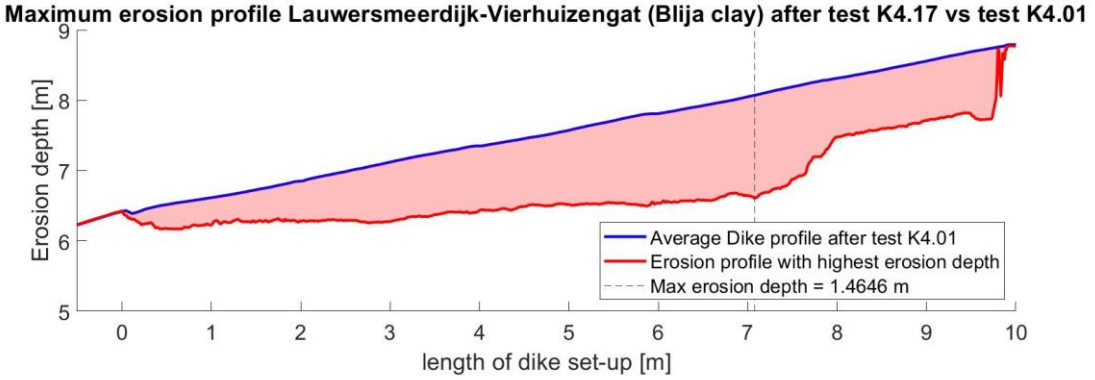
Maximum erosion profile Lauwersmeerdijk-Vierhuizengat (Blija clay) after test K4.17 vs test K4.01
Erosion depth [m]
length of dike set-up [m]
Average Dike profile after test K4.01
Erosion profile with highest erosion depth
Max erosion depth = 1.4646 m

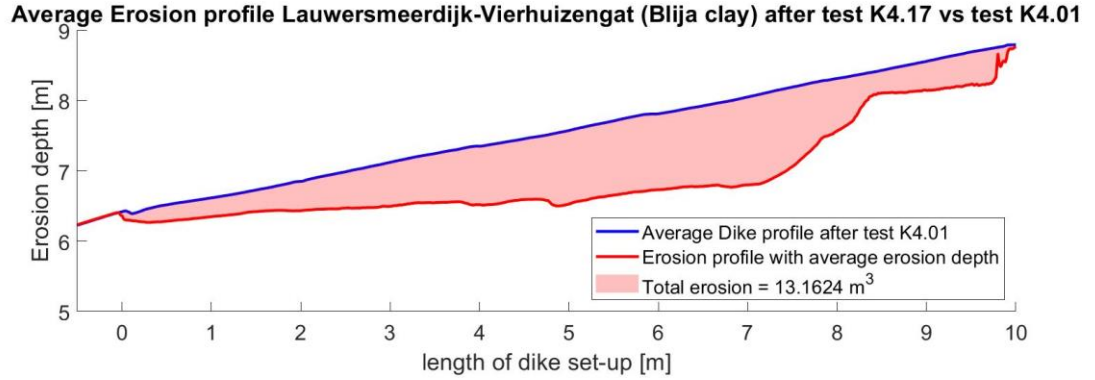
Average Erosion profile Lauwersmeerdijk-Vierhuizengat (Blija clay) after test K4.17 vs test K4.01
Erosion depth [m]
length of dike set-up [m]
Average Dike profile after test K4.01
Erosion profile with average erosion depth
Total erosion = 13.1624 m3

C.10 Erosion surface experiment K5

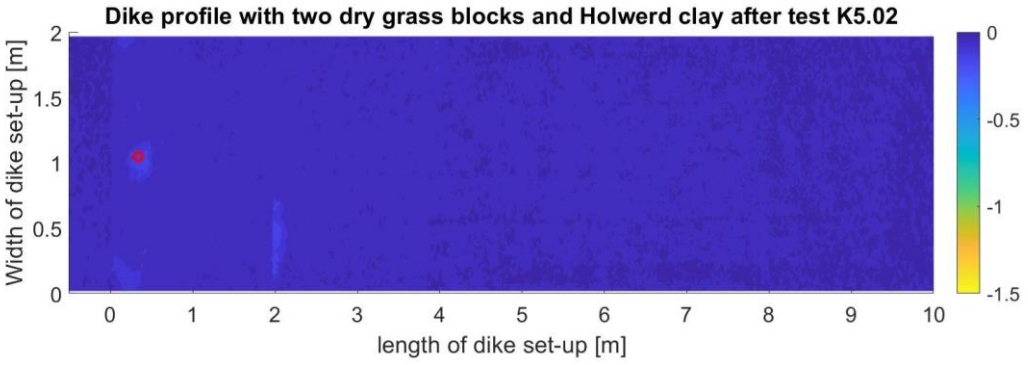

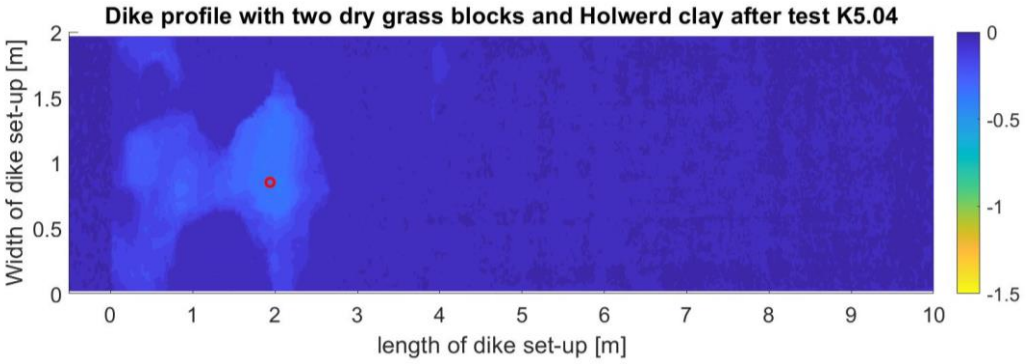

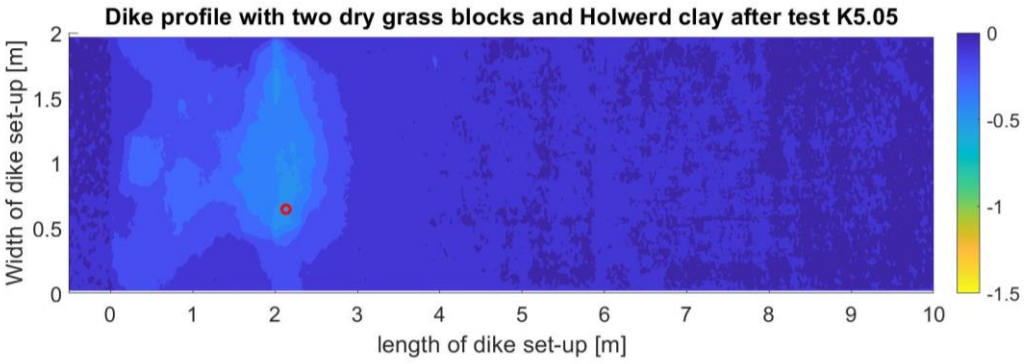

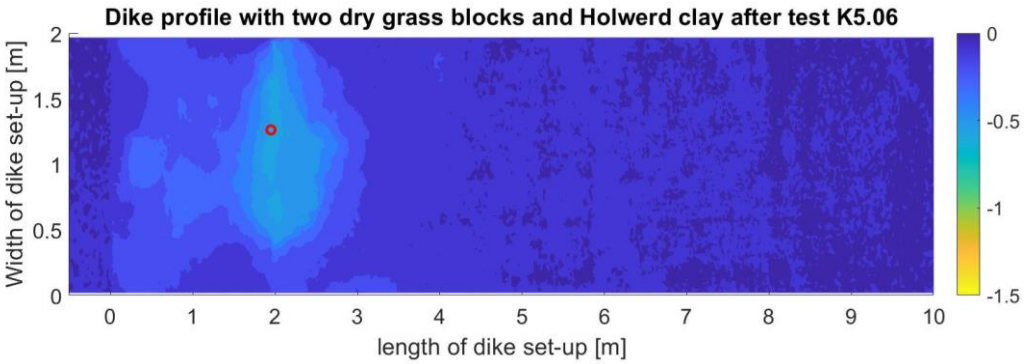

C.11 Erosion cross-section experiment K5

Maximum erosion dike profile with two dry grass blocks and Holwerd clay after test K5.04 vs test K5.01

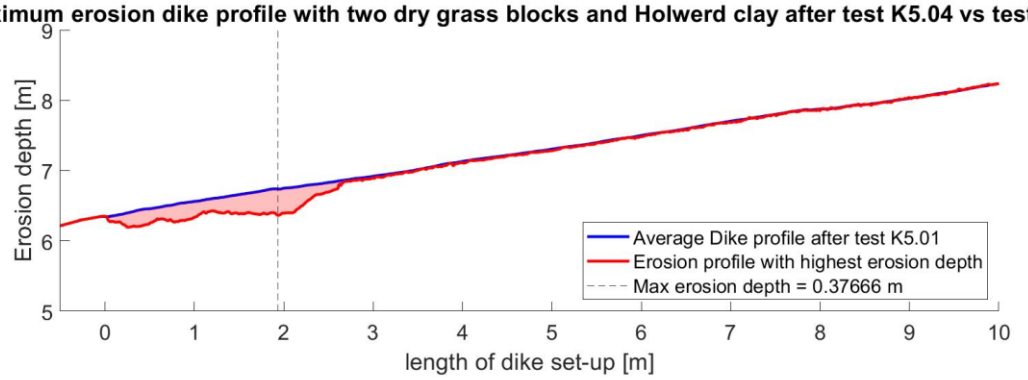

Average erosion dike profile with two dry grass blocks and Holwerd clay after test K5.04 vs test K5.01

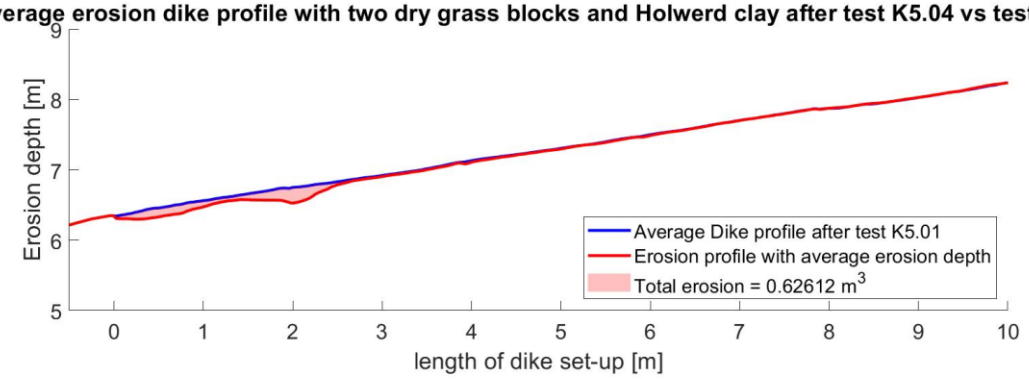

Maximum erosion dike profile with two dry grass blocks and Holwerd clay after test K5.06 vs test K5.01

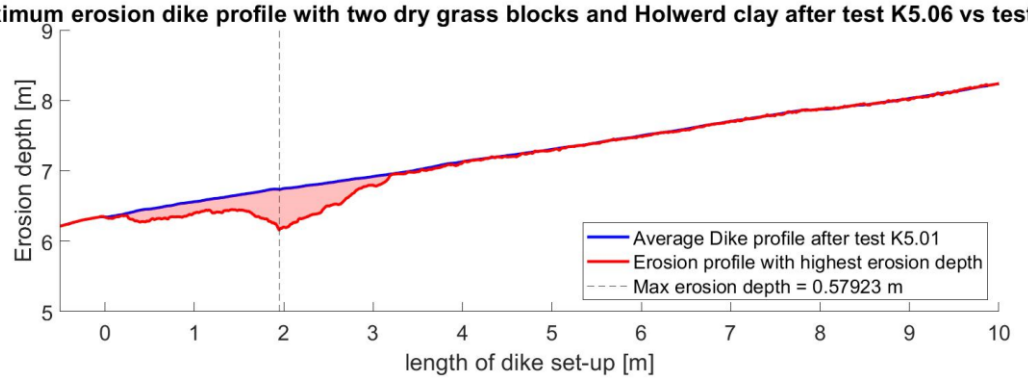

Average erosion dike profile with two dry grass blocks and Holwerd clay after test K5.06 vs test K5.01

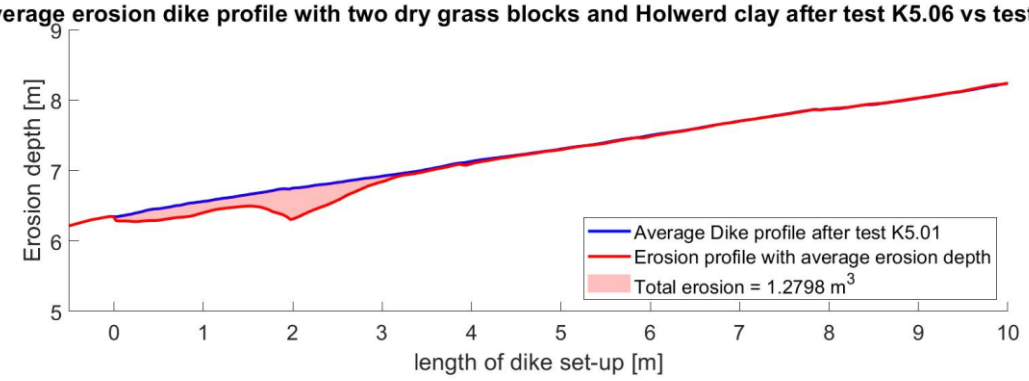

C.12 Erosion surface experiment K6

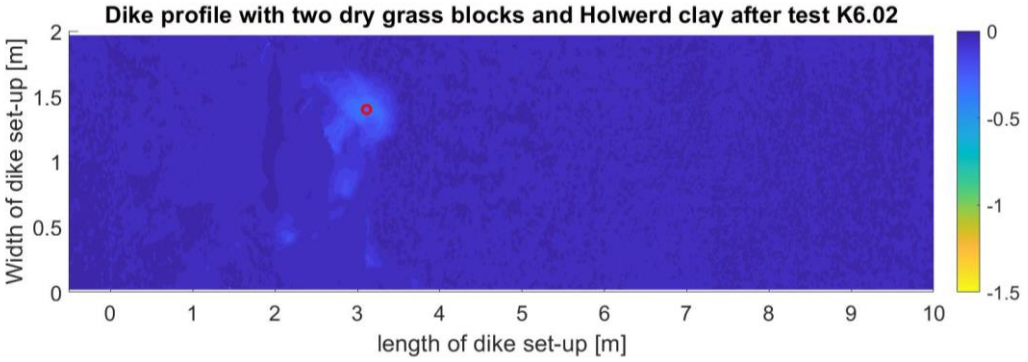

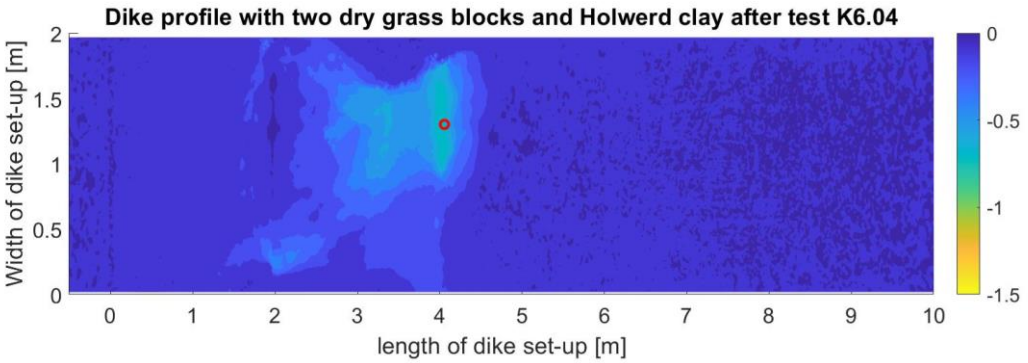

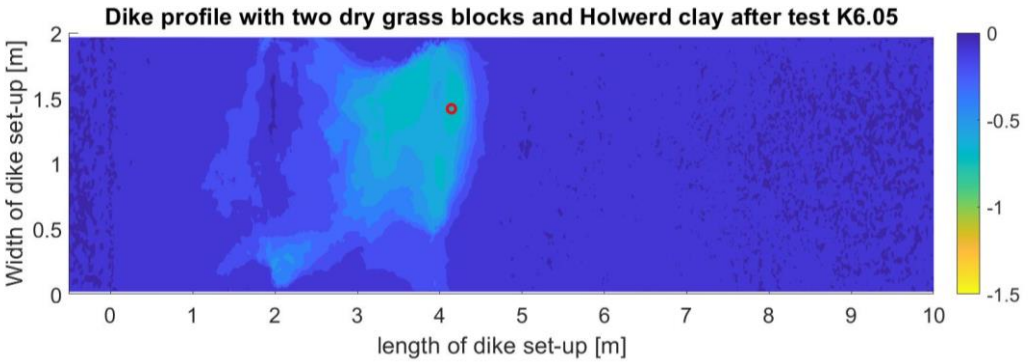

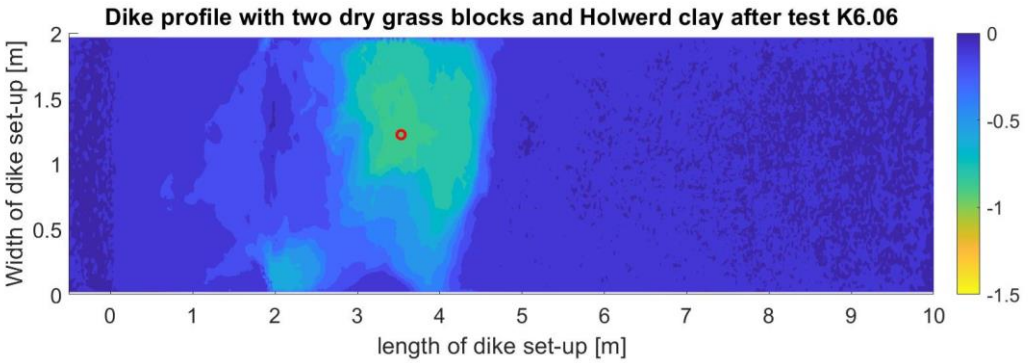

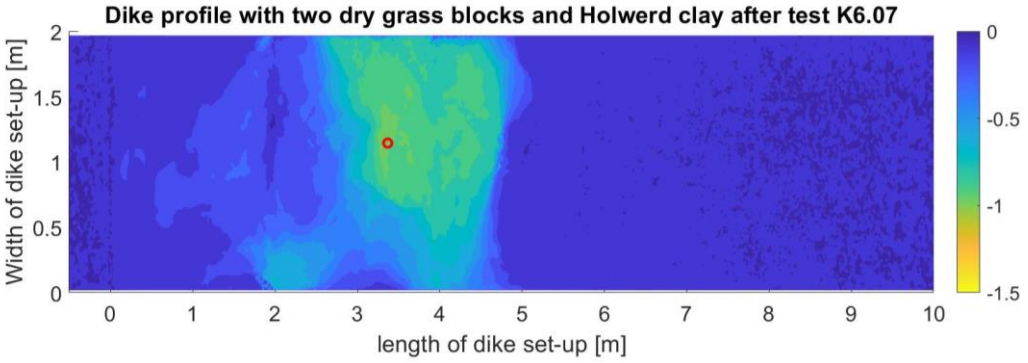
Dike profile with two dry grass blocks and Holwerd clay after test K6.07
Width of dike set-up [m]
length of dike set-up [m]
0
0.5
1
1.5
2
0
1
2
3
4
5
6
7
8
9
10
0
-0.5
-1
-1.5

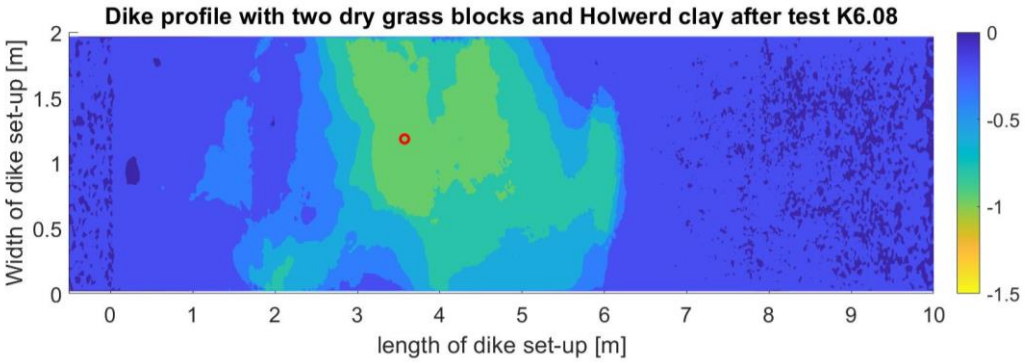
Dike profile with two dry grass blocks and Holwerd clay after test K6.08
Width of dike set-up [m]
length of dike set-up [m]
0
0.5
1
1.5
2
0
1
2
3
4
5
6
7
8
9
10
0
-0.5
-1
-1.5

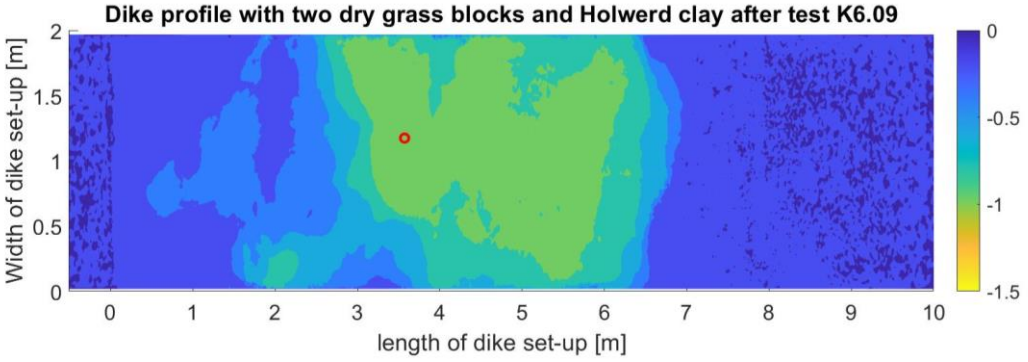
Dike profile with two dry grass blocks and Holwerd clay after test K6.09
Width of dike set-up [m]
length of dike set-up [m]
0
0.5
1
1.5
2
0
1
2
3
4
5
6
7
8
9
10
0
-0.5
-1
-1.5

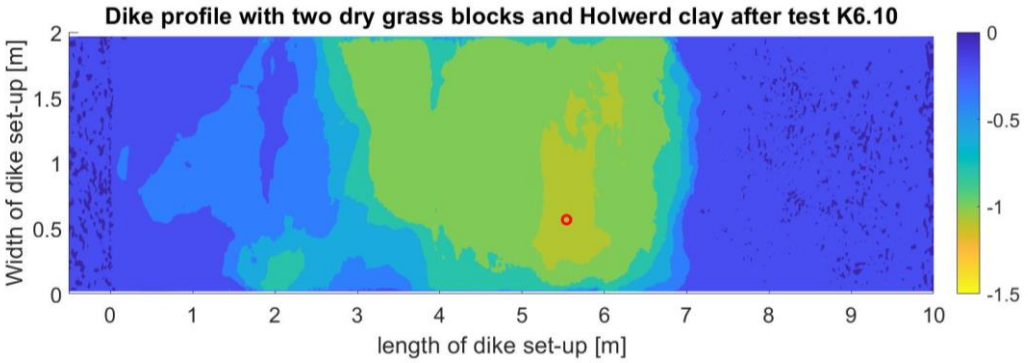
Dike profile with two dry grass blocks and Holwerd clay after test K6.10
Width of dike set-up [m]
length of dike set-up [m]
0
0.5
1
1.5
2
0
1
2
3
4
5
6
7
8
9
10
0
-0.5
-1
-1.5

C.13 Erosion cross-section experiment K6

Maximum erosion dike profile with two dry grass blocks and Holwerd clay after test K6.02 vs test K6.01

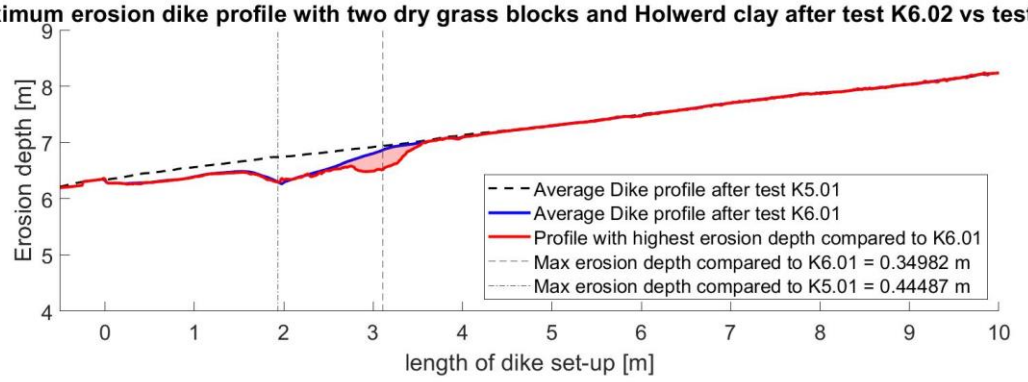

Average erosion dike profile with two dry grass blocks and Holwerd clay after test K6.02 vs test K6.01

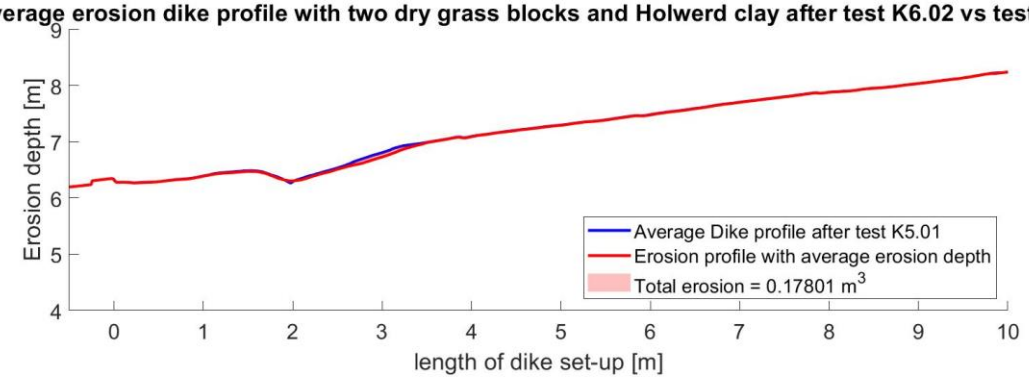

Maximum erosion dike profile with two dry grass blocks and Holwerd clay after test K6.04 vs test K6.01

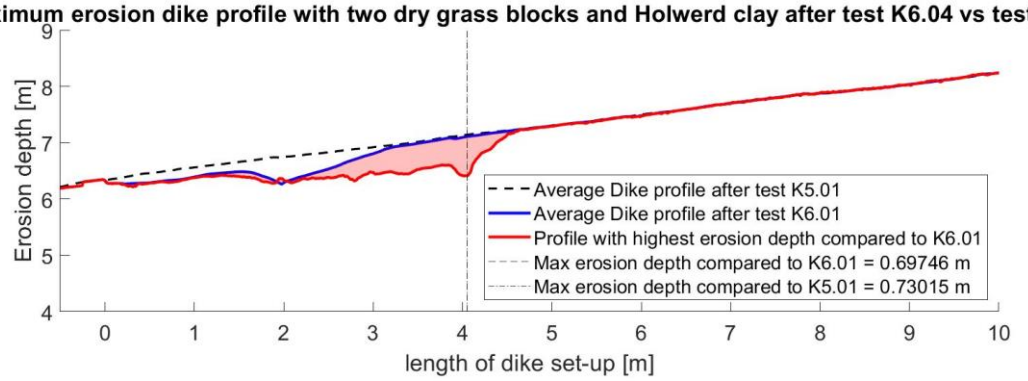

Average erosion dike profile with two dry grass blocks and Holwerd clay after test K6.04 vs test K6.01

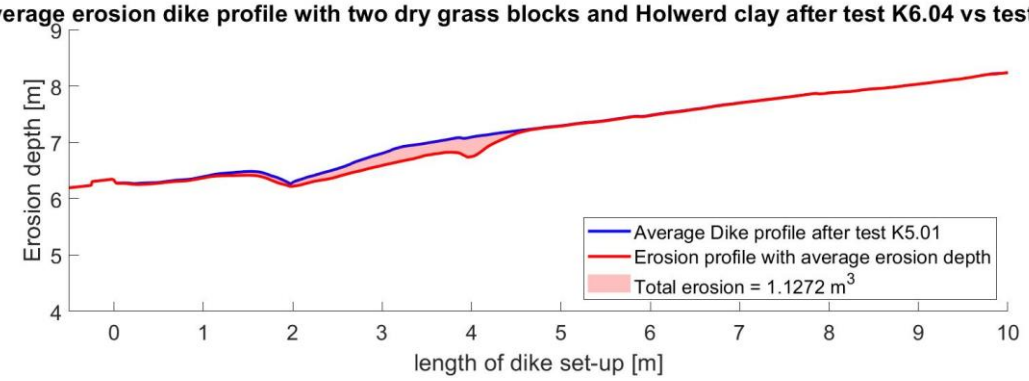

Maximum erosion dike profile with two dry grass blocks and Holwerd clay after test K6.08 vs test K6.01

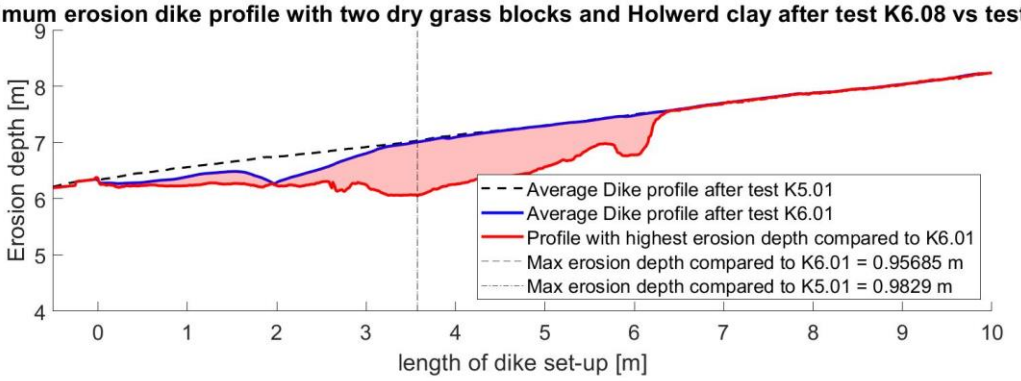

Average erosion dike profile with two dry grass blocks and Holwerd clay after test K6.08 vs test K6.01

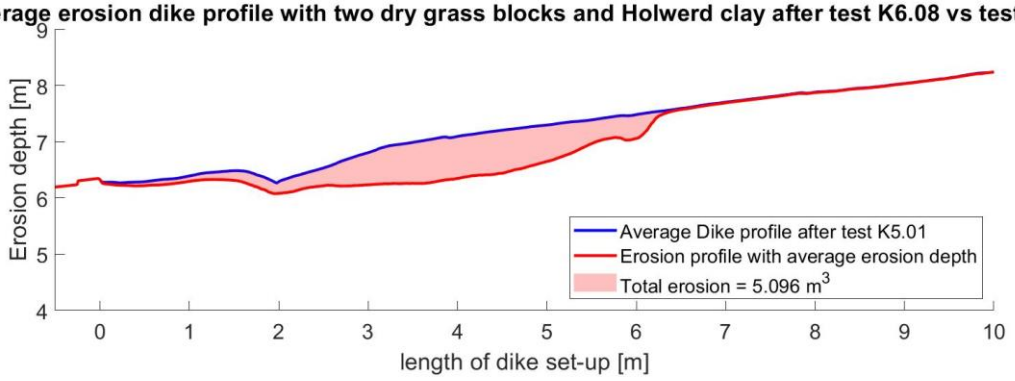

Maximum erosion dike profile with two dry grass blocks and Holwerd clay after test K6.10 vs test K6.01

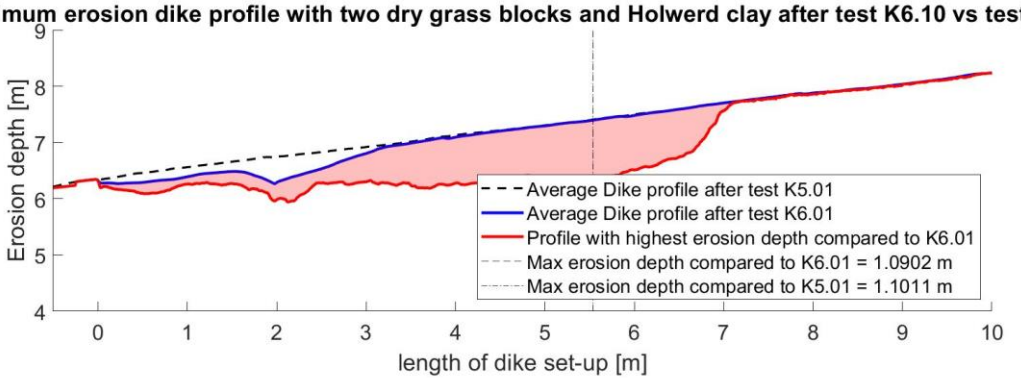

Average erosion dike profile with two dry grass blocks and Holwerd clay after test K6.10 vs test K6.01

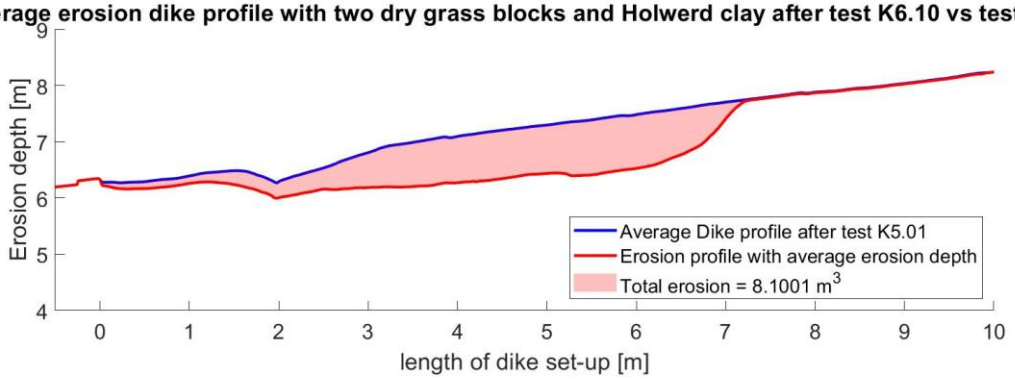

D Appendix 4: OpenFOAM model meshes

Below the meshes used for simulating experiment K101 and K114 in OpenFOAM.

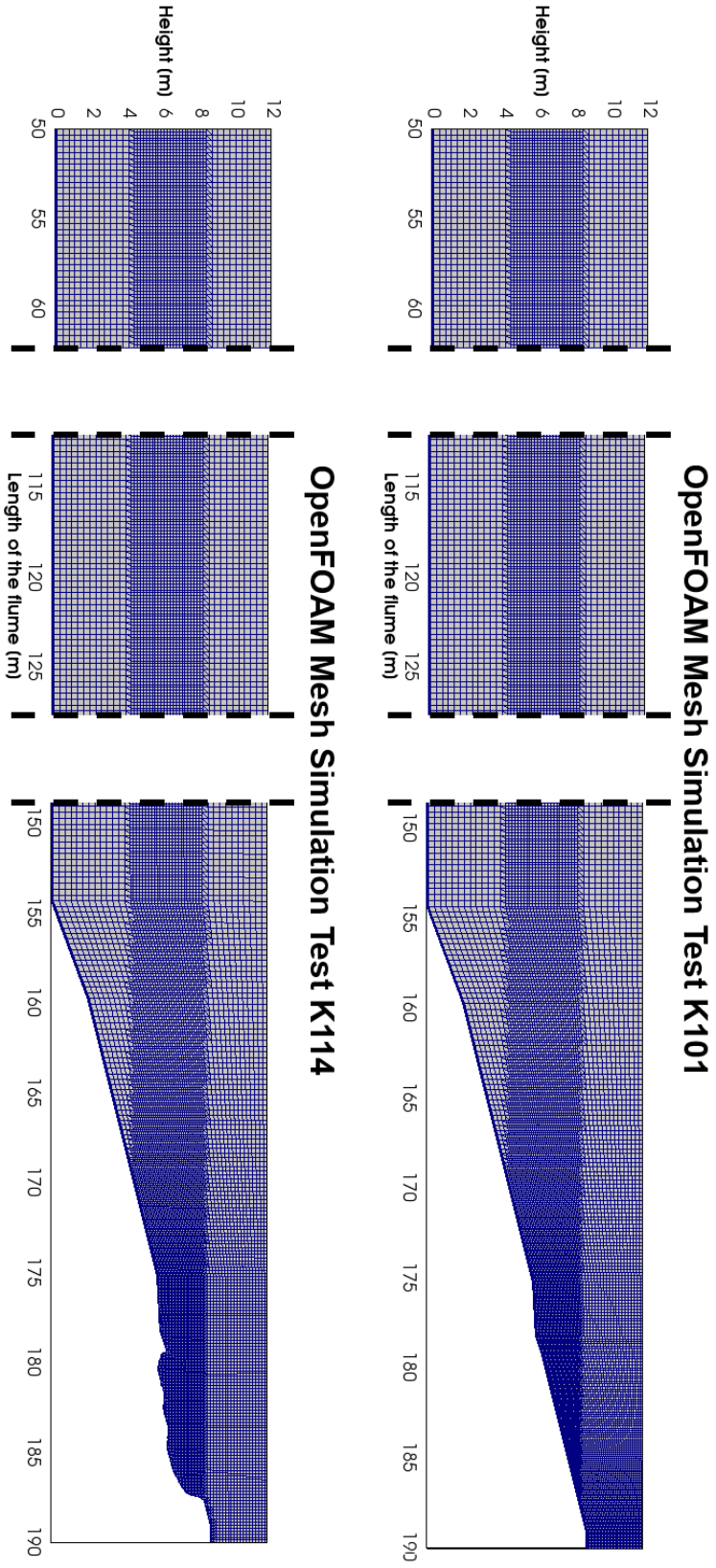

Figure D-1 OpenFOAM meshes for simulating wave impact test K101 and test K114.

E Appendix 5: OpenFOAM model mesh and probes calibration

E.1 Effect refinement surface on model results experiment K114

In order to reduce the computational time, the refinement surface was cut off after x = 165 m instead of extending it to the dike surface, reducing the computational time by approximately 30%. The effect was tested on the erosion mesh of experiment K114. The mesh with the short refinement surface is shown in Figure E-1 and the mesh with the long refinement in Figure E-2. The mesh with the long refinement surface has a considerable number of extra cells causing a longer computational time, but using no refinement surface over the eroded area causes a rough surface with lower quality mesh.

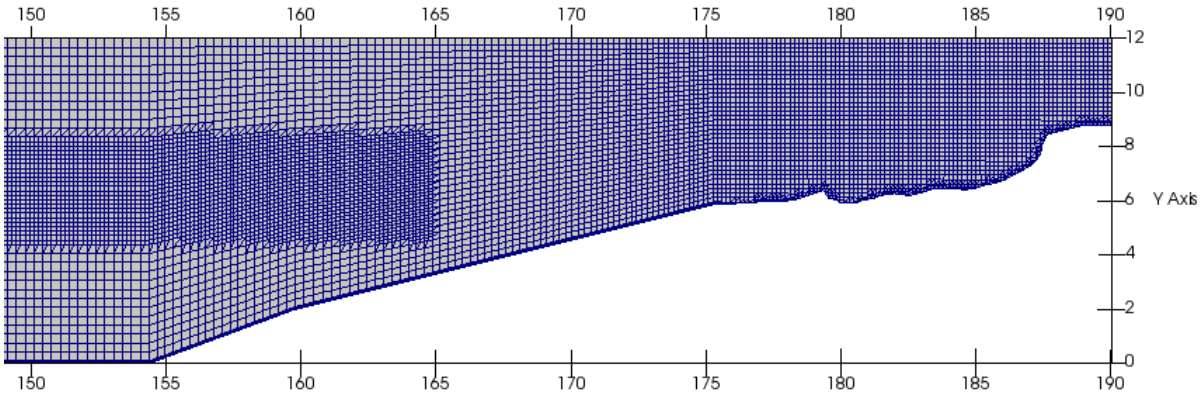

Figure E-1 OpenFOAM blockMesh model Lauwersmeerdijk-Vierhuizengat experiment K114 short refinement surface.

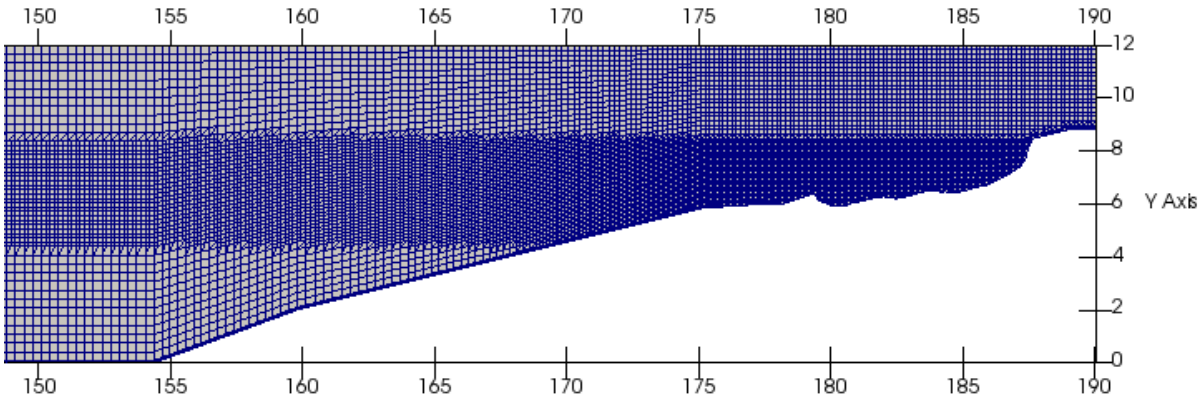

Figure E-2 OpenFOAM blockMesh model Lauwersmeerdijk-Vierhuizengat experiment K114 long refinement surface.

The effect of extending the refinement surface has been compared using the 2% exceedance maximum wave impact pressures for the first 50 seconds of the experiment as shown in Figure E-3.

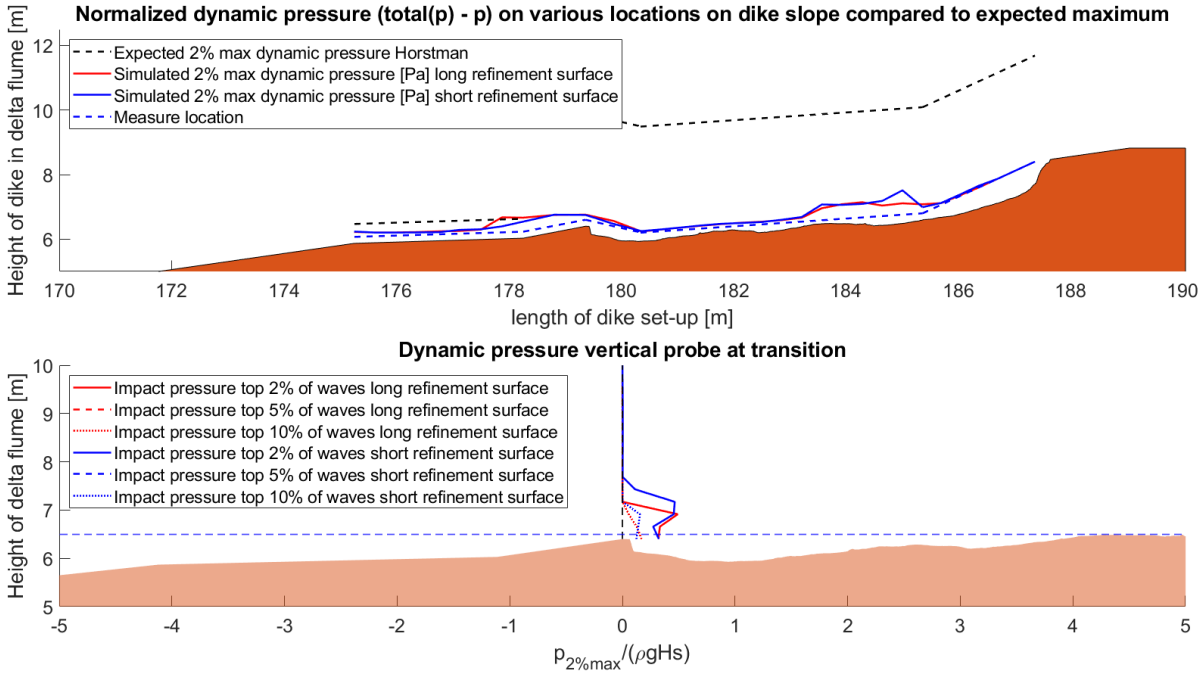

Figure E-3 Impact pressures grass revetment Lauwersmeerdijk-Vierhuizengat short vs long refinement surface.

The refinement surface does have some effect on pressure results. However, the impact pressures were tested with the first 50 s of simulation, so no very high impact pressures were yet present. Measured data are not available to validate the accuracy of the simulated parameters. Therefore, the data from the model with extended refinement surface is deemed to be more accurate since higher cell density increases model performance. Consequently, the mesh with long refinement surface is used for simulation of the experiment K101 and K114.

E.2 OpenFOAM model calibration probe location using impact pressures

Probes were added in the OpenFOAM model to obtain variables that were post-processed into pressures and velocities used for computing the erosion. The pressure is measured with vertical probes placed 6 m from each other over the dike surface. This distance was chosen to limit the number of probes and therefore the data required to calculate and validate the pressures. An extra vertical probe has been placed at the transition between hard and soft revetment as well as an extra layer of probes 10 cm above the grass revetment. Each vertical probe measures from the bottom or dike slope to the top of the domain at 12 m. Each probe has a measure point every 20 cm and were applied in the OpenFOAM model. The probe information is summarized in Table E-1.

	Number of probes	Location X [m]	Location Z [m]
Vertical probe 1	60	154	0 - 12
Vertical probe 2	50	160	0 - 12
Vertical probe 3	43	166	0 - 12
Vertical probe 4	34	172	0 - 12
Vertical probe 5	30	178	0 - 12
Vertical probe 6	23	184	0 - 12
Vertical probe transition	28	179,368	7.2 - 12

Diagonal probe grass revetment	90	179,368 - 189.048	6.5 - 8.92

Table E-1 Description of probes for pressure validation OpenFOAM model experiment K101.

The probe locations have also been visualized in Figure E-4 showing all the probes on the surface of the dike model of experiment K101.

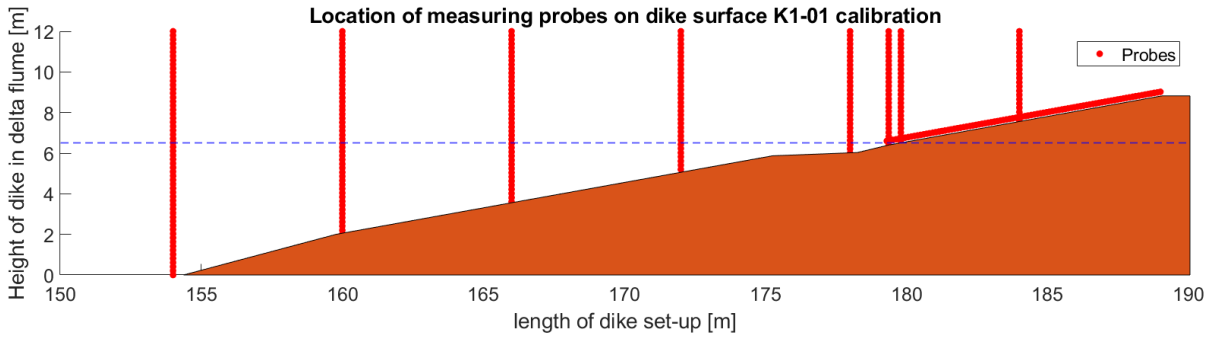

Figure E-4 Probe locations of model validation set up.

However, using the number of probes as shown in Figure E-4 results in a lot of data, while most of the data were not used. Therefore, the height above the surface where the maximum dynamic pressure occurs has been used as the only probe location for the final model reducing the amount of data points significantly.

Simulated pressures

The dynamic pressure over depth has been measured during the OpenFOAM simulation at different locations to determine the location of the maximum dynamic pressure. The height above the dike at which the maximum dynamic pressures occur is an important parameter to determine for measuring the maximum impact pressures. Identifying the location of maximum dynamic pressure allows to put a line at that height with multiple probes, rather than using numerous vertical probes which extend simulation duration and increase the amount of data. The 2% of maximum impact pressures from p_rgh and total pressure minus hydrostatic pressure data from the vertical probes have been compared in Figure E-5. A constant dynamic pressure distribution over depth is visible in the top plot of the figure where p_rgh is displayed. The dynamic pressure in the bottom plot is only visible in the wave impact and run-up zone. The hydrostatic pressure before wave breaking is almost equal to the total pressure in the bottom plot.

The green line shows the location of maximum dynamic pressure which is around the wave movement at the surface before wave breaking and close to the dike surface at the impact and run-up zone. It was observed that the waves generally break at the berm (at x = 175 m in Figure E-5) thus dynamic pressure probes will be placed along the green line from the start of the berm until the crest of the dike. The green line is 0.2 m above the dike surface.

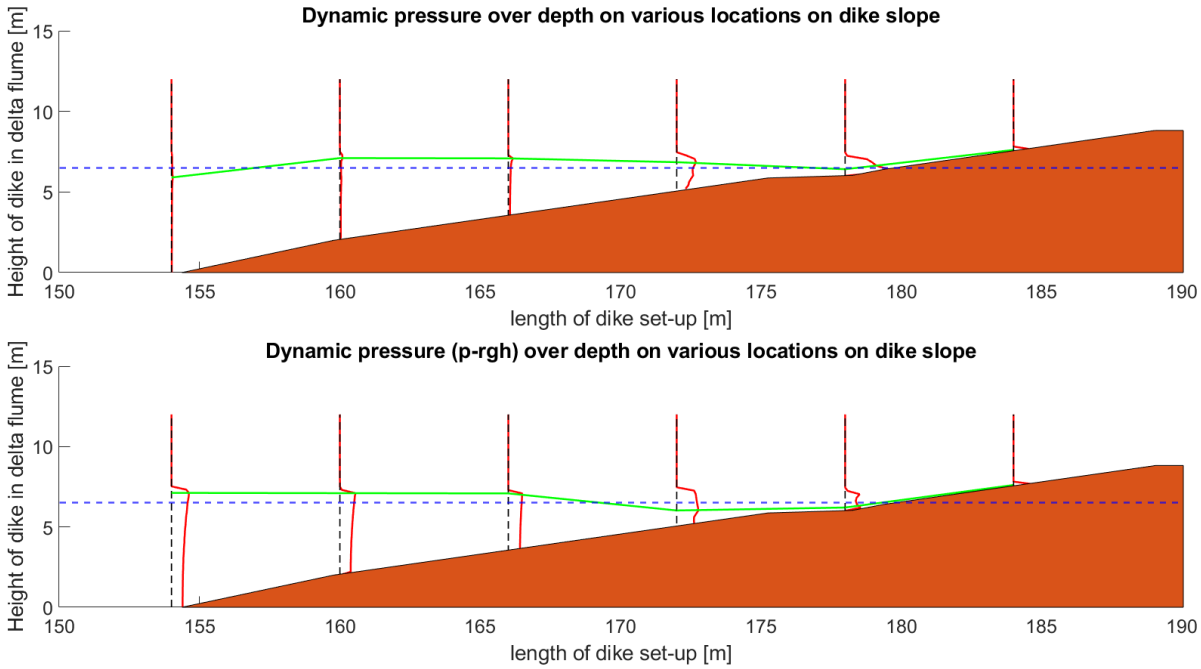

Figure E-5 Dynamic pressures from wave impact p_rgh vs total(p) – p.